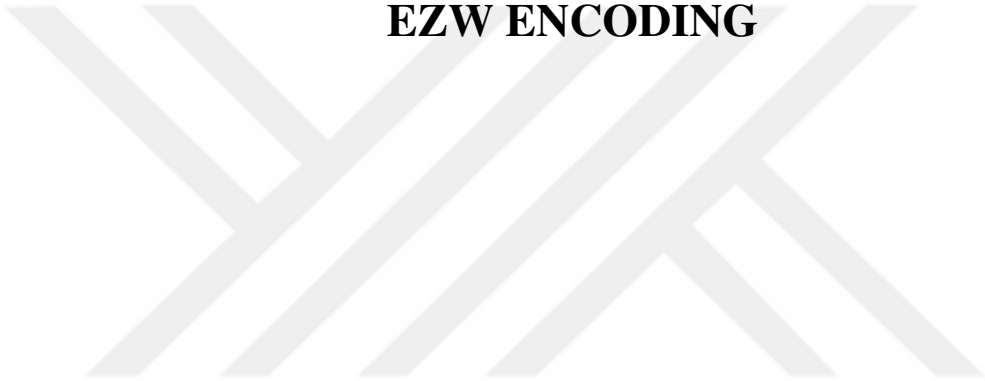


DOKUZ EYLÜL UNIVERSITY
GRADUATE SCHOOL OF NATURAL AND APPLIED SCIENCES

MEDICAL IMAGE COMPRESSION APPROACHES
BASED ON RUN-LENGTH, CHAIN CODE AND
EZW ENCODING



by
Erdoğan ALDEMİR

July, 2019
İZMİR

MEDICAL IMAGE COMPRESSION APPROACHES BASED ON RUN-LENGTH, CHAIN CODE AND EZW ENCODING

**A Thesis Submitted to the
Graduate School of Natural And Applied Sciences of Dokuz Eylül University
In Partial Fulfillment of the Requirements for the Degree of Doctor of
Philosophy in Electrical and Electronics Engineering Program**

**by
Erdoğan ALDEMİR**

July, 2019

İZMİR

Ph.D. THESIS EXAMINATION RESULT FORM

We have read the thesis entitled “**MEDICAL IMAGE COMPRESSION APPROACHES BASED ON RUN-LENGTH, CHAIN CODE AND EZW ENCODING**” completed by **ERDOĞAN ALDEMİR** under supervision of **PROF. DR. GÜLAY TOHUMOĞLU YILDIRIM** and we certify that in our opinion it is fully adequate, in scope and in quality, as a thesis for the degree of Doctor of Philosophy.


Prof. Dr. Gülay TOHUMOĞLU YILDIRIM

Supervisor


Doc. Dr. M. Alper SELVER

Thesis Committee Member


Doç Dr. Adil ALPKOÇAK

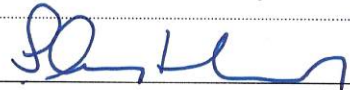
Thesis Committee Member

Doç. Dr. Devrim ÜNAY



Examining Committee Member

Doç. Dr. Şevket GÜMÜŞTEKİN



Examining Committee Member


Prof. Dr. Kadriye ERTEKİN

Director

Graduate School of Natural and Applied Sciences

ACKNOWLEDGEMENTS

First, I would like to declare my most heartfelt appreciation to my supervisor, Prof. Dr. Gülay TOHUMOĞLU YILDIRIM. It has been a pleasure to work under her guidance for the years. Her advice, energy, encouragement, and dedication have been inspirational. She always encourages my research and allows me to grow as a scientist.

I am especially indebted to Assoc. Prof. Dr. M. Alper SELVER who have been always supported my whole Ph.D. study and who encourage me to pursue my goals.

I am also grateful to my mother and father for whom it would never be possible to see this story without them. My family's love and guidance have always been with me.

I also thank my friends; they have always supported me even if at the most desperate times.

This dissertation was supported by The Scientific and Technological Research Council of Turkey (TÜBİTAK) -Scientific and Technological Research Projects Funding Program- under grant number 116E133.

Erdoğan ALDEMİR

MEDICAL IMAGE COMPRESSION APPROACHES BASED ON RUN-LENGTH, CHAIN CODE AND EZW ENCODING

ABSTRACT

In information theory, utilization of channel bandwidth efficiently, establishing the practical telemedicine networks and even though archiving of medical images are importantly considered to transfer data. The expression of an image using a fewer number of bits with or without loss of information is defined as image compression or coding. In order to image coding, there are many compression techniques.

In this dissertation, various compression algorithms are examined to reveal the redundancy of 3D medical images more effectively. The context-based and contour-based coding approaches are proposed bi-level compression pipelines. In the first circumstance, the run-length coding is specialized for two-dimensional slices of volumetric-medical images. Inter-voxel relationships and intra-pixel relationships are revealed by different scanning procedures such as Hilbert, chevron, and perimeter. Secondly, chain codes are applied to 2D-slices to code contour knowledge. In this method, the contour defining algorithm is used and modified to code symbols representation efficiently. The embedded zerotree wavelets (EZW) and sparsity are gray-level compression approaches, and they utilize different wavelets.

In this study, proposed algorithms are experienced on the computed tomography (CT) and magnetic resonance imaging (MR) datasets, which are acquired from Dokuz Eylül University Hospital. The run-length and chain codes systems are applied for bi-level CT and MR datasets and compression ratios approximately 100:1 and 200:1, respectively. These achievements show proposed systems outperform JBIG and CCITT that are well-known bi-level compression standards. The EZW algorithm only tested for gray-level MR images. The results are presented in terms of common lossy compression metrics.

Keywords: image compression, chain-code, medical image, run-length encoding

KATAR UZUNLUĞU, ZİNCİR KOD VE EZW KODLAMALARI TABANLI TIBBİ GÖRÜNTÜ SIKIŞTIRMA YAKLAŞIMLARI

ÖZ

Bilgi teorisinde, kanal bant genişliğinin verimli kullanılması, pratik teletıp ağlarının kurulması ve tıbbi görüntülerin arşivlenmesi, verilerin aktarılması için önemli olduğu düşünülmektedir. Bilgi kaybı olacak şekilde veya kayıpsız olarak az sayıda bit kullanılarak bir görüntünün ifadesi, görüntü sıkıştırma veya kodlama olarak tanımlanır. Görüntü kodlaması için birçok sıkıştırma tekniği vardır.

Bu tez çalışmasında, 3D medikal görüntülerin fazlalığını daha etkin bir şekilde ortaya çıkarmak için çeşitli sıkıştırma algoritmaları incelenmiştir. Bağlam tabanlı ve çevre tabanlı kodlama yaklaşımları iki seviyeli sıkıştırma boru hatları olarak önerilmiştir. İlk durumda, katar-uzunluğu uzunluğu kodlaması iki boyutlu hacimsel tıbbi görüntülerin dilimlerinin sıkıştırılması için özelleştirilmiştir. Vokseller-arası ilişkiler ve pikseller-arası ilişkiler, Hilbert, chevron ve çevre gibi farklı tarama prosedürleriyle ortaya çıkarılmıştır. İkinci olarak, zincir kodu, kontur bilgisini kodlamak için 2D dilimlerine uygulanmıştır. Bu yöntemde, kontur tanımlama algoritması, sembollerini temsil etmek için verimli bir şekilde kodlamak üzere kullanılmış ve geliştirilmiştir. Gömülü sıfır-ağac dalgacık (EZW) ve seyreklik gri seviyeli sıkıştırmada kullanılan yaklaşımlardır ve farklı dalgacıklardan yararlanırlar.

Bu çalışmada, Dokuz Eylül Üniversitesi Hastanesi'nden elde edilen bilgisayarlı tomografi (BT) ve manyetik rezonans görüntüleme (MR) veri setlerinde önerilen algoritmalar deneyimlenmiştir. Katar-uzunluğu ve zincir kod sistemleri, iki seviyeli CT ve MR veri kümelerinde uygulanmış ve sırasıyla yaklaşık 100:1 ve 200:1 sıkıştırma oranları elde edilmiştir. Bu sonuçlar, önerilen sistemlerin iyi bilinen iki seviyeli sıkıştırma standartları olan JBIG ve CCITT'den daha iyi performansa ulaştıklarını göstermektedir. EZW algoritması yalnızca gri seviyeli MR görüntüleri için test edilmiştir. Sonuçlar, ortak kayıplı sıkıştırma ölçütleri olarak sunulmuştur.

Anahtar kelimeler: imge sıkıştırma, zincir-kodu, tıbbi imge, katar-uzunluęu kodlaması



CONTENTS

	Page
Ph.D. THESIS EXAMINATION RESULT FORM	ii
ACKNOWLEDGEMENTS	iii
ABSTRACT	iv
ÖZ	v
LIST OF FIGURES	xiii
LIST OF TABLES	xiv
CHAPTER ONE – INTRODUCTION	1
1.1 Motivation	2
1.2 Telemedicine Networks and Medical Image Compression	3
1.3 Scientific Novelty of the Dissertation	5
CHAPTER TWO – BACKGROUND.....	8
2.1 Fundamentals of Data Compression.....	8
2.1.1 Performance Assessment of Compression Scheme	14
2.2 Information Theory and Data Compression.....	17
2.2.1 Optimal Coding for Lossless Compression	19
2.3 Related Works and Literature Review	20
CHAPTER THREE – IMAGE COMPRESSION	25
3.1 Transform Based Image Compression	25
3.2 Lossless Image Compression	29
3.3 Lossless Compression Systems	30
3.4 Lossless Compression Algorithms.....	34
3.4.1 Huffman Coding	35
3.4.2 Arithmetic Coding.....	36
3.4.3 Contour Encoding	37

3.4.4 Lempel–Ziv–Welch	38
3.4.5 Run-length Encoding	38
3.5 Lossless Bi-level Image Compression Standards	40
3.5.1 The JBIG Standardizations for Bi-level Image Compression	40
3.5.2 CCITT Standards	41
CHAPTER FOUR – REDUNDANCY IN MEDICAL IMAGES	43
CHAPTER FIVE – PROPOSED BI-LEVEL COMPRESSION SCHEMES	50
5.1 Extended Run-Length Encoding for Bi-level Medical Images	51
5.1.1 The RLE with Multiple Scanning Procedure	53
5.1.2 A New Volumetric Run-Length Encoding Approach	59
5.2 Chain Rule based Compression System (CrS)	66
5.3 Transform based Compression System	68
5.3.1 Predictive Mapping and RLE based Hybrid Compression	68
5.3.2 Embedded Zerotree Wavelet Image Coding	70
5.3.3 Wavelet Transform	71
5.3.4 Embedded Zerotree Wavelet Algorithm.....	74
5.3.5 Sparse Representation Approach.....	78
CHAPTER SIX – SIMULATIONS AND RESULTS	80
6.1 Medical Image Data Sets	80
6.2 State-of-The-Art Binary Image Compression Standards	83
6.3 Run-Length Encoding based Compression Scheme	85
6.3.1 Volumetric RLE based Compression Algorithm: 3D-RLE	87
6.4 The Chain Rule based Compression System.....	101
6.5 The EZW Compression	107
6.6 Sparse Representation based Compression.....	108
6.7 The Implementation Challenges.....	114
6.7.1 The 3D-RLE	114
6.7.2 The Chain Rule-based Compression System	114

CHAPTER SEVEN – CONCLUSIONS AND FUTURE WORKS.....	116
7.1 Future Works	118
REFERENCES.....	119



LIST OF FIGURES

	Page
Figure 2.1 Segments of the raw data regarding the compression process	9
Figure 2.2 The fundamental blocks of the encoder	10
Figure 2.3 The fundamental blocks of the decoder	11
Figure 2.4 Main processes of designing a compression algorithm	13
Figure 2.5 Entropy function regarding propability of symbols	18
Figure 3.1 Generic block diagram of transform based compression.....	26
Figure 3.2 Uniformly distributed random and medical images having different level of compactness	30
Figure 3.3 Main operation blocks of lossless image compression	32
Figure 3.4 The binary tree of the Huffman symbols	35
Figure 3.5 Generic block diagram of coding.....	36
Figure 3.6 Chain code representation as lossless compression algorithm	37
Figure 3.7 The run-length encoding based lossless compression system (encoder)	38
Figure 3.8 The traditional scanning forms of the RLE.....	39
Figure 4.1 Different level of redundancy for medical and multimedia data (Foundation, 2019)	44
Figure 4.2 The CT-liver (medical) and boat (natural) images having different level of compactness (Petitcolas, 2018)	46
Figure 4.3 Natural and medical images having different level of non-stationarity, the image (a) and image (b) (Petitcolas, 2018)	49
Figure 5.1 Proposed flowchart: Once the 3D rendering is obtained, the existing systems (red region at the bottom) use snapshots or image/video exporting to store and transfer the results (provides only limited interaction). The proposed system efficiently compresses and store the segmented data and use it to fully reconstruct the visualization at the remote locations or off-line studies (preserving full interaction capabilities).....	52

Figure 5.2	The Morton scanning with different scanning orders	54
Figure 5.3	The 2D-RLE based compression scheme	56
Figure 5.4	Linear scanning with a) (x,y) , b) (y,x) , c) $(-x,y)$ and d) $(-y,x)$ orders	57
Figure 5.5	Boustrophedonic scanning with a) (x,y) , b) (y,x) , c) $(-x,y)$ and d) $(-y,x)$ orders	57
Figure 5.6	Zig-zag scanning with a) (x,y) , b) (y,x) , c) $(-x,y)$ and d) $(-y,x)$ orders	57
Figure 5.7	Perimeter(spiral) scanning with a) (x,y) , b) (y,x) , c) $(-x,y)$ and d) $(-y,x)$ orders	57
Figure 5.8	Morton scanning with a) (x,y) , b) (y,x) , c) $(-x,y)$ and d) $(-y,x)$ orders	58
Figure 5.9	Hilbert scanning with a) (x,y) , b) (y,x) , c) $(-x,y)$ and d) $(-y,x)$ orders	58
Figure 5.10	Chevron scanning with a) (x,y) , b) (y,x) , c) $(-x,y)$ and d) $(-y,x)$ orders	58
Figure 5.11	The main blocks of the 3D-RLE method.....	60
Figure 5.12	The illustration for the 3D-RLE algorithm in the case of slice depth \mathcal{D} is 2.....	61
Figure 5.13	Example for the uniquely decipherable property	66
Figure 5.14	Chain rule derivations a) F8 b) F4	67
Figure 5.15	Main block diagram for chain code based compression	69
Figure 5.16	Two level wavelet decomposition for 2D data	72
Figure 5.17	Subband scheme for 1 and 2 level, 2D wavelet transform	73
Figure 5.18	Decomposition of 2D medical data (Sudheimer et al., 2019)	74
Figure 5.19	Decomposition of 2D natural data (Sudheimer et al., 2019).....	75
Figure 5.20	Significance map for EZW encoding.....	76
Figure 5.21	Scanning order of the subband for encoding a significance map (a) The sub-band of the parents to the sub-band of the children is indicated by the arrows. The sub-band of the lowest frequency is located at the top of the left and the maximum one is located at the lowest part of the right (b) Parent should be scanned before the children	77
Figure 6.1	Images data set: (b)-(f) T1 weighted segmented bi-level MR sequence (h)-(l) abdominal aortic aneurysms aortic (AAA) tree (CT-Angiography)	82

Figure 6.2	Test data: (a) Rendered MRI image (b) rendered segmented binary image and (c) uniformly distributed random data	83
Figure 6.3	Compression performance of the RLE for zigzag and perimeter scanning	85
Figure 6.4	Compression performance for the RLE system using different scanning forms.....	86
Figure 6.5	The compression efficiencies of proposed and state-of-the-art techniques for the CT images set (the average for all patients)	87
Figure 6.6	The compression efficiencies of proposed and state-of-the-art techniques for the MR images set (the average for all patients)	88
Figure 6.7	The bit per voxel metric for (a) CT and (b) MR data set	89
Figure 6.8	The performance of the scanning forms for (a) CT and (b) MR data set	90
Figure 6.9	Test data: computed tomography slice and uniformly distributed random data.....	92
Figure 6.10	Optimality of slice depth.....	93
Figure 6.11	Compression ratio for segmented binary abdominal organs acquired by (a) MR-T1 and (b) MR-T2 sequences	97
Figure 6.12	Compression Ratios for segmented organs acquired by CT (CT-AAA and CT-liver)	98
Figure 6.13	Segmentation boundary extraction of the independent regions of the livers (a) Segmented liver slice (b) Boundary extracted form of the segmented liver slice (c) The first part of separated slice (d) The second part of separated slice	102
Figure 6.14	Compression performance of the CrS system employed $F8$ compared to other standards	103
Figure 6.15	Compression performance of CrS system compared to other standards	106
Figure 6.16	Compression ratios for MR-T1 and MR-T2 using the CrS	107
Figure 6.17	Haar and curvelet decomposition for sparse approach (Sudheimer et al., 2019).....	109
Figure 6.18	Sparse approach in compression using haar basis with hard threshold (Sudheimer et al., 2019).....	110

Figure 6.19 Sparse approach in compression using haar basis with hard threshold (Sudheimer et al., 2019).....	110
Figure 6.20 Sparse approach in compression using haar basis with soft threshold (Sudheimer et al., 2019).....	110
Figure 6.21 Sparse approach in compression using haar basis with soft threshold (Sudheimer et al., 2019).....	111
Figure 6.22 Sparse approach in compression using curvelet basis with hard threshold (Sudheimer et al., 2019)	112
Figure 6.23 Sparse approach in compression using curvelet basis with soft threshold (Sudheimer et al., 2019)	113



LIST OF TABLES

	Page
Table 2.1 Categories of the compression strategy according to lossy and lossless approaches	12
Table 4.1 Measurement of characteristic of the natural and medical images.....	47
Table 4.2 Non-stationarity measurement of the natural and medical images.....	48
Table 5.1 Scanning orders and directions of the zigzag, boustrophedonic, linear, and Morton forms.....	54
Table 5.2 Scanning orders and directions of the perimeter, Hilbert, and Chevron	55
Table 5.3 The 3D-RLE algorithm (Pseudo code PART 1)	63
Table 5.4 The 3D-RLE algorithm (Pseudo code PART 2)	64
Table 6.1 Categories of the compression strategy according to lossy and lossless approaches	84
Table 6.2 RLE techniques applied using standard zigzag and perimeter scanning rule	86
Table 6.3 Compression ratios for all data sets.....	95
Table 6.4 Relative compression ratios for all data sets (reference is jpeg2000 which is common standard employed by telemedicine networks)	96
Table 6.5 Efficiency of compression for the CrS compression systems on MR data sets	104
Table 6.6 Efficiency of compression for the CrS compression systems on CT data sets	105
Table 6.7 PSNR metrics assessment (medical image)	108
Table 6.8 PSNR metrics assessment (natural image)	111

CHAPTER ONE

INTRODUCTION

The image compression algorithms are developed for natural images, and these methods became standards over the years for any kind of image ranging from medical to web-multimedia images. However, the medical images have intrinsically different characters from natural ones. The state-of-the-art standards, which are designed for natural data, could not reach the frontier of compression for medical images. Therefore, the modern general purpose methods cannot achieve satisfactory compression performance for medical images. Therefore, there is a substantial amount of uncovered redundancy data in existing medical images (Hsu, 2015; Bankman, 2008). Furthermore, current compression standards are not compatible with telemedicine protocols. The limitations regarding efficient medical image compression (Scholl et al., 2011) is elucidated in the following chapter.

With a grand increase of data from various sources (Gantz & Reinsel, 2012), image compression has become an efficient tool for modern communication systems such as telemedicine networks. And there are myriad studies have been carried out on the subject (Karimi et al., 2016; Ageenko & Fränti, 2000; Lee et al., 2003; Anantha Babu et al., 2016). As sub-area of image compression, medical image compression, which become an indispensable tool for an e-health network, is one of the most commercial and technically crucial application area (Taquet & Labit, 2012; Prabhu et al., 2013). However, there is not available sufficient compression standard geared to bi-level and gray level medical images. The DICOM standard rely on the ISO/IEC and ITU-T standards, e.g. JPEG and JPEG-LS (Bruylants et al., 2015; NEMA, 2017). Also, binary compression mode is not provided by the DICOM container. While the JPEG achieves considerable performance, the information that sacrificed by the method is inadmissible in the field of medicine. The lossy wavelet-based methods are also introduced scalable compression to increase performance of the telemedicine networks (Maglogiannis et al., 2009; Ramakrishnan & Sriraam, 2006). These limitations result that the performance of the current compression standards remain in limited range for medical data.

The DICOM not only utilizes size-reduction algorithms but also contain metadata, which is the textual information of the medical process and patients (NEMA, 2017; Bairagi, 2017). However, the majority of compression standards do not have the ability to convey the metadata except the standard of PNG (Graham et al., 2005). This brings another restriction for usage of the up-to-date standards in telemedicine networks.

In this context, to achieve considerable compression performance for binary and gray-level medical data, lossless compression schemes have been analyzed to improve the codification performance. To this end, the algorithm of the run-length, chain and wavelet-based compression schemes have been improved by considering the image characteristics such as entropy, morphological structure, and compactness of the objects in the image matrix. It is shown that proposed methods reveal inter-slice and coding redundancies that the up-to-date pipeline cannot overcome.

1.1 Motivation

By the digital revolution, the data has become more crucial and indispensable than ever, and a tremendous amount of data emerges in our daily life. Furthermore, with each passing day, the digital universe produces a massive amount of data, and it is hard to foresee the size of this growth. The proportion of embedded and medical data in big data will proliferate from 10% to 30% from 2015 to 2020 (Gantz & Reinsel, 2012). Technologies such as developed medical data modalities, virtual/augmented reality applications, and light field imaging, which produce volumetric data at ultra-high resolutions, are among the primary sources of data (Olshannikova et al., 2015; Karimi et al., 2016; Chang et al., 2006). These tremendous quantities of data need to be transferred, archived, and retrieved, which is a challenging task even for advanced data processing and transmission systems. This creates a strong demand for algorithms that enable more efficient transmission and storing facilities (Bairagi, 2017). Practical application and medical networks have also become an increasing profound tool with recent developments in health-care (Maglogiannis et al., 2009; Ramakrishnan & Sriraam, 2006; Taquet & Labit, 2012;

Prabhu et al., 2013). And thus, the request for the mobility of medical records requires a high-level bandwidth engaged by telemedicine network and more efficient storage of device in the archiving system. New-generation Magnetic Resonance (MR) and Computerized Tomography (CT) imaging systems are capable of scaling the image resolution. The resulting a whole human body scans with high resolution could exceed gigabytes of data load (Scholl et al., 2011). Consequently, progress in the health-care platform and distributed collaborative applications for the medical diagnostic process have brought a strong vogue of an efficient manner of medical data transmission (Anusuya et al., 2014a).

The image compression and source coding are defined as the processes of presenting raw data using fewer bits with no loss of information or loss of data in the acceptable/reasonable range by computer science and information theory. To this end, the redundancy and irrelevance of the data are revealed by compression algorithms. So that, compression renders possible efficient teleradiology networks and archiving system. Compression algorithms categorised in two main group: lossless (reversible) and lossy (irreversible) techniques. All in all, compression algorithms become a more and more vital and indispensable tool for modern medical e-health networks and data processing system (Prabhu et al., 2013).

1.2 Telemedicine Networks and Medical Image Compression

Removing the geographical barriers for medical data circulation and spreading the medical services to a great majority of the population by establishing a distributed collaborative platform of medical data is becoming a significant requirement through the progress of communication technologies (Hsu, 2015; Bairagi, 2017). Practical application and medical networks have also become a influential tool with recent developments in health-care systems.

Telemedicine is described as an electronic network which removes the physical restrictions using telecommunications technologies to provide medical information,

medical records, and services. Digital Imaging and Communications in Medicine (DICOM) is a universal protocol for retrieval, archiving, presenting, and distribution of the medical images and other records (NEMA, 2017). Well-defined standards of PACS aims to provide cost-effective archiving, fast retrieval, and access to data captured with various medical imaging modalities (Choplin et al., 1992). Teleradiology is the sub-area of the telemedicine and is described as a practice of the radiologists, who do not physically present in the physical location where the records are produced, interpreting the medical records. These interactive e-health solutions require effective communication which benefits optimal bandwidth and storage facilities. The medical images are generated by various imaging systems, e.g., xray, CT, ultrasound imaging, Positron-Emission Tomography (PET), MRI, four-dimensional CT etc. The aforementioned modalities create tremendous amount of data every single day. The size of these images may exceed gigabytes for a single volumetric CT image. Therefore, the images are the primary and challenging record of the teleradiology networks.

Advancements in the healthcare networks and collaborative distribution platforms for medical records have brought to the conclusion the techniques for compression of the medical records. At this stage, image compression algorithms, which reduce the size of the image over 80%, come into play to alleviate the burden of the systems.

Effective compression process provides an efficient communication facility by decreasing the total amount of stored data, transmission time, bandwidth and cost rate that is an essential requirement for DICOM and PACS systems. Image compression algorithms, which are designed in general propose, provide satisfactory compression performance. However, these algorithms cannot entirely expose the compressibility potential for medical data. The reason behind this limitation is that medical and natural images intrinsically differ from in structural characteristics such as entropy, non-stationarity, compactness, and energy, which primarily affect the compression efficiency. Thus, there does still exist a growing demand for a compression scheme that is particularly designed for medical data to achieve higher compression efficiency.

1.3 Scientific Novelty of the Dissertation

There is an increasing demand for the interactive sharing of medical record through a telemedicine network. This makes compression the process that is the most crucial step of the modern e-health systems. However, a compression scheme that achieves acceptable compression performance for all kind of medical data is not available. For instance, bi-level compression schemes remain in restricted performance for gray level, while the standards specialized for text and documents are also unfavorable for image data. Additionally, the algorithms utilized by common networks are general purpose algorithms that are not capable of compressing the medical images entirely. In this context, the Run-Length Encoding (RLE), contour, and wavelet transformation based three systems have been introduced for yielding compression of binary and gray-level medical images. The methods are specialized aiming to reveal particular redundancy existing in medical images. To accomplish this task, redundant data is analyzed in the sense of characteristics, which are entropy, non-stationarity, energy, and compactness, of medical images that differ from natural images. The scientific contributions of the thesis are given in the following:

- Firstly, the embedded zerotree wavelet transform and sparsity based systems are applied to the medical data set utilizing multiple wavelets (haar, curvelet, bi-orthogonal). The data set and wavelet compatibility have been examined to determine optimal wavelets for different kind of gray -level medical images.
- The second improvement is to develop an RLE based bi-level compression scheme by extended scanning procedure in such a way of achieving morphological coherence among scanning procedure and the mold of the objects in the bi-level images. The RLE algorithm is an easy-to-implement data-to-symbol coding process. However, it is used by compression standards in common scanning procedure that provides a limited performance. The proposed RLE algorithm is designed in the three-dimensional model. It harnesses the coding redundancy stemmed to the inter-slice correlation among voxels. To eliminate these limitations of the RLE, the proposed compression algorithm

provides an extended scanning procedure. By this procedure, which employs flexible scanning rules and orders such as Hilbert and perimeter, the method is able to set an optimality case for scanning model consistent with the morphological structure of the segmented shape, i.e., the organ, existing in the image matrix. This procedure provides high-level flexibility for adaptations of the RLE to the various shape of the organs. Providing a morphological coherence produce a low-entropy symbol sequence.

The RLE is employed in two-dimensional (2D-RLE) and volumetric form (3D-RLE). The 2D-RLE are managed to unveil a significant intra-slice correlation through the instrument of the extended scanning forms and appropriate entropy coder. In a volumetric manner, the 3D-RLE method proposes a new algorithm to code bi-level 3D images by also operating the correlation between the elements of volume (voxels), i.e. inter-slice correlation, together with the intra-slice correlations. The scheme is created in a parametric model to be integrable to telemedicine and e-health infrastructures. The simulation outcomes attest that the 3D-RLE is superior current modern bi-level compression standards.

- Present compression methods maps the image matrix into symbols sequence, i.e., data-to-symbol/transformation and then convert encoded-symbols (entropy coding) into the bitstream. This is the traditional strategy of commercial compression standards. However, in recent years, it has been shown that encoding only boundary of the object existing in the bi-level images by means of a reversible chain rule is sufficient for lossless compression, instead of deciphering the entire matrix data of the image. The compression efficiency of the chain code-based systems achieves up to tenfold of the conventional techniques. Moreover, this achievement primarily depends on the chain rules and can be improved by suggesting new chain rules. In other words, this strategy also includes redundancy of its own symbols. Therefore, these show a looming potential of chain code based compression for bi-level medical images. Motivated by these facts, a chain code based bi-level compression pipeline,

namely the CrS, is proposed. The method employs current and modified chain rules. The proposed method is employed improved chain rules, besides the current chain rules. The chain rules are improved by optimizing the length of the elements of the normalized angle difference (NAD) chain rule to reveal redundancy existing in chain symbols.

The experimental results show that the suggested chain code based system can unveil more redundancy compared to the-up-to-date techniques. Also, modified NAD, namely mNAD, outperforms the existing chain rules and the NAD in the case of occurring high-level of non-stationarity in the segmented objects.

Consequently, the proposed pipelines concentrate on the redundancy, existing in medical data and that cannot be removed by general-proposed compression techniques. The characteristics of the medical images, such as entropy, compactness, non-stationarity, are taken into account in order to achieve this aim. Since any information loss may impose catastrophic effects in the field of medicine, suggested compression techniques are designed in the reversible mode so that there is no loss of any information.

Throughout the thesis, the coding term is used for both *encoding* and *decoding*. The term of *bit stream* and *compressed data* are used in the same meaning. The pixel denotes picture elements of the image matrix. And the voxels refer to volumetric image element also indicating the relationship between adjacent pixel from succeeding frames/slice. The symbols refer to both pixel and voxel, i.e., the elements of image data. Unless otherwise specified, the norm applied to the image is any matrix norm.

The dissertation is organized as the following: Chapter 3 introduces the fundamental concept of the lossless compression systems for images with common algorithms and standards. In Chapter 4, redundancy existing in medical images are elucidated. The RLE, an efficient lossless compression algorithm, is modified for binary medical data in two and three-dimensional approaches. The last chapter presents the discussion of the results and additionally the future work in Chapter 7.

CHAPTER TWO

BACKGROUND

The conceptional background of data compression is clarified in this. Optimal coding determination is explained to inspect the frontier of the lossless compression. Finally, the related works for image compression are presented to figure out the limitations of the existing compression systems.

2.1 Fundamentals of Data Compression

Compression is described as the skill of reshaping raw data in compact form with the aim of representing it using fewer bits. It has been used in a wide range from web transmission to e-health networks. By means of compression, the data can be transmitted, stored and archived using less bandwidth and storage capacities. The raw data is generally divided into three portions:

- Redundancy
- Irrelevancy
- Significance

The significance, i.e. information, is the main fraction intended to be transmitted/stored by the system. The redundant is described as an statistical resemblance among the elements of data, i.e., pixel or voxel which are the elements of two- and three-dimensional images, respectively. Irrelevancy is the partition that cannot be perceived or interested in by the receiver or observer of the systems, which can be the human visual system (HVS) for image compression. The information having high-frequency in medical images and metadata existing in portable network graphics (PNG) formats are the examples of the irrelevance data for the HSV. The compression methods are categorized into two groups concerning the condition of these portions after the reconstruction: *lossless* and *lossy* techniques. While the raw

data can be perfectly reconstructed in the case of lossless mode (also known as reversible compression), in the lossy mode it is obtained in an approximated format (known as irreversible compression) in which the data considered as redundancy is eliminated. The lossless and lossy techniques utilize redundancy and irrelevancy of the data for compression, respectively, see in Figure 2.1.

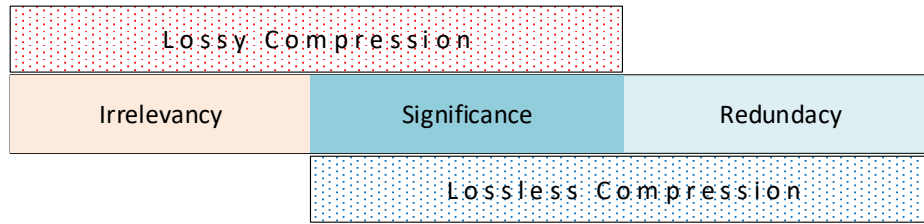


Figure 2.1 Segments of the raw data regarding the compression process

Thereby, the lossless and lossy approaches decrease the size of raw data by reshaping and eliminating the aforementioned data partitions, respectively. The compression efficiency for the lossless methods depends on only their successes of revealing the redundancy data. The difference between reconstructed and raw data, i.e. retrieval error, determine the achievement of the lossy techniques. For the reason that the redundancy has different characteristics, lossless methods are concentrate on a specific type of redundant data. This eventuates that the compression achievement of lossless methods is generally lower than the lossy one. Besides these, there exist hybrid models that combine two strategies to achieve higher compression performances.

The redundancy varies according to the data e.g. image, sound, hyperspectral and so on. Thus, compression methods have to be evolved regarding redundancy to achieve remarkable compression performance. The image, where the information is embodied within the form of bitmap raster or vector graphics structure, have their own characteristics intrinsically. This fact leads to evolving and specializing the compression algorithm by harnessing these characteristics to compress the image data more efficiently. To put it baldly, the aim of the image coding methodologies is to bring into the open pixel or voxel correlations, wherever in their domain or

transformed space, during the process. Note that, medical and natural images vary in basic structural characteristics, e.g., the natural images are generally generated by reflection of the light spectrum from object to sensors, while the imaging principle of MR is based on aligning fo the atom with the magnetic field (Toennies, 2017). The capabilities of modalities and characteristics of the medical images have also diversified over the last decades. These developments bring the diverse type of redundancy into being. Current compression standards mostly designed for natural images have become inadequate for efficiently uncover the redundancy of the medical images. As a result, developing a yielding compression technique for medical data records is still a valid demand in the digital age.

In general, data compression systems consist of two fundamental blocks: **encoder**, where the data converted to the bit-stream, which is the appropriate/desired state of data for transmission or storing/archiving, and **decoder** where the original data is reconstructed from the bitstream — in other words, the decoder operates the inverse processes of the encoder to reacquire the original or approximated form of the data. Note that perfectly reconstructed and approximated the form of lossless and lossy mode, respectively. The details of the encoder and the decoder blocks are presented in the following.

Defining a raw data in N dimensional real space, $X \in \mathbb{R}^N$, where $N \in \mathbb{Z}^+$. To compress data X , generic architecture of encoder is shown in Figure 2.2. This codification process has two successive sub-blocks as α data-to-symbol transformation and γ entropy coder.

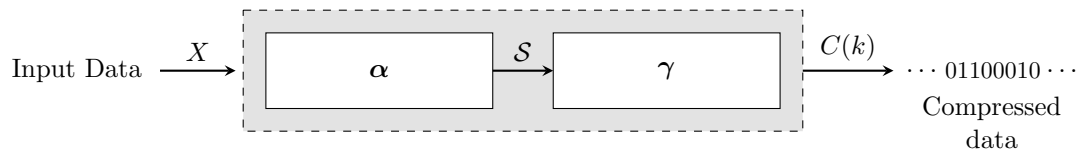


Figure 2.2 The fundamental blocks of the encoder

The data-to-symbol transforms the raw signal X into the symbol sequence S which may be more convenient to *see* the redundant part. Then, the entropy coder block γ ,

that could be variable/fix length coding, generates bit-stream sequence $(C(k) \in \{0, 1\} \mid k = 1, 2, 3, \dots K, \text{ and } K \in \mathbb{Z}^+)$, which is the compressed data and where K denotes the total quantity of bits that needed for representation of the raw data. Lossless encoding methods desire to achieve the lowest possible number of K , which represents the raw data without any loss of information.

Successfully codification of input data generates a sequence of bit stream $C(k)$ which can be stored in an achieving system or easily transferred by communication networks. The compressed data can be reconstructed/uncompressed by performing the decoding operations, whose sub-blocks are shown in Figure 2.3. The decoder has two operations, in turn, inverse entropy coder γ^{-1} where the bit-stream is transformed into symbols, and the symbol-to-data decoding β in which the reconstructed data \hat{X} is generated using the symbols \hat{S} (Goyal, 2001).

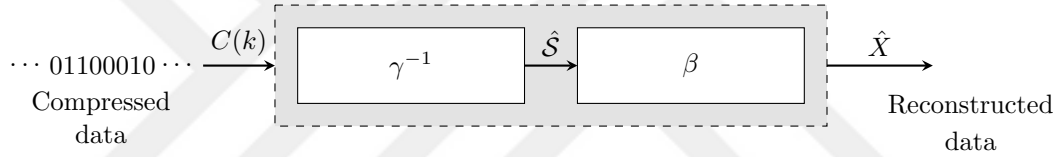


Figure 2.3 The fundamental blocks of the decoder

The process is called lossless approach if the reconstructed data \hat{X} is equal to raw data X , however if \hat{X} is an approximated form of the raw data, it called as lossy approach. The error between the raw and regenerated image is defined as $E(x, y) = [X(x, y) - \hat{X}(x, y)]$ and given a matrix norm $\|\cdot\|$, note that the error $\|E_{lossless}\| = 0$ and $\|E_{lossy}\| > 0$ for lossless and lossy approaches, respectively. The algorithms of lossy and lossless compression methods are listed in Table 2.1.

The irrelevance and redundancy are eliminated by lossy and lossless compression algorithms, respectively. It should be kept in mind that the error E may be a piece of critical information that affects diagnosis in the field of medicine. The lossless and lossy compression methodologies are generally combined by the modern compression schemes. A well-defined standard Joint Photography Expert Group 2000 (JPEG2000) employs wavelet, quantization and arithmetic entropic encoder (Skodras et al., 2001). The hybrid systems achieve considerable compression efficiency (Qin et al., 2018;

Table 2.1 Categories of the compression strategy according to lossy and lossless approaches

Compression approaches		Data-to-symbol coding	Entropy coding
Lossless	<ul style="list-style-type: none">• Reversible transformation<ul style="list-style-type: none">- Burrow wheeler transform- Discrete cosine transform- Wavelet transform• Run-length encoder• Dictionary-Based Methods<ul style="list-style-type: none">- LZ77 / LZ78- Lempel ziv Welch (LZW)• Chain-code representation	<ul style="list-style-type: none">• Arithmetic encoder• Adaptive arithmetic encoder• Huffman• Adaptive Huffman• Fix-length encoder	
Lossy	<ul style="list-style-type: none">• Scalar quantization• Irreversible transformations<ul style="list-style-type: none">- Wavelet transform- Discrete cosine transform• Block truncating coding	<ul style="list-style-type: none">• Quantization• Arithmetic encoder• Adaptive arithmetic encoder• Huffman• Adaptive Huffman• Fix-length encoder	

Lih-Jen Kau, 2003).

The main processes of the designing lossless compression methods are presented in Figure 2.4. The type of image data is identified in the first block, then the image data is characterized in the succeeding sub-block. In step of the third and fourth, appropriate transformations and algorithms are utilized to redundancy manipulation. In this dissertation, the proposed methods takes into account the image characteristics to effectively uncover the redundancy of the medical images.

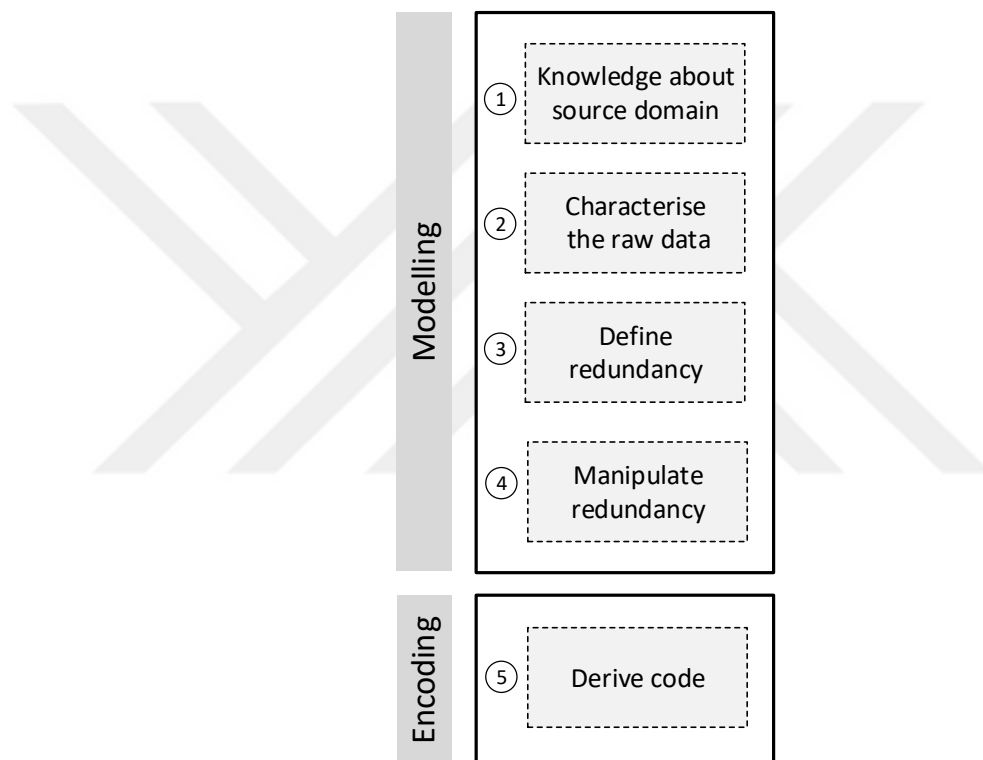


Figure 2.4 Main processes of designing a compression algorithm

The algorithms given in Table 2.1 are employed by modern compression standards. Since the compression has a huge commercial significant for modern communications networks, there are myriad compression algorithm/pipeline have been developed. Block truncation, fractal encoding, and irreversible transformation based standards such as JPEG, JPEG2000 are the common lossy techniques (Salomon, 2008). The methods of JPEG-extended range (JPEG-XR), Joint Bi-level Image Experts Group

family (the members are the JBIG and JBIG2), PNG, Tagged Image File Format (TIFF), JPEG lossless (JPEG-LS), graphical interchange format (GIF), Windows Bitmap (BMP), and ZIP are some of the most well-known lossless compression algorithms (Hoffman, 2003). The standards JBIG2 (Howard et al., 1998), JPEG2000 (Skodras et al., 2001), JPEG (Wallace, 1992) have both lossless (reversible) and lossy (irreversible) modes.

To summarize, considering lossless compression, the original record can be reconstructed identically while in the lossy mode, the compressed data is an *approximated* form of the original data. In medical signal processing, lossy compression techniques could cause loss of information during the compression, which may lead to further misdiagnoses. Therefore, lossy techniques are not generally preferred by the medical applications which any loss of information may induce catastrophic effects. These techniques are commonly preferred in web multimedia transmission and applications. Even though the performance of the lossless techniques remains under the lossy one, they are preferred in the field of medical more that.

2.1.1 Performance Assessment of Compression Scheme

Evaluation of performance for the compression techniques is categorized into two groups: fidelity metrics for lossy compression and compression efficiency for lossless one. This evaluation metrics is elucidated in the following.

Performance of the lossless compression methods is measured by the universal index: compression ratio. The metric is described in the amount of redundancy achieved by the methods.

Definition 2.1.1. (Lossless compression metric) The raw and compressed data are denoted as X and C , respectively. The *Compression Ratio* (CR) is formulated as

$$CR = \frac{\eta(X)}{\eta(C)} \quad (2.1)$$

where $\eta(\cdot)$ is the function that quantifies the size of data as number of bits (Salomon & Motta, 2010). That is, the CR is the quotient of the number of bits representing raw data and bit-stream $C(k)$ that is the form of data that will be stored or transmitted.

A lossless compression efficiency measure is relative data redundancy, R_r (Gonzalez & Woods, 2008). It is a common metric that indicates at what level the redundancy in the data had been removed. Relative data redundancy R_r defined as

$$R_r = 1 - \frac{1}{CR} \quad (2.2)$$

The R_r is an indicator showing how much redundancy that the image contains. For instance $CR = 9$ states that 9 bits of the uncompressed image is represented in 1 bit by the compressed image \hat{X} representation. This expression can be seen as 9 : 1 in literature. Considering $CR = 9$ implies that relative redundancy is $R_r = 8/9$. This means that 88.88% of the X data is redundant.

To assess the lossless compression performance, we have suggested another index, namely the relative compression ratio (CR_r). The index provides a level of compression efficiency according to achievement of a reference technique. Considering the CR_f as the compression ratio of method f , then the relative compression ratio of the technique f is defined as follows.

$$CR_r = \left(1 - \frac{CR_f}{CR_b}\right) \times 100 \quad (2.3)$$

where CR_b is the compression ratio of reference method.

The other evaluation metrics for lossless image compression are *Bit per pixel (bpp)* and *bit per voxel (bpv)*. These evaluation metrics are the measurement of the number of bits that requires representing compressed data.

Definition 2.1.2. (Lossless compression metric) Consider a image function $I : \mathbb{Z} \times \mathbb{Z} \mapsto \mathbb{Z}$. The image matrix expressed as $I(x, y) = l_i$ of dimension M and N , in which x and y denotes the coordinates in the spatial domain and $\forall l_i \in \{0, 1, 2, 3, \dots, L\}$ is the intensity level of pixels and $\{i_k\}_{k=1}^{M \times N}$. The bit per pixel is defined as

$$bpp = \frac{M \times N}{\eta(C)} \times L \quad (2.4)$$

where $\eta(C)$ denotes the quantity of bits of the compressed file. The bit per voxel (bpv) is defined in the similar manner with bpp but the only difference is that the raw data $\left[I(x, y, z) \right]_{M \times N \times K}$ is three-dimensional. Thus, the bpv formulated as $bpv = \frac{M \times N \times K}{\eta(C)} \times L$. The metric is employed to assessed the compression systems in the volumetric strategies.

The evaluation metrics of lossy techniques are also known as fidelity metrics. The common metrics are Mean Square Error (MSE), which is defines as the error signal between the raw and reconstructed data, and the Peak value of Signal Noise Ratio (PSNR), which indicates the level of distortion. Lossy compression systems aim to minimize distortion in the file after decompression while aim to receive maximum compression efficiency. The error between the raw and reconstructed images, which is denoted by the MSE metric, is defined in the following.

Definition 2.1.3. (fidelity index) Consider raw and reconstructed image I and \hat{I} , respectively. The MSE fidelity metric is expressed as

$$MSE = \frac{1}{MN} \sum_{x=1}^M \sum_{y=1}^N \left(I(x, y) - \hat{I}(x, y) \right)^2 \quad (2.5)$$

where the image matrix dimensions are given as M and N (Sayood, 2017).

The second fidelity metric is the PSNR, whose definition is provided in the following.

Definition 2.1.4. (fidelity index) Consider raw and reconstructed image I and \hat{I} , respectively. The MSE fidelity metric is defines as

$$PSNR = 20 \log_{10} \frac{\max |I(x, y)|}{MSE} \quad (2.6)$$

where $\max |I(x, y)|$ denotes the maximum number of pixel intensities of the image, e.g., $2^8 = 256$ for 8 bit intensity level images (Salomon & Motta, 2010).

The aim of the lossy techniques is to reconstruct the image with low-distortion and high level of PSNR.

2.2 Information Theory and Data Compression

The theory of the information identifies the frontiers of the data compression. To make it clear, any data could be represented in a compact form whose boundary is determined by the information measurement, i.e., the entropy of data. The entropy can be interpreted as the quantity of the uncertainty of a data sequence (Cover & Thomas, 2005). That is, the redundant data is proportional to the entropy. Therefore, the concept of information for entropy will be detailed in the aspect of data compression.

Considering the image $I(x, y) \in \mathbb{R}^{M \times N}$, intensity levels is a alphabet $\mathcal{A} = \{0, 1, \dots, L-1\}$, and $\forall I(x, y) = l_i \in \mathcal{A}$, x and y are spatial coordinates, and M and N are dimensions of image. The probability of occurrence of every $M \times N$ elements l_i are presented in set of $P = \{p_j\}_{j=1}^L$, e.g. p_j is the probability of $I(x, y) = l_j$ element.

Definition 2.2.1. The definition of entropy for the $I(x, y)$ image data is formulated as

$$H(I) = - \sum_{j=0}^{L-1} p_j \log_2 p_j \quad (2.7)$$

in which L represents the number of intensity level of the I image matrix and each I_j occurs with the probability p_j (Salomon & Motta, 2010).

The entropy function subject to corresponding probability is shown in Figure 2.5. It can be concluded from the Figure 2.5 that the maximum level of the information arises in the case of the maximum uncertainty, which indicates also maximum entropy, and that is the probability equal to 0.5. The entropy is construed as a measure of the smallest number of bits which is necessary to codify the pixel or voxels of an image data (Karam, 2009). In other words, the entropy is the *expected amount of information* that represent the data.

Images can be divided into categories such as artificial, natural, and biomedical according to the scope of their entropy level. The performances of the methods vary according to the data type as they are in different entropy classifications. Thus, the entropy is a vital parameter in designing of compression schemes. Before demystify

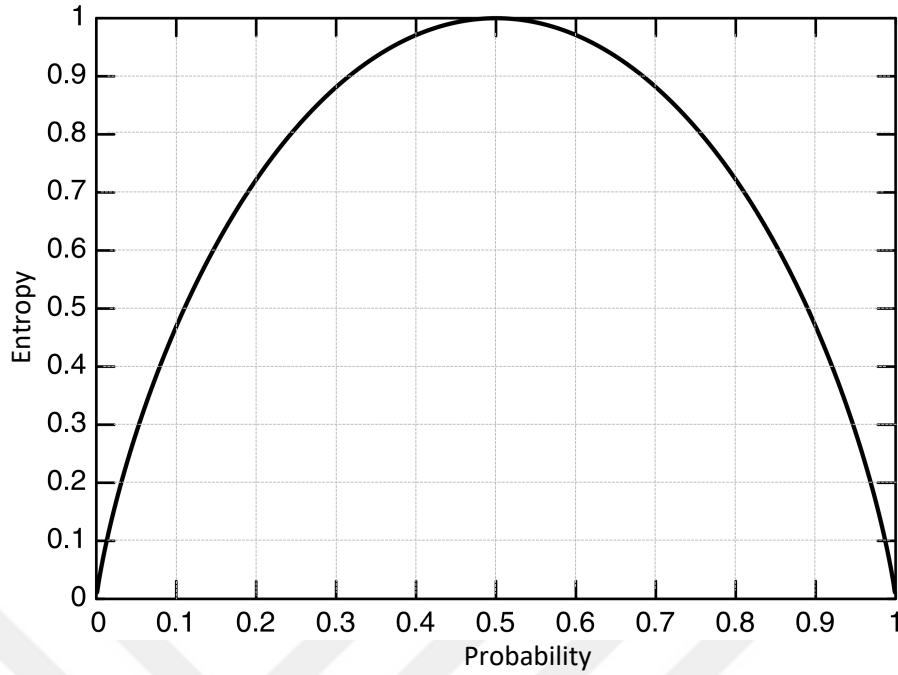


Figure 2.5 Entropy function regarding propability of symbols

optimality concepts for lossless compression, we need to define *prefix* and *Uniquely Decipherability* (UD) properties. A codeword is said to be uniquely decipherable if there exists only one possibility for decoded form. In other words, consider that the compression process is a function whose domain is the representation of raw symbols and its range is compressed codewords (Hoffman, 2003). This function satisfies the UD property if and only if it is one-to-one- mapping. Otherwise, the decoder cannot retrieval the original data, or there will be ambiguity in the decoded bit-stream. This is why the UD code is a crucial property for lossless compression. The prefix denotes the condition that no code-stream part can be the prefix of another part of code-stream. For example, the code-stream parts $c_1 = 11010$, $c_2 = 010$, $c_3 = 0110$ are the prefix codes. The case of prefix coding is a subset of the UD property (Pu, 2005). Note that the property of uniquely decipherable must be satisfied for a lossless compression system. The Huffman and arithmetic coding algorithms satisfy prefix condition.

The entropy of a raw data can be manipulated by transformation or entropy reduction algorithms to achieve minimum uncertainty case. This is the major idea behind the lossless compression schemes, and it will be demystified in further.

2.2.1 Optimal Coding for Lossless Compression

Since compression aims to procure the shortest possible code length for effective communication and archiving, determination of the boundaries for codifying has importance. Any source of data can be represented in compact form with optimal conditions. The optimality of lossless compression, i.e. minimum code length, depends on characteristics of the data such as entropy, compactness, etc.

Considering a raw image $I(x,y) = l_i, \forall l_i \in \mathcal{A}$ that is represented by elements of dictionary $\mathcal{A} = \{0, 1, \dots, L-1\}$, the probability distribution of pixels of raw image is denoted as P . Now, suppose we represent every element of \mathcal{A} with $\mathbf{C} = \{c_j\}_{j=1}^L$ and the length of these code words are $\mathcal{L} = (l_1, l_2, \dots, l_L)$. To achieve optimal code length of representing image I in compressed form, we need minimize the code length. This is an optimization problem expressed as follows,

$$\min_{l_i} l^*(P, \mathcal{L}) \quad (2.8)$$

where $l^*(P, \mathcal{L}) = \sum_{j=1}^L P_j l_j$. The main problem is to minimize equation (2.8) subject to the constraint l_i . And the question is that does exist a limit for l^* or in other words, what are the limits for an average number of code symbols that represent the image data. Consider a binary prefix code stream whose average code length is formulated as $l^* = \sum_{j=1}^L p_j l_j$, where l_i is codewords representing elements of \mathcal{A} dictionary and the frontier for l^* can be described as an inequality which is

$$H(I) \leq l^* \leq H(I) + 1 \quad (2.9)$$

This inequality simply says that the expected length of any instantaneous array code for a random variable I is equal to or greater than the entropy $H(I)$. The proof of the inequality (2.9) can be found in (Pu, 2005). It obvious from the expression (2.9) that it is not possible to express any information in lossless mode unless the bit length in the average of representing code is greater than the entropy of the raw data. These interpretations are the theoretical endorsements for the *entropy manipulation or reduction algorithm* being key point of the lossless compression schemes which is arisen in Figure 2.4. Since the limitations of the compression posed in term of

entropy, any method or transformation that reduced the entropy may yield the better compression efficiency.

In this dissertation, the techniques of entropy manipulations for bi-level medical images have been investigated. Thus, the image data has been reformed in low-entropy sequences by scanning through the pattern compatible with the organ existing in the segmented image. Furthermore, volumetric predictors have been employed to reduce the entropy of 3D-images.

2.3 Related Works and Literature Review

This section will present a wide range of literature review of image compression which categorized regarding the type of data being compressed (gray- and bi-level images) and the form of reconstructed data (lossless and lossy compression). There is a sharp distinction between gray level and bi-level image structure, i.e., a raster of pixel/voxel (Soille, 2013). The intensity level of picture elements diversities is limited in bi-level data. Therefore, there does exist an apparent relationship (high correlation) between neighboring symbols (pixels and voxels) in the binary image data compared to gray-level ones. The primary source of intra-slice and inter-slice redundancies in the images are the correlated pixels/voxels, respectively (Salomon, 2008). In consideration of the information, a compression algorithm, that takes cognizance of the construction of bi-level images, can attain more compression efficiency. Lossy compression algorithms are preferably used in multimedia and Internet applications which may compromise image quality (Xu et al., 2016; Suresh, 2015). On the contrary, lossless compression methods are used mostly in the biomedical and secure communication where the loss of data cannot be tolerated (Anusuya et al., 2014a; Shen & Rangayyan, 1997). Besides, the DICOM committee does not have strict restrictions on the type of compression (Toennies, 2017); the lossless one is significantly demanded in medical image analysis (Anusuya et al., 2014b; Cho et al., 2004; Venugopal et al., 2016; Liu et al., 2017; Aldemir et al., 2018a).

There are various modern lossy image compression standards that provide satisfactory compression ratio in gray levels medical images such as JPEG, and JPEG2000, wavelet coding standards (Goyal, 2001; Usevitch, 2001). Owing to the property of frequency-domain localization, the importance of the wavelet transform has increased dramatically (Shapiro, 1993; Graps, 1995; Sydney et al., 1998). In modern compression systems, transform based algorithms using linear transformations have been progressively come into prominence (Sayood, 2017; Tu & Tran, 2002). Discrete cosine, discrete Walsh-Hadamard, and wavelet are some of the commonly used transformations in modern compression (Rao & Yip, 1990; Ramabadran & Chen, 1992). The 3D wavelet-based system is applied to medical data in lossy-to-lossless approach (Bruylants et al., 2015). Three-dimensional integer wavelet-based algorithm has also enabled loss-to-lossless compression for medical images (Xiong et al., 2003). However, the integer wavelet-based compression schemes have disadvantages on computational complexity. The transform based system (discrete, wavelets) are generically designed in lossy mode and have considerable computational load (Prabhu et al., 2013; Maglogiannis et al., 2009).

The PNG, JPEG-LS, GIF, TIFF are common used gray-level lossless compression standards. The lossless compression systems must satisfy the UD to perfectly reconstruct the data (Sayood, 2003; Miaou et al., 2009). It has to keep in mind that since any information loss in medical data may cause a catastrophic effect in the sense of diagnosis, the segmented medical images must be compressed by the lossless compression methods. Therefore, the lossless compression techniques are generally given preference in the field of medical data analysis (Anusuya et al., 2014a). Besides the aforementioned lossless systems are employed for medical image compression, they are designed in general-purpose. Therefore, the entire redundancy cannot be eliminated by these methods.

E-health systems have to overcome the logistic problem process/transmission Tera-to Petabyte of biomedical records (Gantz & Reinsel, 2012). Image compression will be the major point in developing e-health applications, which also attain acceptance from the medical practiser (Scholl et al., 2011). In the literature, various

lossy and lossless binary compression systems have been experienced on the natural and medical images (Karimi et al., 2016; Brahimi et al., 2017a; Venugopal et al., 2016). However, the DICOM which is one of the most common medical compression standard does not include a bi-level compression procedure (NEMA, 2017).

The RLE which is seeking for recurrent of the pixels along the way of the scanning form is a simple and accomplished compression strategy to obtain coding redundancy. The methodology has been experienced on a spread range of data from DNA to medical images (Hara & Kawano, 2015; Liaghati & Pan, 2016). There are run-length coding and JPEG based hybrid compression techniques (Yang & Wang, 2009). There are practical volumetric medical data compression standards based on different techniques (Schelkens et al., 2003; Xu et al., 2004). These codification procedures cannot totally eliminate redundant parts in the binary images due to that the bi-level images are naturally divergent from the gray level image. Therefore, there is not exit a universal compression standard for medical image compression (Liu et al., 2017). To overcome this limitation of the RLE based systems, an algorithm forming according to objects occurring in the binary images structure might achieve a better compression performance. The conformability of the scanning form and shape of the objects existing in the bi-level image plays a significant part in specifying the number of recurrence of the intensity levels of adjacent pixels. The linear and zig-zag (cantor diagonal) are the common scanning forms used in the RLE based compression algorithms (Strasser et al., 2015). In this context, addition to the standard scanning forms (scanning pattern); perimeter (spiral), boustrophedonic, Morton (quadrant scanning), Chevron, and Hilbert (Pi) using different orders have been applied to the binary medical data. Numerical simulations have shown that the scan form which is compatible with the shape of the image morphologically has provided better compression performance (Aldemir et al., 2019). Therefore, scan forms determination a proper scan form relevant to organ shape is the key point of the compression performance.

The universal bi-level schemes, e.g., Joint Bi-level Image Experts Group (JBIG) family (Howard et al., 1998; Regentova et al., 2005), the CALIC, and Octree (Wu &

Memon, 1996; Moursi & El-Sakka, 2007), Adaptive Bi-Level Image Compression (ABIC) (Mitchell & Rijavec, 2004), CCITT algorithms (Lu & Tan, 2003) are the common state-of-the-art techniques (Sayood, 2003; Memon & Sayood, 1995). The JBIG is one of the most successful binary data compression standards used for natural and medical data (Memon & Sayood, 1995). In the recent study of (Guo et al., 2017), the symbol-dictionary framework based JBIG2 lossless standard is employed to encode binary images. The method is integrated in segmentation based system for document compression (Regentova et al., 2005). Furthermore, JBIG2, an improved member of JBIG family is able to compress binary images in a progressive manner and achieves satisfactory compression ratios (CR) (Howard et al., 1998; Fowler et al., 1995). A method designed for binary images harnesses the variable-size context and forward-adaptive statistical approaches (Ageenko & Fränti, 2000). In the study of (Lee et al., 2003) and (Qin et al., 2018) are two compression scheme designed based run-length algorithm which is the fast and easy-to-implement lossless algorithm. The RLE-based bi-level compression pipeline experienced on medical data and it outperforms well-known binary reversible compression methods such as JBIG and last version of the standardization called the CCITT (Aldemir et al., 2019).

In recent years, chain code representation, which is well-known a pattern recognition and shape descriptor procedures, is evolved to encode the bi-level image data (Rodríguez-Dagnino, 2005; Zahir et al., 2007; Schiopu & Tabus, 2013). The chain coding is a shape representation technique that expresses the objects using their boundary information. The main motivation of the chain code based compression systems is to generate shorter code with low-entropy using less computational complexity. The chain code rules are reversible and thus satisfied the uniquely decipherable (UD) property. The chain code procedures preserve whole information providing to allow considerable data reduction. The chain code based systems are effectively employed as lossless compression in 2D and 3D approaches (Žalik et al., 2015; Aguilar & Bribiesca, 2015). These systems become a powerful rival to modern techniques during recent years (Huerta-Hernández & Sánchez-Cruz, 2014; Verdoja & Grangetto, 2017). The chain code is employed as data-to-symbol transformation by

the systems that combined chain coder with entropy coder such as Huffman or arithmetic coders (Liu et al., 2007; Liu & Žalik, 2005; Sánchez-Cruz et al., 2007). There are more variations of the chain rules such as unsigned Manhattan (Žalik et al., 2016), slope chain code (Bribiesca, 2016) and the chain code for volumetric data representation (Chen & Lee, 1991). The main motivation of the chain code derivations is to generate shorter code with low-entropy using less computational complexity.

It has been figured out that chain rule based compression systems superior to the modern bi-level standards, including JBIG (Rodríguez-Dagnino, 2005) and JBIG2 (Zahir et al., 2007; Sánchez-Cruz & Rodríguez-Díaz, 2009), two well-established robust bi-level compression standards. Motivated by these studies, various chain code based compression schemes have been proposed (Bribiesca, 2008; Žalik & Lukač, 2014; Bribiesca & Bribiesca-Contreras, 2014). And the methods of RLE and the chain-code are employed in hybrid compression scheme (Bailey, 2010; Liu et al., 2012). However, chain-code based systems are generally developed for compression of text and trivial shape natural/artificial shapes in computer graphics. Consequently, the chain code based systems hold great potential for compressing binary medical data. In this thesis, we propose a chain-code based system, namely the CrS, to reversible compress medical data.

In this dissertation, we take up the lossless bi-level compression methods aim to increase the compression performance for the medical images. After introducing common lossless techniques in details, the proposed bi-level lossless compression algorithms geared to medical images, which are the 3D-RLE (developed by a new context-based algorithm) and chain-code (CrS), are elucidated. The performances have been assessed on a wide range of data set consisted of different modalities (MRI and CT) and on the various morphological structure (liver, spleen, and abdominal aorta). Thus the compression performance of the current and proposed methods have been comprehensively assessed.

CHAPTER THREE

IMAGE COMPRESSION

In the last decades, the demand for the mobility of the multimedia products and of the medical records has increased dramatically; concordantly, the requirement of the bandwidth for networks and of storage capacity has also escalated. And the data compression has become a crucial point for efficient communication and its applications such as telemedicine and special networks. The coding of data is the process of reducing the amount of data (one-dimensional (1D) signals, 2D and 3D images, videos, etc.) to describe the information content with fewer bits. The (still) image compression is an outstanding branch of data compression. To exemplify the importance of image compression: a 360-degree image frame stream resolution of 16K needs 3Gb for one-minute video records, and compression technique can reduce bandwidth requirement from 6×10^3 Kbps to 4×10^6 Kbps (Bassbouss et al., 2018). As a sub-area of still image compression, the medical images have great importance. A volumetric CT image of the heart needs over 1 Gigabyte storage of data. This makes image compression vital for modern communications and e-health networks.

In this chapter, lossy and lossless image compression algorithms and standards are described. The limitations and disadvantages of the existing systems are analyzed regarding the characterization of redundant data to develop new approaches for medical images.

3.1 Transform Based Image Compression

Transform based compression stands for applying an additional operation, linear transformation, in both encoder and decoder. To explain, the encoder operation consists of two fundamental sub-blocks *quantizer* and *binary encoder* and in addition to the generic block, a new process, called *transformation* is applied before the quantization. The generic block diagram of transform based compression techniques (Creusere, 1997; Shusterman & Feder, 1994) for N dimensional data is given in

Figure 3.1.

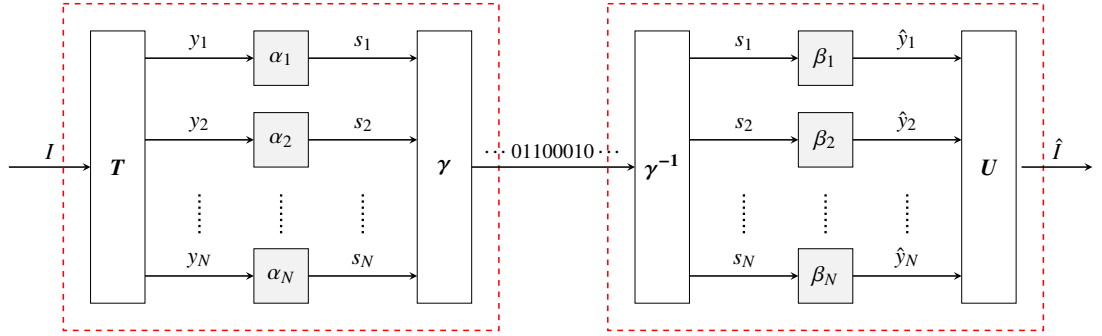


Figure 3.1 Generic block diagram of transform based compression

Transform block refers to the conversion of data to the transformation coefficients that represent the data in the sense of some unique features in transformed space, e.g., in Fourier space as frequency harmonics or in wavelet space as details (high frequencies in the data) and approximation coefficients (low-frequency components in the data). As the generic compression diagram indicates, the transform block is optional, not all the compression methods use it, however, it is commonly used in the majority of techniques due to the transformation such as the transform of discrete cosine and wavelet, provides a more effective quantization process and binary encoding. In this system, wavelet is used as a transformation block, owing to the advantages explained in Chapter 2.

Main diagrams of the transform-based compression scheme is depicted in Figure 3.1 will be expounded (Goyal, 2001). The first step of transform based compression is to apply an reversible/irreversible transformation. Let define $\mathcal{T} : \mathbb{R}^{N \times M} \mapsto \mathbb{C}^k$, $\mathbf{y} = \mathcal{T}\mathbf{I}$ mapping whose coefficients are $\mathbf{y} = \{y_i\}_{i=1}^k$. The transformation generates coefficients \mathbf{y} , which signify the features belonging to N-dimensional I data in transformed space, e.g., wavelet space. The second operation is the scalar quantization α_n in which the coefficients of data are digitized in terms of gray level magnitudes (symbols), see details for DCT coefficients of the JPEG architecture in (Ansari et al., 2009). In other words, the coefficients are mapped into symbols, which are the representing a finite set of the value. The loss of data appears in the quantization block as can be figured out. The final step of the codification is entropy encoding γ which allocates the quantified levels of coefficients to the sequence of bits, i.e. compressed data.

It is evident that if the transformation is chosen as reversible one such as Burrow-Wheeler and Golomb, the loss of information is only stemmed from quantization. And recall that the entropy encoders, e.g., Huffman and arithmetic, are lossless algorithms.

Decoder is the block that processes code stream to reconstruct the *original data*. First of all, the encoded data (bit stream) are inverted to a discrete set of symbols s_n in γ^{-1} entropy coder block. It is obvious that s_n is recaptured by lossless mapping. The second step of the decoder is the scalar quantizer block β_n that converts the s_n values to \hat{y}_n transform coefficients. The final step of the decoder is U transformation which is the inverse of T transform, $U = T^{-1}$. The output of U block is \hat{I} that is the approximation form of the original data I . The error between the raw and reconstructed images is defined as $E = \|I - \hat{I}\|$. The transform-based compression systems aim to minimize code length of compressed data with the minimum possible amount of errors E .

As indicated in the codification structure, \hat{I} is an approximation form of the raw data I , as a result of information loss which appears in both the encoder and the decoder quantizer. Additionally, there is further loss of information caused by the transform block. The loss of information appearing in the transformation block stems from truncating the insignificant coefficients. Floating point number is registered in the integer allocated memory blocks. In wavelet and fractal transforms the operations such as conversion float to integer and thresholding are applied to the coefficients.

In this thesis, wavelet-based and sparse representation transformations are proposed for the gray-scale medical image compression. Once the wavelet transform based technique will be explained in details, their strengths and weaknesses have been laid emphasis on. Then, the wavelet transform based compression technique, namely Embedded Zero-tree Wavelet (EZW), will be introduced. The EZW technique is an effective and simply-applicable compression method for gray-level images. Having associated the transform based compression algorithm to wavelet transform, it has been explained which the wavelets are appropriate for medical image. The EZW algorithm is explained in detail through the advantages and drawbacks. The second

transform based strategy is a sparse representation based compression scheme. The main idea behind the sparsity is that the medical images have irrelevance details that are considered as sparse data.

The EZW algorithm is commonly used in compression. The algorithm is regarded as the fundamental of modern compression algorithms (Usevitch, 2001; Babu & Alamelu, 2009). The method is applied to 2D natural (Brahimi et al., 2017b; Kadhim et al., 2019) and medical images (Babu & Alamelu, 2009; Rani et al., 2018). Since the success of the compression depends on the wavelets, the performance of the algorithm corresponding to the selected wavelet basis has been assessed. In this thesis, various wavelets such as orthogonal, bi-orthogonal, and symmetric bases leading to the determination of optimal wavelet bases have been experienced.

Throughout the past decades, sparsity-based algorithms are employed in various field of applications, including solving the inverse problem, image denoising, and image compression, data denoising, and compressed sensing, and so on (Candès & Wakin, 2008; Aldemir & Tohumoglu, 2016; Donoho, 1993). Sparse representation approach has also been applied to the field of data compression (Fang et al., 2015; Liu et al., 2015; Zhou et al., 2016). By this approach, sparsity is considered as truncating wavelet coefficients using compressing sensing theory to reduce the bits representing data (Chen et al., 2016). Implementations have been applied using symmetric and orthogonal bases.

Study of optimal bases determination corresponding the structure of image component, modification of the EZW, and sparsity techniques are still under development. The EZW based compression system can be designed in both lossy and lossless modes by providing scalable properties. Also, entropy encoders will be integrated into these algorithms to accomplish a complete compression system. Therefore, bases determination and comparison of the EZW and sparsity techniques constitute one of the focus of future works.

3.2 Lossless Image Compression

Lossless compression methods are intended to express an image data with the possible smallest quantity of data without sacrificing any information. The main idea of lossless compression algorithms is that image data contains a large of *redundancy* which intrinsically occurs and is not related to the image. Motivated by this fact, any part of the data is compressed without being lost by removing the redundancy part of the data. Three kinds of redundancy can be found in the digital image data (Gonzalez & Woods, 2008). Types of redundancy may occur in an image are defined as follows:

1. **Coding redundancy:** Code word is a system of symbol that represents a data. The code word can be bits, number or letter e.i. ASCII code of B is 0102 (octal), 66 (decimal). Since the code word is not unique, code word longer than the minimum code length that the data can represent cause redundancies. For example, image intensity values encoded using 8-bit integer data units can be expressed with more bits than needed. Fixed-length coding is another example of coding redundancy. The difference average number of code between variable and fixed length coding is the amount of this redundancy.
2. **Spatial and Temporal redundancy:** Since neighboring pixel values have a high spatial correlation in an image data, the image can be expressed with information more than needed. This type of redundancy is also designated *inter-pixel/inter-voxel* correlation. The Figure 3.2 depicted high intra-frame correlation 3.2b between the pixels compared to uniformly distributed random images in 3.2a. Similarly, inter-slice of volumetric data have high correlation between voxels.
3. **Irrelevant information:** This kind of redundancy is the data that can not be perceived by the mankind visual system. Therefore, the algorithms that are designed for human beings can increase compression performance by ignoring such information. The redundancy stemmed from this source is also named as *psycho-visual* in the literature.

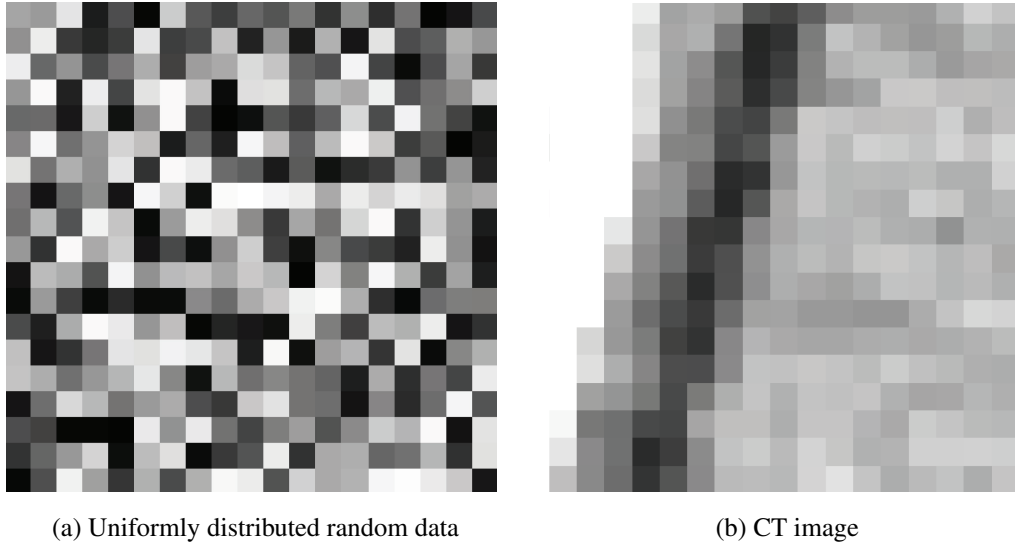


Figure 3.2 Uniformly distributed random and medical images having different level of compactness

The main redundancy type that has been enable lossless compression is *coding* and *spatial/temporal* redundancy. Fix length codes that are used for representing the image intensities could contain more bits that are needed to express the data. The data elements of data (pixel or voxels) are proportional to the spatial/temporal redundant data, i.e. the cross-correlation. Considering 16-bit 2D-MRI images set, there is a high degree of spatial correlation between pixels. In 3D-MRI, additional to the spatial relationship between slices, there is also inter-slice correlation across voxels. Irrelevance information constitutes unnecessary data that exploited by lossy techniques.

The slice and frame are defined as consecutive image matrix for video and three-dimensional data, respectively. Therefore, the successive matrix pf volumetric images will be represented as *slice*, throughout the dissertation.

3.3 Lossless Compression Systems

The lossless compression systems is composed in two main parts: **encoder** and **decoder** blocks. The sub-blocks are shown in Figure 3.3. Input image data is converted to a bit stream which is ready for archiving or transmission by the decoder. There does

not occur any information loss while the encoder process. In the decoder blocks, the identically inverse operations of the encoder process are performed, which means that the raw image is perfectly reconstructed.

Define a raw image $I \in \mathbb{R}^{(N \times M)}$ in real space, as uncompressed and \hat{I} reconstructed image, then error is $|E(I - \hat{I})| = 0$ for lossless compression. The encoder has three sub-blocks: *transformation* block where the input data are mapped in appropriate space or domain in which the redundancy can be easily made out (transformation coefficients). Any reversible transformation can be exploited such as burrow wheeler or Walsh-Hadamard. *Data-to-symbol coding* generates symbol sequence which has lower entropy compared to the transformed data. Finally, entropy encoder produces compressed data by assigning the shortest dictionary elements to the symbol occurred in the highest probability.

In the decoder process, the bit stream (compressed data) is exposed to the operations identically inverse of the encoder ones. First, the bit stream is used to regenerate the symbols by *entropic decoder*. The resulting symbols are converted to transformation coefficients *symbols to data* blocks. Then, \hat{I} data is inversely transformed by the identical transformation that applied in the encoder. Finally, the data I is perfectly reconstructed at the output of the decoder block. The resulting code-stream is the form of the raw data which can be effectively transmitted or stored.

The first two operations, identity transformation and data-to-symbol Mapping can be evaluated as a pre-process to make the image data more compatible and efficient with the lossless coding algorithms since the entropic encoders are independently generates a bitstream (Karam, 2009). However, in modern compression systems transformations and data-to-symbols coder are indispensable operations. Because of that the decoder operations are identically inverse operations of those of the encoder, only encoder blocks are explained. Definitions of the encoder blocks are given as follow:

1. **Transformation:** A reversible and one-to-one mapping is applied as identical transformation block. This operation aims to convert the I data to a more

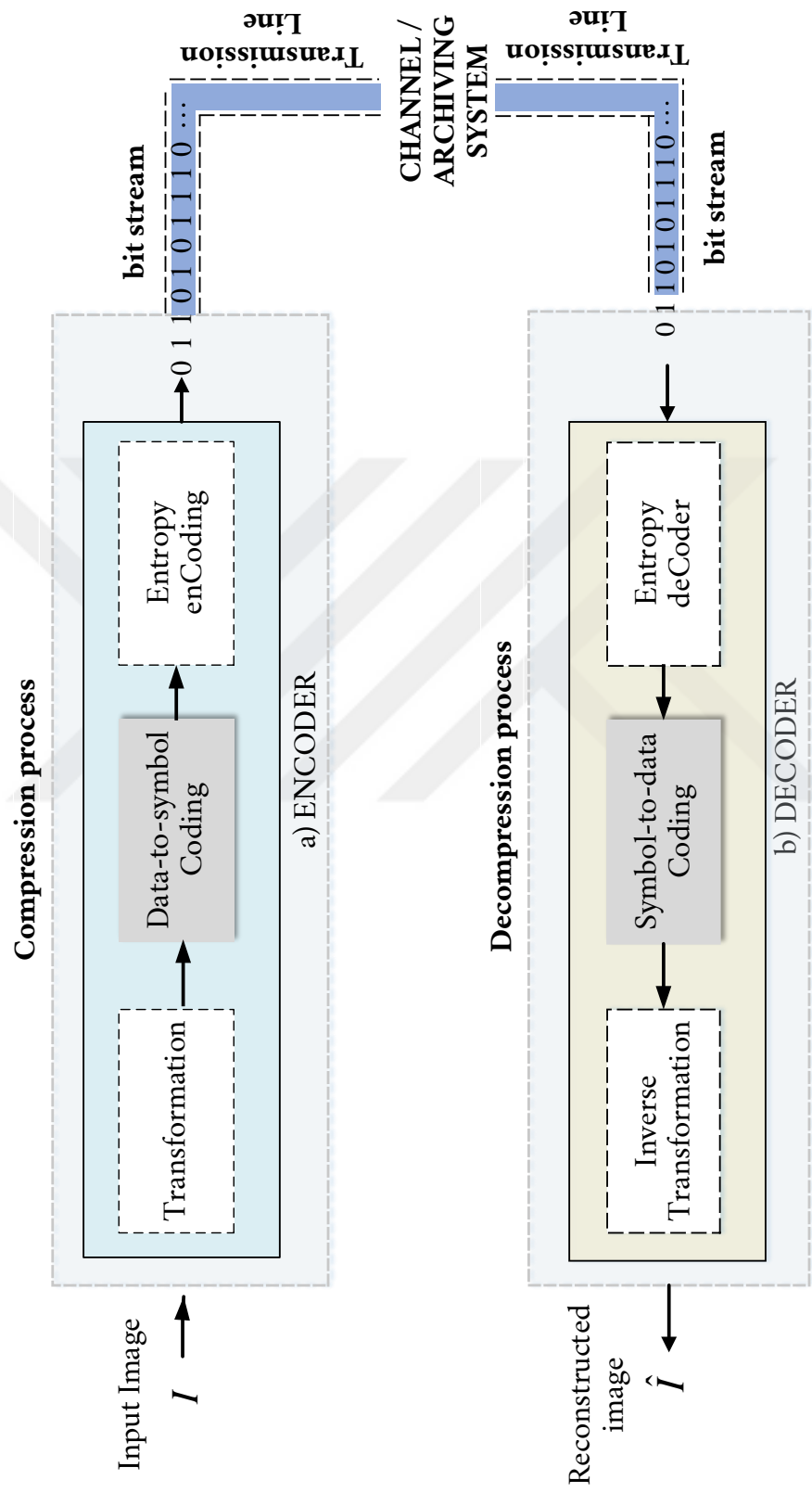


Figure 3.3 Main operation blocks of lossless image compression

amenable form to unveil redundant data existing in \hat{I} . Word of 'amenable' refers that the data is represented as a set of coefficients in a new space where achieving better compression ratio and low entropy. To achieve this purpose, the block may increase the correlation between coefficients and therefore, obtains a new statistical distribution. Differential/predictive mapping, Discrete Cosine Transform (DCT) (Rao & Yip, 1990) and Red-Green-Blue (RGB) space to luminance and chrominance (YCbCr) colour representation are some transforms that commonly used in lossless compression scheme. As result of that, it is impossible to separate the transformation from the application selection of techniques depends on the application field.

Most of the state of art compression system use predictive mapping to decrease the entropy of the image. For instance the JPEG and robust technique PNG are utilized different linear predictive models. Throughout dissertation, two-dimensional predictive coding modes is used as transformation to improve coding efficiency for medical data. The predictive coding uses the inter-pixel correlation between the image data element. Additionally, 3D predictive coding is improved by using intra-frame correlation across the volumetric medical image slices.

2. **Data to Symbol Mapping:** The resulting data of transformation sub-block (coefficient in spatial or frequency domain) is converted to the symbols. This may be done through the RLE and/or partitioning, chain code representation. In this stage, the image data is divided into neighboring pixel values or reshaped through to minimize entropy and complexity of data. The grouping of the data units that provide the use of the possible correlation between the image data provides a higher compression ratio while may cause to increase coding complexity. The coding/decoding complexity does not pose any problem if the implementation of the compression is applied to databases in off-line. On the other hand, the computational load and complexity must be considered during on-line applications.

One of the most well-known techniques used in data to symbol mapping is the

RLE, which is an easy-to-implement and effective algorithm. The improvements will be made on the RLE (by a context-based algorithm) to improve compression performance for binary biomedical images throughout this thesis.

3. **Lossless Symbol Coding:** In this phase, the bit stream is generated from the symbols by applying a variable or fixed length coding algorithm. Variable-Length Code (VLC) algorithms estimate the probability of every symbol then assigns a codeword to each symbol considering their probabilities. In Fixed-Length Code (FLC) approach, each symbol is assigned with a codeword of the same length. Of these methods, VLC handles code redundancy, while the other method, FLC, ignores the coding redundancy, which leads to worse compression performance (Karam, 2009). Therefore, the VLC approach is mostly used by the modern compression systems such as Joint JPEG, JPEG-Lossless (JPEG-LS), Joint Bi-level Image Expert Group (JBIG) in state of art symbol coding. In the case of the VLC, the symbol that occurs high number frequency is assigned to the shorter codeword (Hoffman, 2003). The well-known VLC algorithms are (adaptive) Huffman and (adaptive) arithmetics coders.

3.4 Lossless Compression Algorithms

Lossless image compression is a branch of the image coding that attracts attention due that no loss of knowledge. The aim of the lossless technics is to represent an image data with the possibly minimum number of bits providing no loss of information, it is the key point. In lossless image compression, the original and reconstructed image must be identical in the terms of quantitative and qualitative metrics. Huffman coding, that dictionary-based coding, is a commonly used by the lossless standards (Yang & Wang, 2009; Liu et al., 2012). The arithmetic coding, Huffman, Lempel-Ziv Coding, run-length encoding are the lossless compression algorithms that have been lucidly expounded in this section. They are made use of by common lossless compression standards such as JPEG, PNG, JBIG family (Karam, 2009; Hoffman, 2003).

3.4.1 Huffman Coding

Huffman algorithm is a common entropy coder used in the lossless compression systems, previously shown in Figure 3.3, in entropy encoder sub-block. It is an algorithm that generates a variable length codeword according to the probability values of the symbols.

The method starts with listing the probabilities of symbols in decreasing order to construct Huffman tree. It creates a set of resource reductions by sorting the probabilities of the considered symbols. Then algorithm combines the lowest probability symbols with a single symbol that changes in the next resource reduction. Then, it accumulates the probabilities of symbols from leaf to root by starting with the smallest probability in each level of the tree. The process is repeated until the main root, which means that the tree has been completed, last reduced source remain with two symbols. Finally, the left and right side of the tree are assigned 0,1 codes, respectively. The strength of the method is that it assigns the most repetitive symbols (the sample has the highest probability) to the shortest code word, which reduces compression significantly. The coding process is illustrated in Figure 3.5.

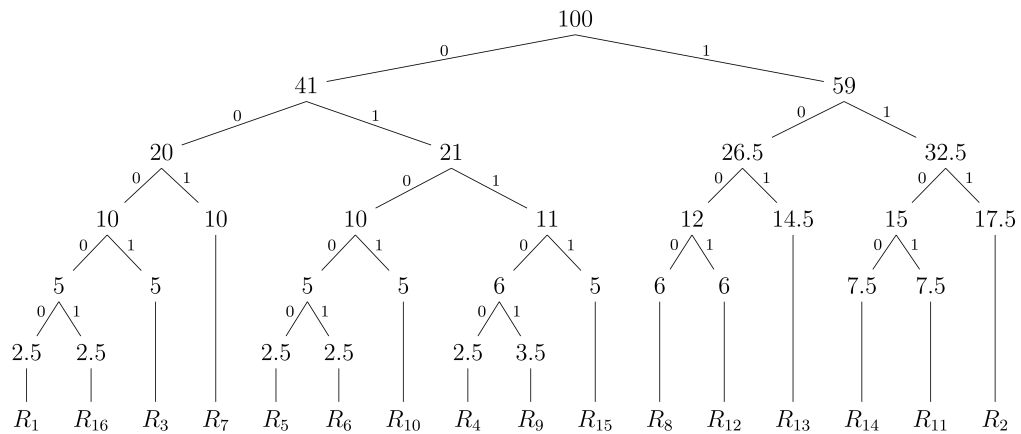


Figure 3.4 The binary tree of the Huffman symbols

Let define the symbol data pairs as

$$R_k = \{r_1, v_1, r_2, v_2, \dots, r_{(k-1)/2}, v_{(k-1)/2}, r_{k/2}, v_{k/2}\}$$

and probability of R_k samples are given as

$$P_{R_k} = \{p_1(2.5), p_2(17.5), p_3(5) \dots, p_k(2.5)\}$$

Huffman tree for R_k symbol sequence is given in Figure 3.4.

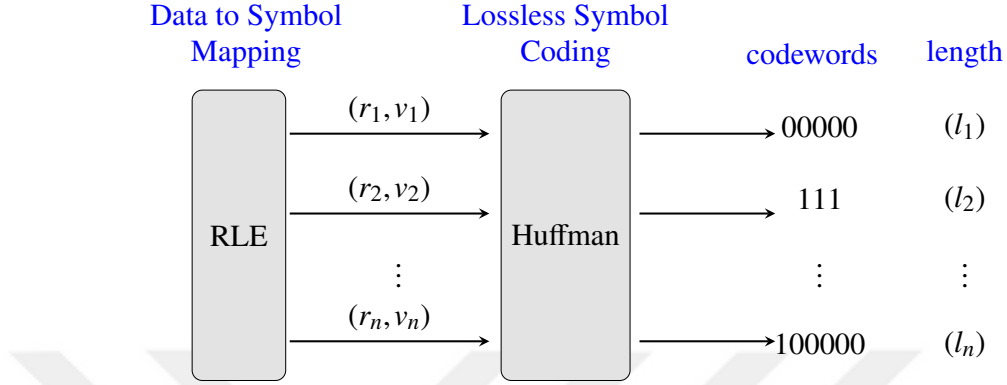


Figure 3.5 Generic block diagram of coding

The occurrence probability of the run-length symbols for medical bi-level images have been analyzed. These intensity level probabilities bring to exist the condition of the negative power of 2. This case is the optimal for the Huffman algorithm to provide the highest compression efficiency. Thus the Huffman coding has been utilized by the run-length based proposed systems as the VLC. The implementation details illustrated in Figure 3.5.

3.4.2 Arithmetic Coding

Arithmetic coder is a lossless compression algorithm that employed as entropy coder by compression pipelines. The arithmetic coder deciphers the symbols regarding to the probability distribution of the intensity of the image elements (Rissanen & Langdon, 1979), e.g., bi-level images local structure that have pixel same pixel intensity: 1/0. It codifies an input symbol stream with a single portion as the compressed data, instead of displacing every single input symbol with a codeword (Pu, 2005).

The arithmetic coder outperforms the Huffman coder in the case of the alphabet of limited range. However, the alphabet range of scanned bi-level does not remain in

a limited range. And thus, for RLE-based proposed systems Huffman is preferred as entropy encoder.

3.4.3 Contour Encoding

Chain coding is a shape representation technique that expresses the objects using their boundary information. It is also employed as the well-defined lossless compression technique for binary data, see Figure 3.6.

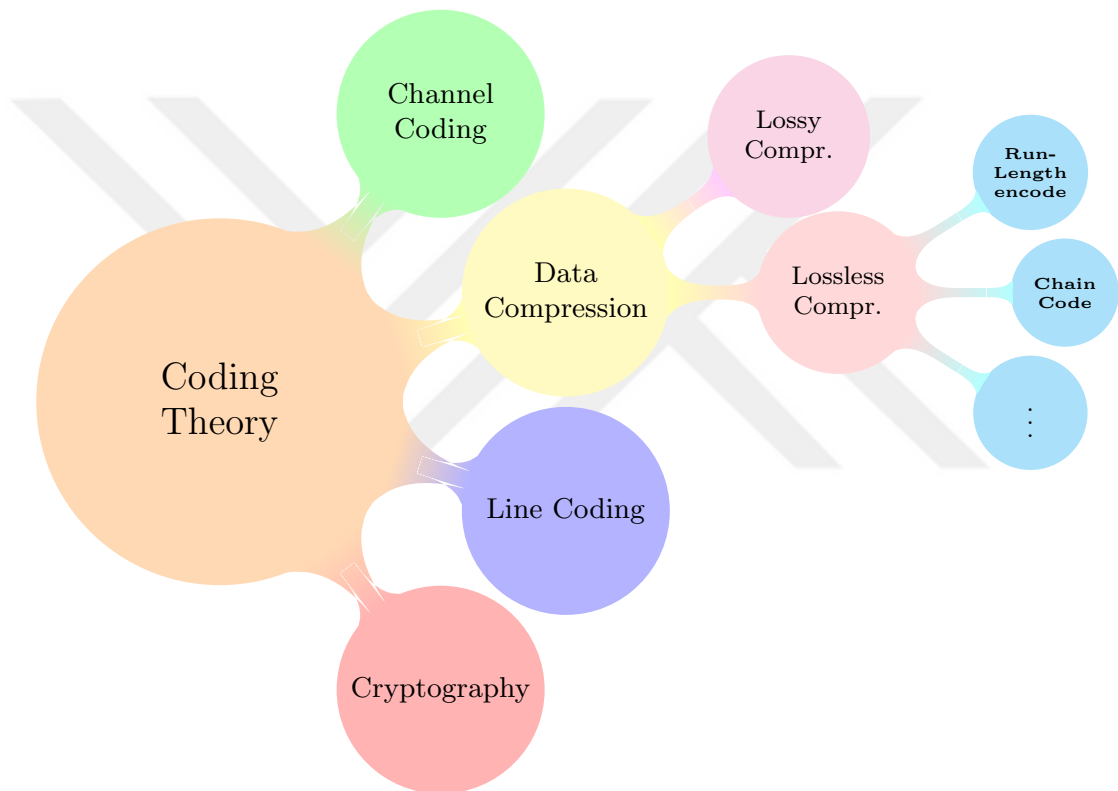


Figure 3.6 Chain code representation as lossless compression algorithm

The fundamental idea of the method is to transform the boundary pixel or voxel information to a reversible and decipherable code. In other words, the contours of the segmented regions of the bi-level images are coded by chain rules. The chain code based systems hold a great potential for compressing binary medical data. In this dissertation, a chain code based compression scheme has been proposed for bi-level segmented medical images.

3.4.4 Lempel–Ziv–Welch

Lempel-Ziv-Welch is dictionary based and commercially common used compression algorithm. It has three most popular distributions that are LZ77, LZ78 and LZW (Ziv & Lempel, 1977, 1978). Firstly, the longest pattern for each segment of the source is described by the LZW algorithm. Then it encodes them by the indices in the dictionary. In the case of no matching in the dictionary, the segment will become a new element. And next time, this segment will match the element of the dictionary. By this basic update principle, the dictionary elements are optimized during the process (Pu, 2005).

3.4.5 Run-length Encoding

Run Length Coding is an algorithm that used in mapping of data-to-symbol by lossless compression standards. The idea of compressing the image data using RLE algorithm is based on the observation that choosing a random pixel in the image will probably have the same colour as its neighbours (Salomon & Motta, 2010). In other words, there does exist high correlation between the consecutive pixels/voxels. The performance of the methods highly depends on the correlation between the neighbouring pixels. The methods present the image in form of symbols that indicates the *run* and *value* which are the number of succeeding image elements and the intensity value, respectively, see in Figure 3.7.

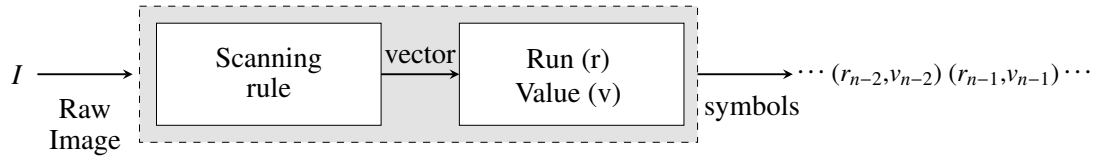


Figure 3.7 The run-length encoding based lossless compression system (encoder)

The image matrix reshaped in 1D sequence by matrix-to-vector scanning procedures. The common scanning rules, linear, zigzag and boustrophedonic, are illustrated in Figure 3.8. The input data $I \in \mathbb{R}^{M \times N}$ is image matrix. The RLE produces a *(run, value)* pair called symbol from the I data sequence. The value is the intensity

of the data sequence. The *run* states for the number of times of continuously repetitions of the value. As a result, the pixels represented as vector sequence. The resulting vector is matched to a set of symbol pairs $\{(r_1, v_1) (r_2, v_2), \dots, (r_n, v_n)\}$. Since

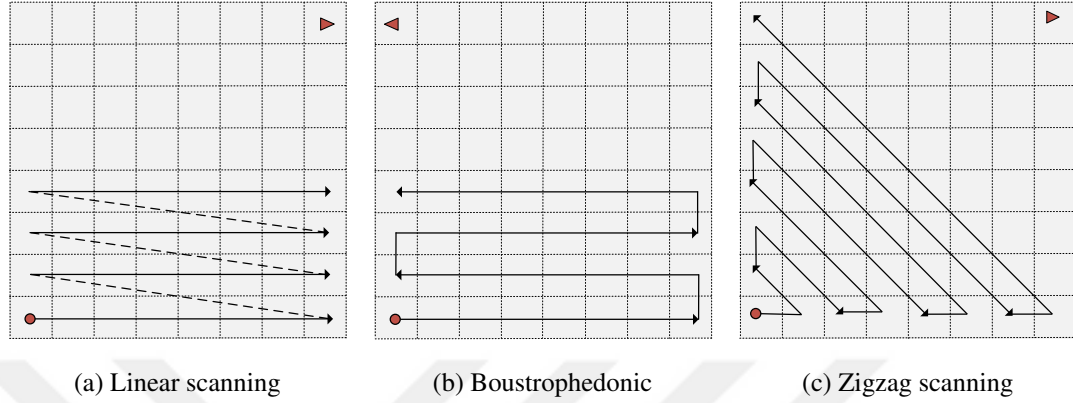


Figure 3.8 The traditional scanning forms of the RLE

the scanning rules are reorder the matrix as sequence, it is primarily affects the (r, v) pairs. In other words, the entropy of the symbol sequence is determined by the scanning rule. The scanning rules must be reversible that the vector-to-matrix must be applied to one-dimensional sequence.

The RLE coding is used in various compression system such Bitmap (BMP) for both grey level and bi-level data (Bradley, 1969; Associated & Adverse, 2015). Furthermore, it is particularly more effective than other compression algorithms for binary images due to that bi-level data has two level of intensity. The probability of the contiguously repeating of the bi-level data is more than grey level images. This means that adjacent pixel or voxels are more likely to be identical (Gonzalez & Woods, 2008). There is various scan forms that applied gray level image (Maniccam & Bourbakis, 2001).

The RLE is a practical tool for binary image compression. The considerations that make RLE based compression algorithms effective for binary data are discussed below.

- Binary data have only two type of intensity values. Therefore, running the matrix in a proper scanning form can catch the intensity repetitions effectively.

- 2D-RLE compression approach does not need a header bit to generate a UD code due to that only two intensity values exist.
- The RLE based volumetric compression has $2^{\mathcal{D}}$ bits, where \mathcal{D} denoted scan frame depth, as indicators for satisfying lossless decodable code stream.

In this dissertation, the RLE based improvement lossless compression scheme is applied on the binary 2D and 3D medical image data. Firstly, the scanning rules are extended by new scanning rule. Secondly, a novel algorithm has been proposed for compression of the volumetric images utilizing both intra- and inter-slice redundancy.

3.5 Lossless Bi-level Image Compression Standards

The grayscale and binary images have their own characteristics that need to be examined with different approaches. These distinct attitudes are one of the most important criteria for the success of algorithms (Gonzalez & Woods, 2008). With the increase of volumetric imaging algorithm, the gap increased. Therefore, the universal compression standard could not eliminate redundancy in both gray scale, continuous tone, and binary image category. State of art compression standards are not totally designed as taking account the bi-level data structures.

Since any loss of the data may lead to misdiagnoses, lossless techniques are dominantly used in the field of medical data compression. Numerous lossless compression schemes using various algorithms are applied to medical data (Khan et al., 2017; Schelkens et al., 2003). A compression technique which is compatible with bi-level can eliminate the redundancy data more than gray level based compression techniques.

3.5.1 The JBIG Standardizations for Bi-level Image Compression

The bi-level image coding schemes are standardized by the group of Joint Bi-level image Expert, JBIG. The standards of JBIG (officially called as ITU T.82) and JBIG2

are well-established compression techniques that designed explicitly for bi-level data (Hoffman, 2003). The JBIG family is special-purpose lossless standards (Hampel et al., 1992). It is developed for the transmission of the bi-level image progressively. The architecture of the methods employed deterministic prediction as a transformation block — in addition to that the methods have gray-level compression support.

The JBIG2 has been developed by the same group to increase the performance of the JBIG. The JBIG2, which is the next generation version of JBIG, harnesses model-based strategy to take into account the knowledge of the image data (Ono et al., 2000). The standard analysis of the image in the text, halftones, and others. The partitions are compression by applying different models to the segmented regions. Furthermore, improved standards are able to compress in lossy and lossless form (Salomon & Motta, 2010; Howard et al., 1998).

On the other hand, these methods are not designed specifically for binary medical data. Besides the JBIG2 performs adjusted strategies to the different data region of images such as text and generic region, it cannot factor in the characteristics of the medical data, in total. Since JBIG is designed for bi-level text compression as fax standards (Regentova et al., 2005), the performance of the methods remains in limited range for medical bi-level compression (Marks, 1998). As a result, a compression algorithm that designed by considering bi-level medical data is a vital demand in the field of medical image analysis.

3.5.2 CCITT Standards

The CCITT compression standards introduce various bi-level compression standards for text and fax transmission. The first released standards developed by the ITU-T were T2 (also known as CCITT Group-1) and T3 (CCITT Group-2). These pipelines are currently inoperative, and T4 (CCITT Group-3) and T6 (CCITT-Group 4) are employed. The latest version of the CCITT standardization exploits the RLE and Huffman coding. The latest version of CCITT, group-4, has been implemented on

medical data throughout the thesis for a comprehensive assessment of the proposed methods

To summarize, there are various compression standards for both bi-level and gray-level image compression. However, these algorithms utilized by common networks are general purpose algorithms that are not capable of compress the medical images entirely. These standards are not specifically designed for medical images. The following requirement is crucial for medical image standardization:

- The compression standards should be compatible to storing metadata which are the text including patient information, annotation of image modalities.
- For telemedicine integration (PACS, DICOM), the methods should be parametrized in sense of compression and telemedicine networks parameters.
- The algorithm should take account the structure of the image have different characteristics. For instance, the inter-slice distance for CT and MRI are different from each other. Therefore, the inter-slice parameter may be determined according to the modalities.
- Since the telemedicine network have huge burden, the computational load and complexity must be considered

The aforementioned properties should be considered while developing a special-oriented lossless medical image compression system. The proposed systems are developed taking into account these properties.

CHAPTER FOUR

REDUNDANCY IN MEDICAL IMAGES

What is the characteristics difference between the natural and medical images from the points of compression? The answer lies behind the sources of redundancy existing in two image categories which are generated by distinct acquisition principles. The natural images are formed by recording amplitude of reflected light from the object. The acquisition principle of the medical images are entirely different from the natural images, e.g., CT images are produced by passing radiation through the various locations of the body being imaged and the recording level of attenuation of the signals (Seeram, 2015). Currently, there does exist numerous medical imaging technologies that work with different imaging principles such as MRI, ultrasound imaging. Furthermore, it results in significant disparities between the redundancies existed in these sources. See the fundamental difference in the inter-slice and inter-frame redundancies of video and consecutive volumetric images, respectively, in Figure 4.1. It is obvious that inter-slice correlation are entirely different in natural (difference of frame 1 and frame 2 (Foundation, 2019)) and medical images (difference of CT-slice 1 and CT-slice 2) in Figure 4.1. Consequently, the medical image modalities yield different levels and types of redundancy compared to natural images.

To achieve higher compression performance comparing general-purposed standards, ones should consider the structure of the modalities during the determination of the redundancy. The redundant data are formed regarding data characteristics that are given below:

- **Entropy** is defined as unexpectedness of the image elements, i.e., pixel/voxels. In other words, it is an expression for the measurement amount of information (Cover & Thomas, 2005). The frontier of the compression is determined by the entropy. The higher the entropy, the lower the redundancy and thus lower the level of lossless compressibility. The expression of the entropy is formulated as probabilistic distribution of the symbols, see the equation 2.2.1 at the Section 2.2.

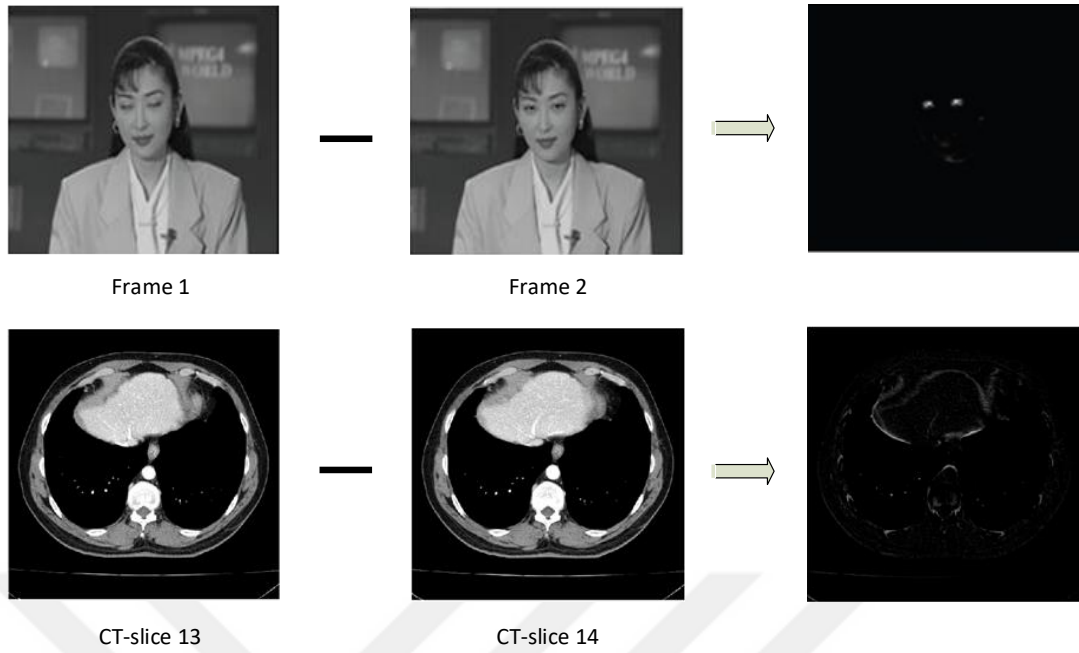


Figure 4.1 Different level of redundancy for medical and multimedia data (Foundation, 2019)

The probability distribution of the source determines the uncertainty through the element of data. The higher amount of information the higher number of bits that required to represent the source.

- **Compactness** is an intrinsic characteristic of a discrete object. It does not refer to the property of closed and bounded subsets as defined in topology (Munkres, 2014). Compactness is described as the quotient of perimeter and area of discrete objects existing in the binary images, i.e., a set of connected pixel (Bribiesca, 2008, 1997). High level of compactness results in less redundant data, in general. The compactness of the object in the segmented bi-level image is defined as,

$$C_p = \frac{P^2}{A} \quad (4.1)$$

where P and A are the perimeter and area of the object, respectively. The compactness is measured based on pixel and voxel for discrete images. The compactness characteristics are significant in the sense of information conveyed by the segmented organs. The compactness is significant for both two-dimensional and volumetric compression strategies.

- **Non-stationarity** is described as a subjective quality index that measures

structural context similarity of two images. The index provides what level of change occur in morphological structures between two images, e.g., the consecutive slices of volumetric CT-slices (Aja-Fernandez et al., 2006). The high degree of non-stationarity corresponding to successive slices, the higher the inter-slice correlation.

- **Energy** of the image matrix is an absolute value of pixel/voxel intensity levels, for binary images enclosed curve or volume. To determine the energy of an image, we exploit Frobenius norm, see appendix. The index does not provide knowledge about where the energy is concentrated. Thus, it is a contributory measurement used with the indexes mentioned above. The energy of image matrix I having dimensions of M and N is described by the Frobenius norm which defined as

$$\|I_{xy}\| = \left[\sum_{x=0}^{M-1} \sum_{y=0}^{N-1} |I(x,y)|^2 \right]^{1/2} \quad (4.2)$$

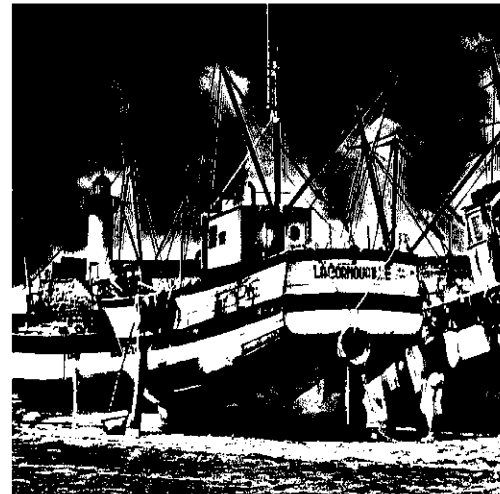
The measure of the energy of an image gives a practical perspective to identify coefficients of transformation in the frequency domain. The energy index also provides knowledge about the segmented organs, which can be regarded as a parameter of compression schemes (Salomon & Motta, 2010).

The principle of medical image acquisition systems is entirely different from the optical sensor photography. Therefore, the types of redundancy should be specifically analyzed by compression schemes. See the different level of compactness belonging to binarized natural and medical images in Figure 4.2b and Figure 4.2d, respectively. The natural and medical images in these figures are different as regards the level of compactness and entropy. Considering successive slices of the medical images, one can see that the morphological structures are consistent with each other. This gives rise to the low-level of non-stationarity.

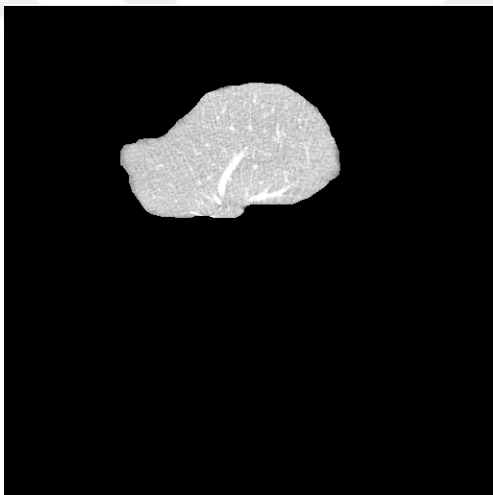
Beside the aforementioned characteristics, inter-/intra- slice correlation, set redundancy, - which is the mutual data occurring in more than one image in a sequence of analogue images (Karadimitriou & Tyler, 1997)-, are also primary characteristics that affect the achievement of the lossless methods for image



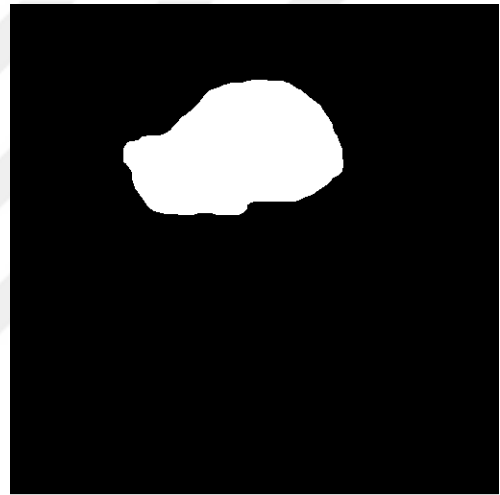
(a) Natural image - boat



(b) Binarised boat image (Otsu method)



(c) CT-liver



(d) Segmented CT-liver (Selver et al., 2008)

Figure 4.2 The CT-liver (medical) and boat (natural) images having different level of compactness (Petitcolas, 2018)

codification. Set redundancy is not considered during the lossless compression algorithm in this thesis. See different image characteristic in Figure 4.2a (Petitcolas, 2018) and Figure 4.2c. These characteristics of binary and grayscale images can be analyzed to uncover more redundancy compared to traditional compression strategy. The characteristics analysis of the typical natural and medical images is presented in Table 4.1.

Table 4.1 Measurement of characteristic of the natural and medical images

Characteristics	Image Sets					
	Lena	Cameraman	Boat	Liver-CT	Liver-MR	Spleen
Entropy	18.0	16.6	18.0	14.6	12.6	10.5
Compactness	10	86.6	109.8	303	28.4	30.1
Energy	510	316	519	158	51	39

Non-stationary processes intrinsically occur images where texture/patterns are present. For medical images, the successive images of the volumetric set have a change of structural behavior that may contribute to revealing of inter-slice redundancy. The metric Quality Index based on Local Variance (QIVL) introduces the measurement of non-stationary between images $I(x,y)$ and $J(x,y)$, which represent the slices of the volumetric image data set (Aja-Fernandez et al., 2006). The QIVL is formulated as

$$QILV(I, J) = \frac{2\mu_{V_I}\mu_{V_J}}{\mu_{V_I}^2 + \mu_{V_J}^2} \times \frac{2\sigma_{V_I}\sigma_{V_J}}{\sigma_{V_I}^2 + \sigma_{V_J}^2} \times \frac{\sigma_{V_IV_J}}{\sigma_{V_I}\sigma_{V_J}} \quad (4.3)$$

where μ_{V_I} and μ_{V_J} are local variances of images I and J , respectively. The expression $\sigma_{V_I} = \left(E\{(Var(I_{i,j}) - \mu_{V_I})^2\}\right)^{1/2}$ denotes the standard deviation of the local variance of image I , and finally $\sigma_{V_IV_J} = E\{(Var(I_{i,j}) - \mu_{V_I})(Var(J_{i,j}) - \mu_{V_J})\}$ indicates the covariance between the variances of I and J , two consecutive images slices. The $E\{\cdot\}$ denotes expectation value. A set of medical and natural images having different level of non-stationarity is given in Figure 4.3. The QILV measurement of these medical and natural images are presented in Table 4.2. The QILV index implies that there does not exist any non-stationarity between two images in the case of $QIVL = 1$, which can be interpreted as identical images. The consecutive CT images, liver slice 30 and 31,

Table 4.2 Non-stationarity measurement of the natural and medical images

QILV index for non-stationarity analysis.						
Images	CT-liver-1	CT-liver-2	MR-liver-1	MR-liver-2	Lena	Cameraman
CT-liver-1	1	0.96	0.07	0.069	0.031	-0.08
CT-liver-2	0.96	1	0.07	0.07	-0.04	-0.09
MR-liver-1	0.067	0.07	1	0.89	-0.002	-0.007
MR-liver-2	0.069	0.07	0.89	1	-0.004	-0.008
Lena	-0.031	-0.04	-0.002	-0.004	1	0.16
Cameraman	-0.08	-0.009	-0.007	-0.008	0.16	1

have minimum structural changes and maximum structural correlation, i.e., the value of 0.96 indicates there exists considerably high stationarity between the two image structure. This interpretation concludes that highly correlated successive slices will significantly contribute to compression performance whether the inter-slice correlation is considered .

The measurement of non-stationarity is one of the most significant parameters for the volumetric compression systems in which the inter-slice correlation is the primary source of the redundancy. Note that stationarity between the slices of CT images are greater than those of the slice of MR imaging.

The data characteristics, which are entropy, non-stationarity, compactness, and energy directly affects the designing of the compression algorithm. The proposed compression schemes, which are the volumetric context-oriented techniques (the 3D-RLE) and chain-code based compression pipeline (CrS) are designed considering the characteristics aforementioned above.



(a) Natural image: Lena



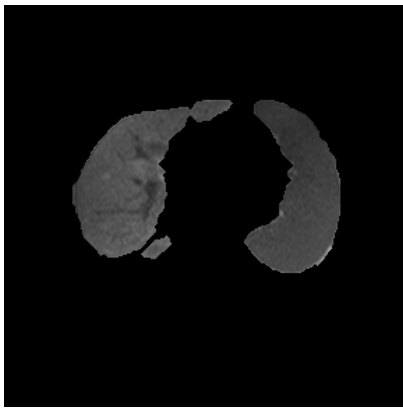
(b) Natural image: cameraman



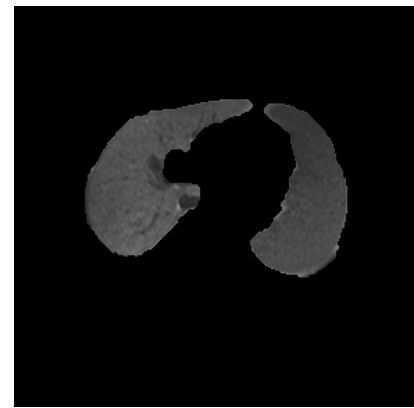
(c) CT-liver: slice 30



(d) CT-liver: slice 31



(e) MR-liver: slice 13



(f) MR-liver: slice 14

Figure 4.3 Natural and medical images having different level of non-stationarity, the image (a) and image (b) (Petitcolas, 2018)

CHAPTER FIVE

PROPOSED BI-LEVEL COMPRESSION SCHEMES

Throughout the thesis, context (3D-RLE) and contour (chain-code) based bi-level lossless compression schemes have been proposed. Wavelet transformation and sparse representation approaches have been designed in lossy compression techniques and applied to medical data sets. The proposed methods are specified in the following:

- The RLE algorithm is extended by utilizing multiple scanning forms. This modification provides flexibility to scan different images having various morphological structures. Furthermore, the extended RLE method has been evolved for compressing bi-level volumetric medical images by taking account inter-slice relationship (correlation between the voxels). The procedure, namely 3D-RLE, is able to determine coding redundancy between slices of the 3D volumetric images. A volumetric context-based technique has been designed by means of a new sweeping algorithm and extended scanning forms. In other words, the code stream has been generated by multiple scanning form which is determined according to image characteristics in the way of volumetrical sweeping the slices. And thus, the methods unveil a considerable redundancy through coherence between the shape of the objects existing in bi-level images and scanning procedure. One-dimensional RLE –using extended scanning forms – has only one slice depth and can be regarded as a restricted form of the 3D-RLE.
- The Chain Rule-based Compression Scheme, namely CrS, is proposed to compress bi-level medical images. The CrS system consists of chain rule as data-to-symbol coder and Huffman as the entropic encoder. The system is employed three-orthogonal direction (3OT), normalized angle difference (NAD), Freeman 4 (F4) and 8 (F8) directional chain rules. Furthermore, the system exploits by modified NAD rule (MNAD), which is a dictionary-optimized version of NAD.

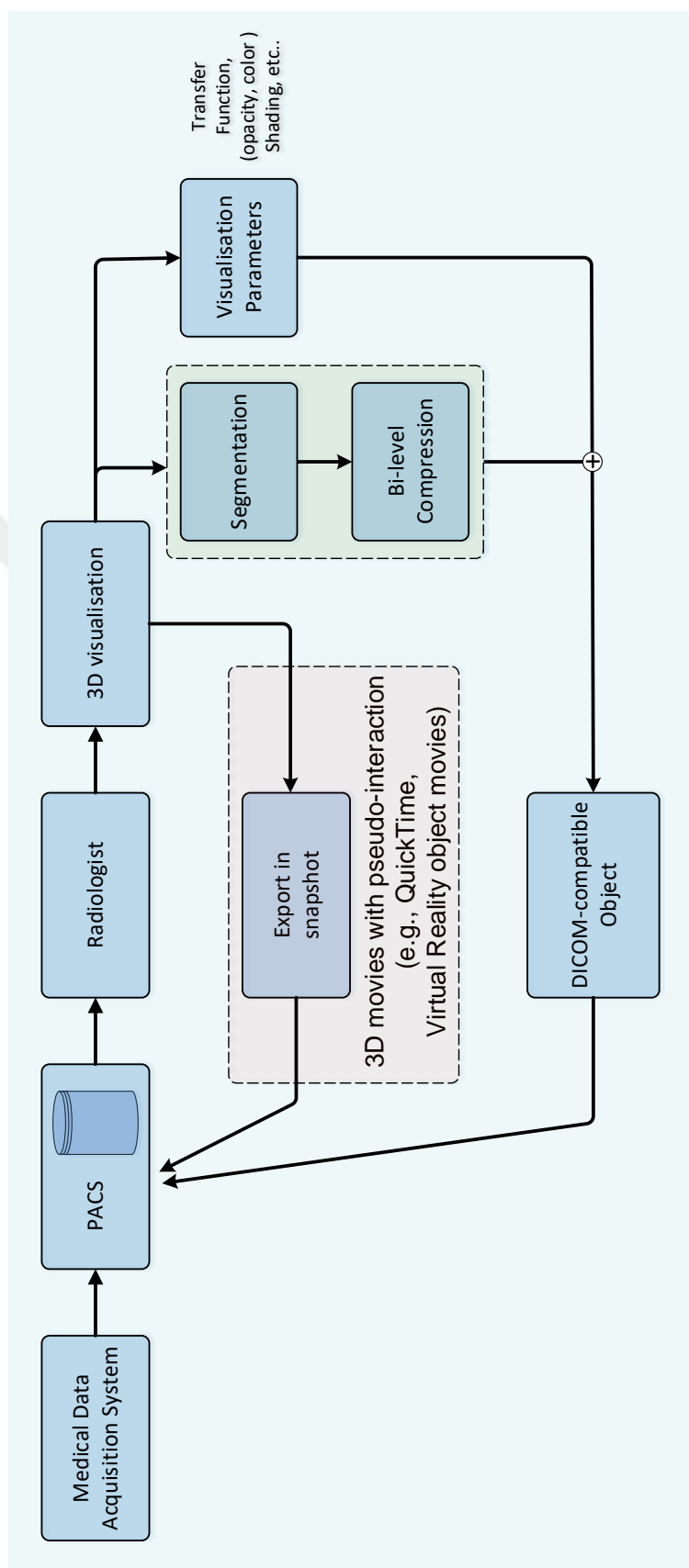
To summarize, context-oriented and chain-based bi-level compression pipelines are proposed for medical image compression. These methods have been specially designed for a new system which includes a necessary step for extending repeatability and transfer of 3D medical imaging. The systems are suggested by developing a DICOM compatible object that covers visualization parameters together with compressed binary-segmented data for efficient transmission in teleradiology applications. Therefore, bi-level compression plays a vital role not only reduces the bandwidth of the transmission line but also providing an efficient reconstruction of gray level images, see the telemedicine system is illustrated Figure 5.1. The proposed systems are elucidated in the following subsection.

5.1 Extended Run-Length Encoding for Bi-level Medical Images

The RLE is one of the most effective and easy-to-implement compression algorithm (Kim & Kim, 2009). The fundamental principle behind the process is to uncover the repetitions of consecutive intensity of the image elements. It has been extended in two ways:

1. To make available a flexible scanning procedure by providing multiple scanning forms and orders. The order and form are defined as positions of and the rule of the scanning procedure, respectively. The RLE can be geared to the morphological structure of the objects in the bi-level image by parametrization the scanning procedure. This provides the optimal level of entropy and increases the capability of the RLE to obtain intra-slice redundancy in more efficiently.
2. A new novel volumetric RLE algorithm that is utilizing inter-slice correlation to unearth coding redundancy between the voxels. The algorithm rasters the volume by the extended scanning procure. By means of the algorithm, both inter-slice and intra-slice coding redundancy can be revealed.

Many RLE based-algorithms harness the common scanning procedures such as linear, zigzag, and boustrophedonic. These approaches restrict the revealing of redundancy.



In this context, to eliminate these limitations of the RLE, the proposed compression algorithm provides - an extended scanning procedure such as spiral and fractal Hilbert to specify an optimality condition for scanning strategy consistent with the physical shape (morphology) of the object (segmented organ) occurring in the image data. This makes a flexible usage of the RLE for the various data sets consist of various morphological structural image. The RLE technique also has been adapted to volumetric data by a novel low-complexity algorithm whose details are presented in the following subsection.

5.1.1 The RLE with Multiple Scanning Procedure

The scanning is the mapping that reorder the pixel in a form with low-entropy sequence. Therefore, the scanning form is crucial to achieve more compression performance. The RLE is extended to multiple scan forms and orders to adjust the shape of the data by the proposed scheme. The RLE is employed as auxiliary operation by the standards of BMP, JPEG, and TIFF (Miano, 1999; Wallace, 1992). The scanning form is extended to boustrophedonic, linear, perimeter, Morton, Hilbert (fractal scanning) and chevron. Moreover, the method has scan start point parameters (order) such as (x,y) , (y,x) , $(-x,y)$, $(-y,x)$ to provide flexibility in the initial scan positions, where (x,y) denotes spatial coordinates located at four quadrants. The sample image matrix is illustrated in Figure 5.2 where the locations of the orders is indicated. Scan form and order primarily effect the performance of the RLE based compression algorithms. Therefore, multiple scan forms have been tested on bi-level medical images to determine optimal scan form and order.

The Table 5.1 and Table 5.2 present the beginning and ending indexes, i.e., (orders), for the extended scanning rules employed by the proposed algorithm. It can be interpreted that the orders (O) becomes more significant in the case existing asymmetric objects in the bi-level images.

By suggested 2D-RLE scheme showed in Figure 5.3 with multiple scanning forms, the methods has been applied to the binary medical image and combined with an

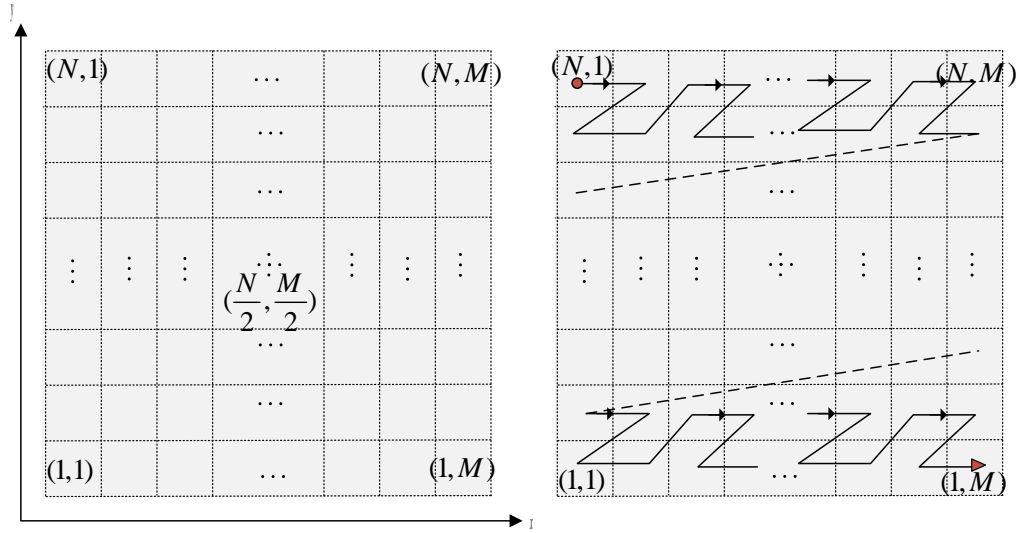


Figure 5.2 The Morton scanning with different scanning orders

Table 5.1 Scanning orders and directions of the zigzag, boustrophedonic, linear, and Morton forms

		Scanning Form							
Order		Linear		Boustrophedonic		Zigzag		Morton	
		Start	End	Start	End	Start	End	Start	End
Direction	$(+x, +y)$	(1, 1)	(N, M)	(1, 1)	(N, 1)	(1, 1)	(N, M)	(1, 1)	(N, M)
	$(+y, +x)$	(1, 1)	(N, M)	(1, 1)	(1, M)	(1, 1)	(N, M)	(1, 1)	(N, M)
	$(+x, -y)$	(N, 1)	(1, M)	(N, 1)	(1, 1)	(N, 1)	(1, M)	(N, 1)	(1, M)
	$(-y, -x)$	(N, M)	(1, 1)	—	—	—	—	(N, M)	(1, 1)
	$(-x, -y)$	—	—	(N, M)	(N, 1)	(N, M)	(1, 1)	—	—

Table 5.2 Scanning orders and directions of the perimeter, Hilbert, and Chevron

	Order	Scanning Form					
		Perimeter		Hilbert		Chevron	
		Start	End	Start	End	Start	End
Direction	$(+x, +y)$	(1, 1)	(N/2, M/2)	(1, 1)	(N, 1)	(1, 1)	(N, 1)
	$(+y, +x)$	–	–	(1, 1)	(1, M)	(1, 1)	(1, M)
	$(+x, -y)$	(N, 1)	(M/2, N/2)	(N, 1)	(1, 1)	(N, 1)	(1, 1)
	$(-y, +x)$	(N/2, M/2)	(M, N)	–	–	–	–
	$(-y, -x)$	(N/2, M/2)	(N, 1)	–	–	(N, M)	(N, 1)
	$(+y, -x)$	–	–	(1, M)	(1, 1)	–	–

efficient entropic encoder (Huffman). Firstly, the optimal scanning rules and orders are initialized. Then, the *run* block is executed to generate RLE symbol and lastly, these symbols are converted to bitstream by Huffman, variable length coding.

The scanning form are illustrated in the following.

Linear scanning is the basic form that used in the RLE and JPEG architecture based compression algorithms (Peter D. Johnson, 2003). Numerical simulations of the linear scanning have provided satisfactory results both 2D and 3D RLE algorithm. Secondly, boustrophedonic matrix scanning form is applied in RLE based algorithms. The procedure of boustrophedonic scan is shown in Figure 5.5. The third scan procedure is zigzag which is commonly used in state of art compression standard such JPEG (Wallace, 1992). Zigzag scan form is shown in Figure 5.6.

Perimeter scan form is fourth scan procedure shown in in Figure 5.7. It has been supposed that spiral form is more appropriate for oval shapes compared to other forms.

Another scanning form that used in RLE is Morton scan. This form which is shown in Figure 5.8 has been provided satisfactory result both for 2D and 3D RLE compression algorithm.

Sixth scan procedure is the Hilbert curve. This scanning form is a fractal curve that

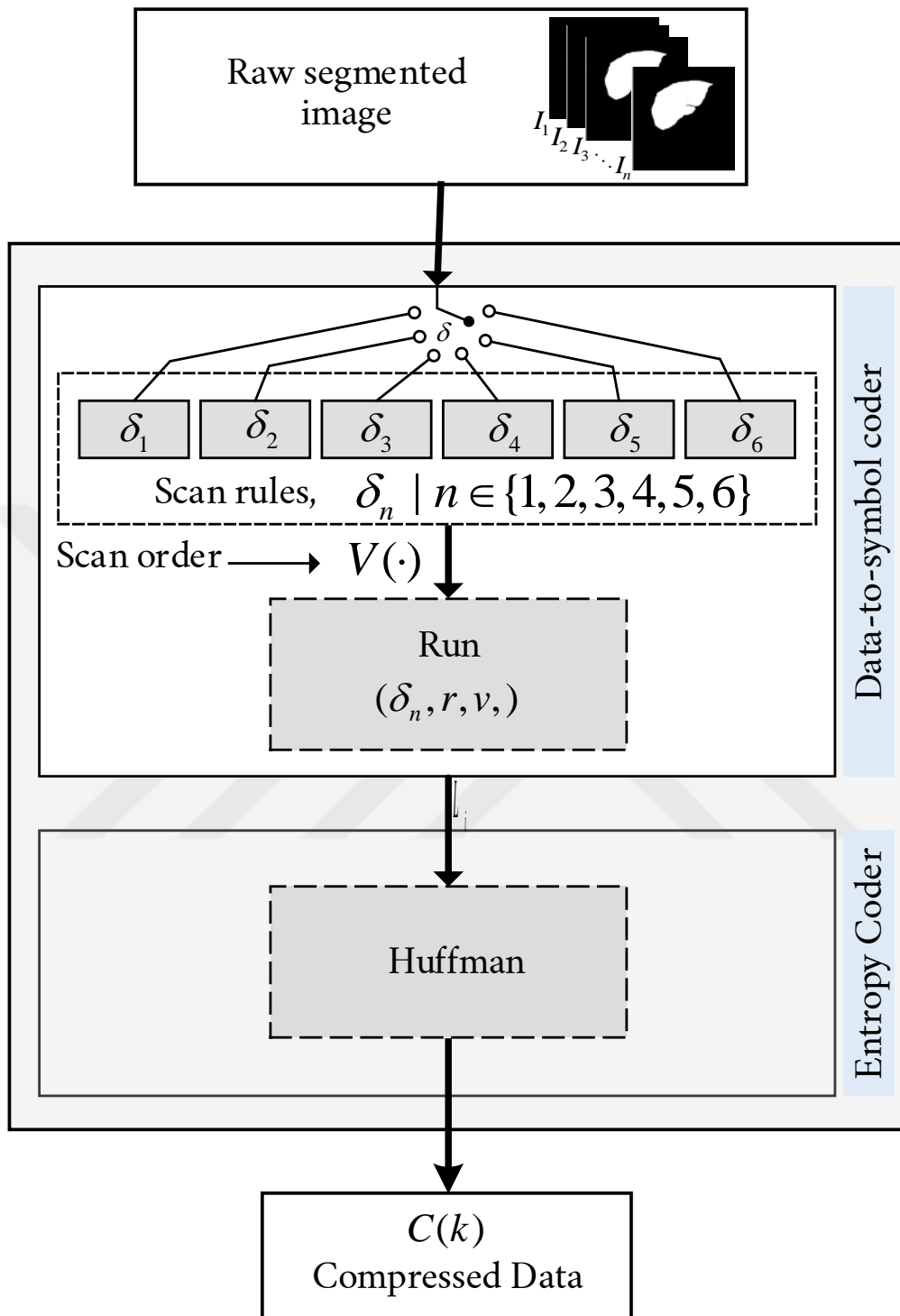


Figure 5.3 The 2D-RLE based compression scheme

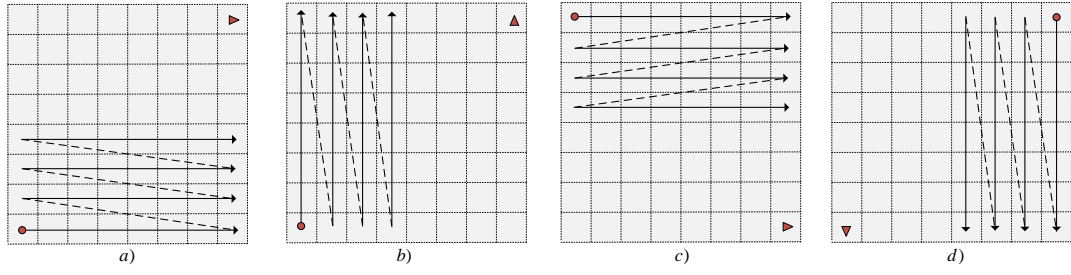


Figure 5.4 Linear scanning with a) (x,y) , b) (y,x) , c) $(-x,y)$ and d) $(-y,x)$ orders

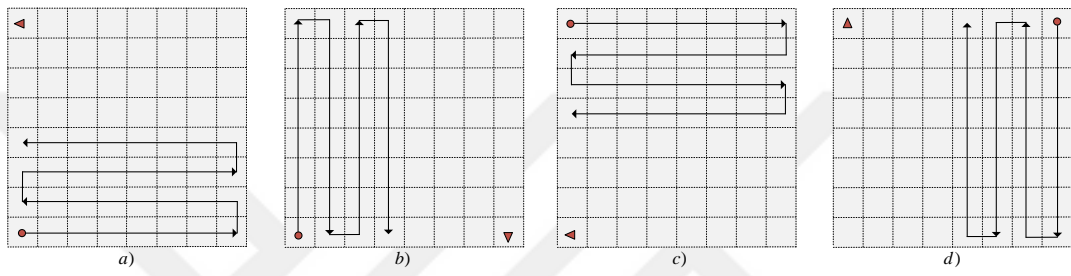


Figure 5.5 Boustrophedonic scanning with a) (x,y) , b) (y,x) , c) $(-x,y)$ and d) $(-y,x)$ orders

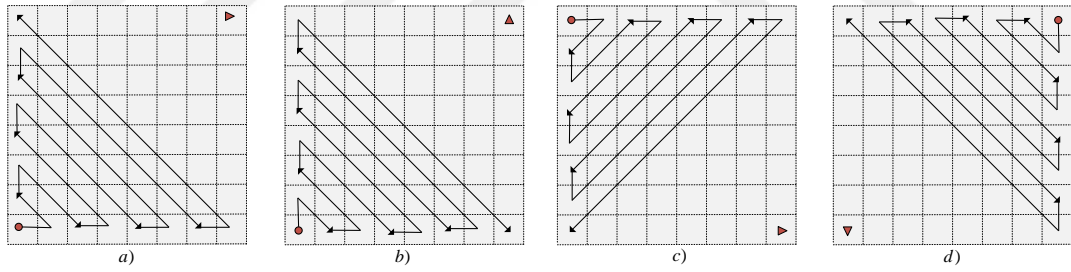


Figure 5.6 Zig-zag scanning with a) (x,y) , b) (y,x) , c) $(-x,y)$ and d) $(-y,x)$ orders

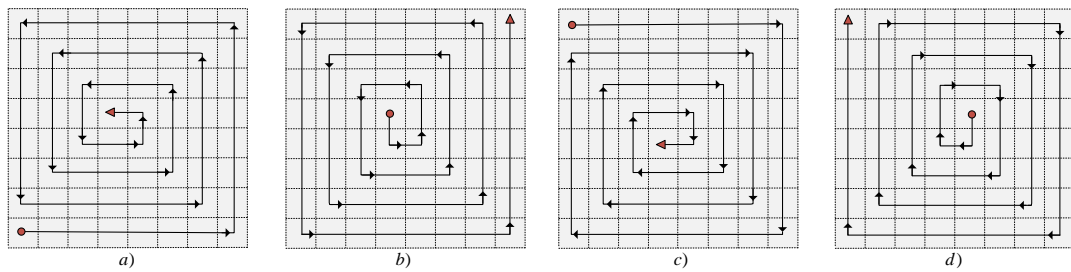


Figure 5.7 Perimeter (spiral) scanning with a) (x,y) , b) (y,x) , c) $(-x,y)$ and d) $(-y,x)$ orders

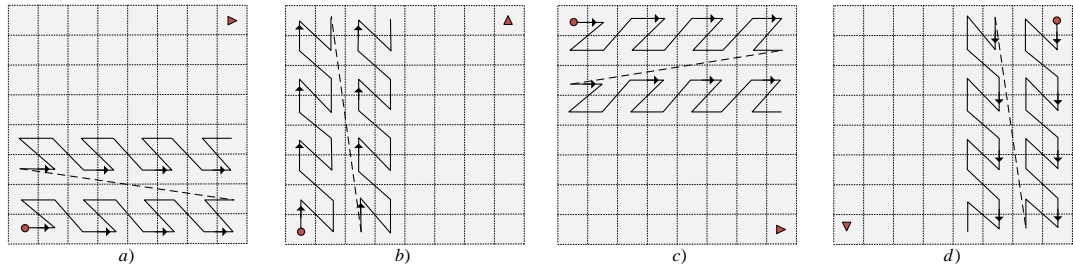


Figure 5.8 Morton scanning with a) (x,y) , b) (y,x) , c) $(-x,y)$ and d) $(-y,x)$ orders

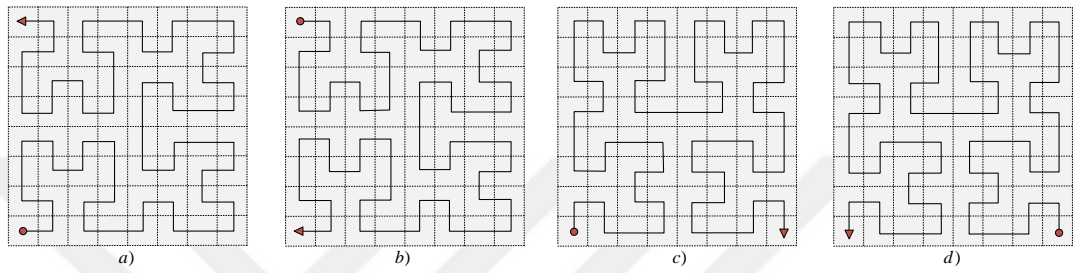


Figure 5.9 Hilbert scanning with a) (x,y) , b) (y,x) , c) $(-x,y)$ and d) $(-y,x)$ orders

is the optimal curve for RLE algorithms. The Hilbert scanning form shown in Figure 5.9 has been provided with the best results in terms of bpp and bpv both for 2D and 3D RLE compression algorithms.

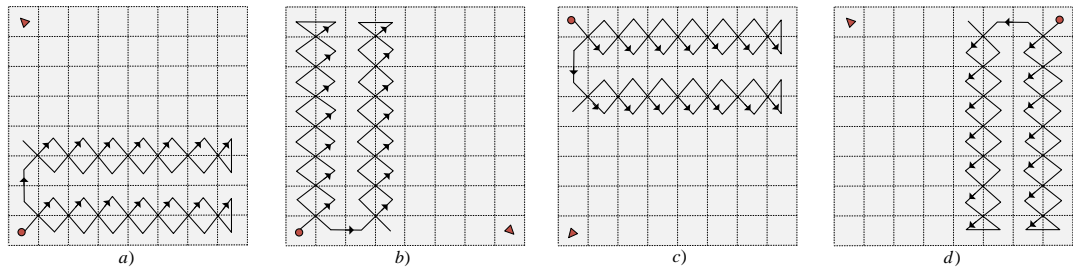


Figure 5.10 Chevron scanning with a) (x,y) , b) (y,x) , c) $(-x,y)$ and d) $(-y,x)$ orders

Chevron is the last scanning form. The scanning forms have illustrated in Figure 5.10 for four orders. This scanning procedure has not provided satisfactory result for RLE algorithms, in general. However, it may achieve considerable compression efficiency in the case of linearly distributed shape of the objects.

5.1.2 A New Volumetric Run-Length Encoding Approach

The run-length encoding algorithm has been extended to compress volumetric image data using inter-slice correlation addition to the intra-slice correlation employed by conventional RLE based systems. The RLE algorithm is basically designed based on the principle of that the high level of inter-slice voxel correlation creates temporal redundancy. Addition to that, the 3D-RLE has taken account the voxels correlations during the compression process. Similar to the intra-slice association, there does exist a spatial dependency between adjacent voxel elements of the 3D images. Utilizing voxel correlation has contributed compression performance due to that the coding redundancy between slices is revealed. Main blocks of the 3D-RLE compression system are shown in Figure 5.11. The code stream is going to be generated by these operations which are elucidated in below.

The sub-block of the 3D-RLE system is illustrated in Figure 5.12. Volumetric data $I(x,y,z)$, shown in Figure 5.12a, are scanned in depth of \mathcal{D} in the first block of the 3D-RLE algorithm. Volumetric scanning for $\mathcal{D} = 2$, which unveil inter-slice correlation of only 2 slice, is illustrated in Figure 5.12b. Three-dimensional scanning generates a V_{3D} matrix. Every row of this matrix consists of an inter-slice correlated scanning vector in \mathcal{D} depth. The V_{3D} matrix has been *run* in the second block throughout a volumetric manner. The $r_{3D,v}$ symbol containing extra uniquely decipherable bits (header bit will be detailed by the pseudo code) comparing (r,v) peers in 2D-RLE algorithm. The last operation is entropy coding. Huffman encoding is used for converting the symbol to the data using variable length coding. The probability of occurrence of the run-length symbols L^{3D} sequences is analyzed. The probabilities of the RLE symbols are satisfying the optimal case which is the probabilities are the negative power of 2. It is the condition that the Huffman algorithm satisfies the optimum codeword as entropy coding. Therefore, Huffman coding is employed to transform the symbols of the run-length into codestream.

The 3D-RLE based volumetric compression has extra header bits as the indicators to satisfy lossless decodable code stream. The extra symbol has been emerged because

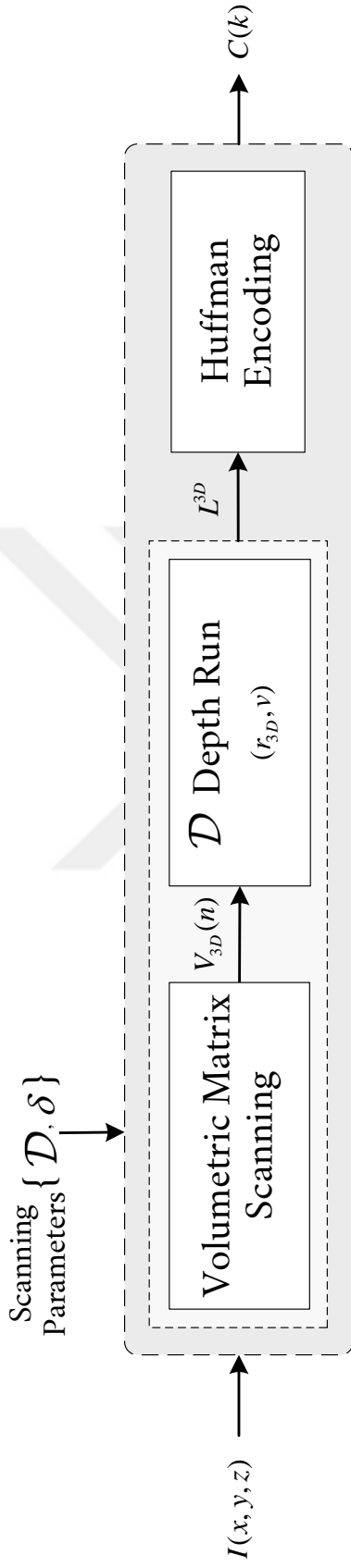
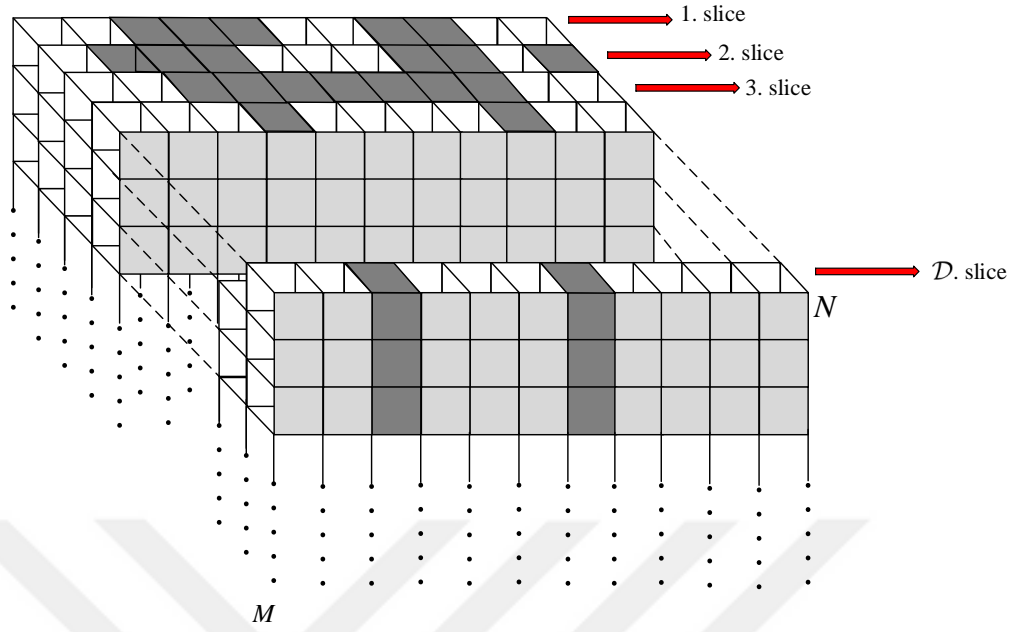
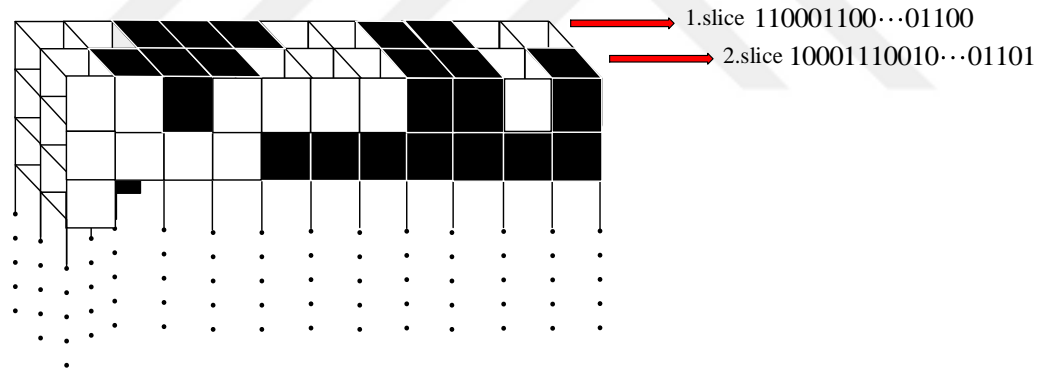


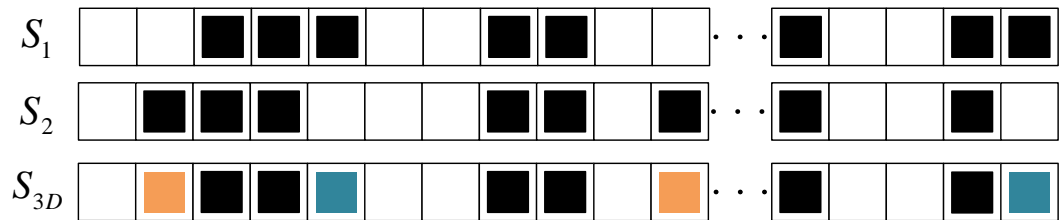
Figure 5.11 The main blocks of the 3D-RLE method



(a) Volumetric $M \times N \times \mathcal{D}$ image data



(b) The algorithm for 2 slice depth



(c) Scanned vector: S_1 : 1. slice, S_2 : 2. slice, S_{3D} : encoded of S_1 and S_2

Figure 5.12 The illustration for the 3D-RLE algorithm in the case of slice depth \mathcal{D} is 2

of the inter-slice combinations to satisfy uniquely decipherable property, see in Figure 5.12c. As it is obvious from the illustration, the higher the inter-slice correlation the fewer the number of header bit. Therefore, the compression efficiency directly depends on these bits. Pseudo code of the 3D-RLE algorithm and codifications have been given in Table 5.3 and Table 5.4 as a two parts. The PART-1 (5.3) expounds the case of $\mathcal{D} = 1$, i.e. no inter-slice correlation. The PART-2 (5.4) reports details of the case of $\mathcal{D} > 1$, i.e. utilization of both inter- and intra-slice correlations.

The proposed algorithm allows compressing the image in forms of 2D-RLE and volumetric based RLE with extended scanning orders and forms. In the case of the 2D-RLE, it utilizes multiple scanning procedures and exploit the algorithm on every slice, individually (pseudo code part **A**). That means only intra-slice correlation is revealed by extended scanning procedure. In the 3D-RLE case, the system executed in form of utilizing both inter/intra-slice codification by the way of three-dimensional scanning strategy (part **B** of the pseudo code).

At the first pseudo part **A**, the image slices are mapped in to the vector

$$V = \{V_n, n = 1, 2, \dots, K, V_n = \mathcal{T}_{\mathcal{S}, \mathcal{O}}(I_n), \forall I_n \in J_{3D}\}$$

by transformation $\mathcal{T}_{\mathcal{S}, \mathcal{O}} : \mathbb{Z} \times \mathbb{Z} \mapsto \mathbb{Z}$ its steps are determined by \mathcal{S} scanning form and \mathcal{O} scanning order where I_n is n^{th} slice of J_{3D} (Process **A**-1). In the following step, the run-length converting \mathcal{R} is performed to every V_n to construct

$$P = \{P_n, n = 1, 2, \dots, K, P_n = \mathcal{R}(V_n), \forall V_n \in V\}$$

where $\mathcal{R} : \mathbb{Z} \mapsto \mathbb{Z}$. where $\mathcal{R} : \mathbb{Z} \mapsto \mathbb{Z}$ (Process **A**-2). Symbol vector P_n are transformed into the bit stream C_n harnessing the Huffman algorithm (Process **A**-3). As a result, whole slices have been compressed and recorded as a bit stream. Note that there does not need for extra-bit required for coding inter-slice relationships. However, it is worth to remark that the scanning rules are reversible so that the UD property is ensured.

In part of pseudo **B** code (the condition of $\mathcal{D} > 1$), the raw data are codifying by harnessing relationships of intra-slice and also inter-slice correlations). The volumetric image slices have been scanned by applying the transformations $\mathcal{T}_{\mathcal{S}, \mathcal{O}}$ and

The volumetric 3D-RLE methods and its algorithm				
INPUTS PARAMETERS				
Raw Image	: $J_{3D} = \{I_n \in \mathbb{Z} \times \mathbb{Z} \mid n = 1, 2, \dots, K\}$ and $K \in \mathbb{Z}^+$ is the slice number of volumetric image			
Scanning Form	: $S = \{1, 2, \dots, 7\}$ 1 : Linear 2 : Boustrophedonic 3 : Zigzag 4 : Perimeter 5 : Morton 6 : Hilbert 7 : Chevron			
Scanning Order	: $O = \{1, 2, \dots, 8\}$ 1 : $(+x, +y)$ 2 : $(+y, +x)$ 3 : $(+x, -y)$ 4 : $(-y, -x)$ 5 : $(-x, -y)$ 6 : $(-y, +x)$ 7 : $(-y, -x)$ 8 : $(+y, -x)$			
Slice Depth	: $\forall \mathcal{D} \in \mathbb{Z}^+$ and $\mathcal{D} \leq K$			
Initialisation $i = 1, i_0 = 1, Q = M \times N, i_1 = 1, i_2 = 1$ and $b = 1$;				
A) if $\mathcal{D} == 1$, then:				
Compress the slices of the image individually				
while $i < K$ do apply the matrix-to-vector mapping with S and O parameters				
1: For each slice, generate re-ordered sequence form of the i^{th} slice $V_i[k] \in \mathbb{Z}$, $k = \{1, 2, \dots, L\}$ by applying \mathcal{T} mapping $J_{3D}[:, :, i] \mapsto V_i$ matrix-to-vector transformation that scans the slices by means of the S and O .				
2: Apply \mathcal{R} run operation to transform V_i into P_i symbol vector consisting of (v, r) pairs.				
3: Symbol to data conversion: perform (Huffman) entropy coder which maps P_i symbol vector to C_i bit stream				
4: save C_i and $i = i + 1$, increment iteration number for the next slice.				
5: Save every C_i bitstream vectors in C_{3D} total code stream.				
Output: $C_{3D} = 10111010 \ 10 \dots$ compressed data (encoded code stream)				

Table 5.4 The 3D-RLE algorithm (Pseudo code PART 2)

The volumetric 3D-RLE methods and its algorithm

INPUTS PARAMETERS:

Raw Image : J_{3D}

Scanning Form : $S = \{1, 2, \dots, 7\}$

Scanning Order: $O = \{1, 2, \dots, 8\}$

Slice Depth : $\forall \mathcal{D} \in \mathbb{Z}^+$ and $\mathcal{D} \leq K$

Initialisation $i = 1, i_0 = 1, Q = M \times N, i_1 = 1, i_2 = 1$ and $b = 1$;

B) if $\mathcal{D} > 1$, then:

Coding the J_{3D} image data by employing inter/intra-slice relationships.

while $i_0 \leq K$ **do** perform \mathcal{T} mapping $J_{3D}[:, :, i_0] \mapsto V_{i_0}$ through
 S and O parameters

6: Create an M_{3D} matrix so that each reordered sequences V_{i_0} are assigned to
a corresponding row of the M_{3D} : $M_{3D}[i_0, :] = V_{i_0}$.

7: Incrementation of the counter for following slice $i_0 = i_0 + 1$.

while $i_2 \leq K$ **do**

while $i_1 \leq Q$ **do**

If $M_{3D}[i_1, i_2] == M_{3D}[i_1 + 1, i_2] \dots = M_{3D}[i_1 + \mathcal{D}, i_2]$, **then:**

8: $V_{3D} = \text{cat}(V_{3D}, M_{3D}[i_1, i_2])$, append V_{3D} to $M_{3D}[i_1, i_2]$

else

9: $h_{i_1} = b + \sum_{k=0}^{\mathcal{D}-1} 2^k M_{3D}[i_1 + k, i_2]$,

10: $V_{3D} = \text{cat}(V_{3D}, h_{i_1})$, append V_{3D} to h_{i_1}

11: $i_1 = i_1 + 1$

12: Concatenate escape character 'ch': $V_{3D} = \text{cat}(V_{3D}, \text{'ch'})$

13: $i_2 = i_2 + \mathcal{D}$

14: Perform run-length to generate P_{3D} symbol sequence

15: Obtain C_{3D} bit stream vector by applying entropy coder to P_{3D} sequence.

16: save C_{3D} codes stream, i.e. compressed data.

Output: $C_{3D} = 10111010\ 10 \dots$ compressed data (encoded code stream)

the resulting symbols sequences are assigned as the row of M_{3D} matrix (see the process **B-6**). As a subsequent operation, the scan along the columns of M_{3D} in non-overlapping blocks having scanning depth of D , and then assign a header (for satisfying uniquely decipherable-UD property) in case of the voxel intensity of scanned block is not identical,

And then, along the columns of M_{3D} in non-overlapping blocks having depth D , if the intensity levels of the all voxels in the block are not same, then the UD header

$$h = b + \sum_{k=0}^{D-1} 2^k M_{3D}[i_1 + k, i_2] \quad (5.1)$$

is calculated and the result is coded in V_{3D} (Process **B-9**). The bias b is used in order not to have 0 and 1 as a value of h , otherwise this contradicts with the fact that block of all voxels having equal intensity level of 0 and 1 have to be coded as 0 and 1 (Process **B-8**), respectively. The *cat* performed in step B-8, B-10 and 12 denotes concatenate

function. In the case of $D = 3, i_1 = 1, i_2 = 1, M_{3D}[1 : 3, 1] = \begin{bmatrix} 1 \\ 0 \\ 0 \end{bmatrix}^T$, the header h has the

value 1 that is not uniquely decipherable, one-to-one mapping, since it is same as the all equal condition $M_{3D}[1 : 3, 1] = \begin{bmatrix} 1 \\ 1 \\ 1 \end{bmatrix}^T$. Therefore, the bias $b = 1$ is added to the sum

to make the code uniquely decipherable. The *cat* denotes the concatenate function. For all slice depth and conditions, the code satisfies UD properties. An example of $I_{3 \times 3 \times n}$ is illustrated in Figure 5.13.

In summary, h_n is the header used as an escape character to distinguish the voxels belongs to different image slices. The identity and non-identity voxels are coded according to proposed algorithm. Thus, non-identity voxels must be coded using h_n to decode in uniquely decipherable form. Same voxel values are coded as a single code along with slice depth but the voxels having different values are coded using h_n header where n is the index of position (h_1 where $n = 1$). For all slice depth and conditions, the code satisfies UD properties.

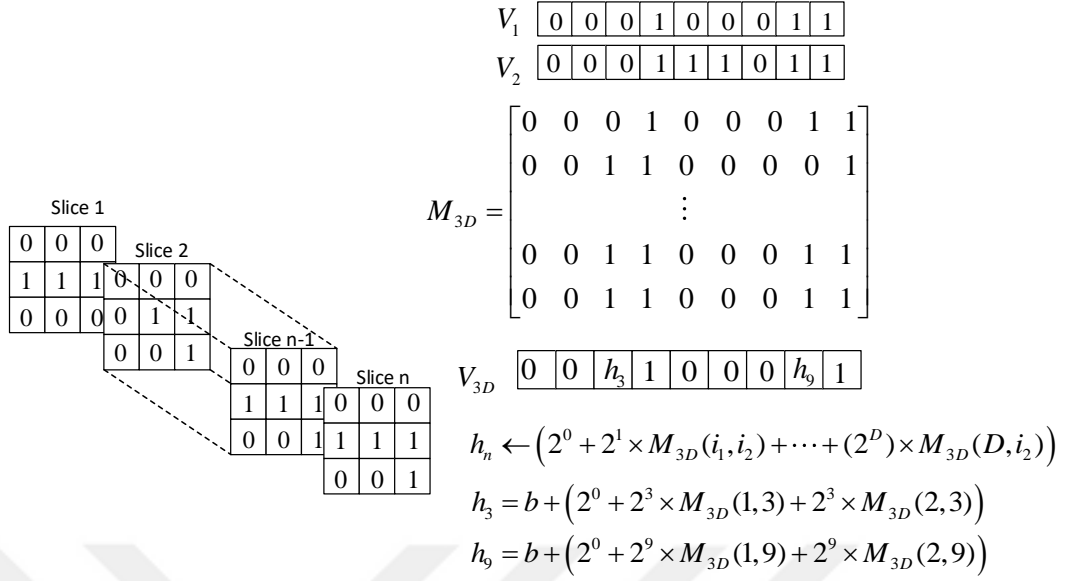


Figure 5.13 Example for the uniquely decipherable property

5.2 Chain Rule based Compression System (CrS)

The basic principle of the chain code based methods is to convert the boundary pixel or voxel information to a lossless and decipherable symbols. In other words, the contours of the segmented regions of the bi-level images are coded by chain rules. Starting with the first introducing of CC representation by Freeman in 1961, various derivations of the chain rules have been proposed.

There are more variations of the chain rules such as Freeman eight (F8) and four (F4) directional (Freeman, 1961, 1974), unsigned Manhattan (Žalik et al., 2016), slope (Bribiesca, 2016), vertex (VCC) (Bribiesca, 1999), three orthogonal (3OT) (Sánchez-Cruz et al., 2007) chain codes and the chain code for volumetric data representation (Martínez et al., 2016). In this dissertation, the F8 chain rule is employed in the bi-level compression system. Aforementioned chain codes aim to reduce lower entropy by reordering the image matrix via chain rules which are the standards input format for numerous shape analysis algorithms. These chain code procedures preserve whole information providing to allow considerable data

reduction. As a consequence, they are effectively employed in lossless compression algorithms in two- and three-dimensional approaches (Žalik et al., 2015), (Bribiesca, 2008). The procedure for the F4 and F8 chain rules are illustrated in Figure 5.14.

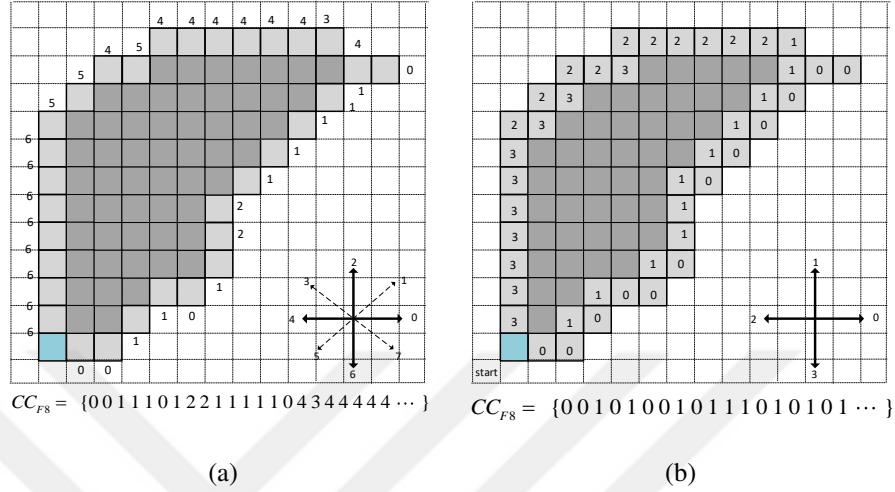


Figure 5.14 Chain rule derivations a) F8 b) F4

The eight directional chain (F8) is the first code that was presented by Freeman (Freeman, 1961). The procedure is based on scanning through the boundary of an object in eight connectivity of the pixels. The F8 alphabet therefore consists of 7 symbols which $\Sigma(F8) = \{0, 1, 2, \dots, 6, 7\}$. The code is generated by $\sigma \in \Sigma$ represents a $45^\circ \times \sigma$ angle from the positive direction of the x coordinate axis. Similar to $F8$, $F4$ represents the boundary using 4 connectivity of neighboring image elements. Thus, the F4 alphabet consists of 4 symbols is $\Sigma(f4) = \{0, 1, 2, 3\}$ and $\sigma \in \Sigma$ represents a $90^\circ \times \sigma$ angle from the positive direction of the x coordinate axis. Three-orthogonal (3OT) is another chain rule that is composed of only three symbols (Rodríguez-Dagnino, 2005). The 3OT alphabet, therefore, consists of three symbols $\Sigma(3OT) = \{0, 1, 2\}$ which is assigned in following rules: if the current coding direction is the same as the coding direction of its predecessor, $\sigma = 0$; if the current coding direction is equal to its first predecessor whose coding direction is different than the direction of its predecessor, $\sigma = 1$; otherwise: $\sigma = 2$ and the symbol sequence is generated. The performance of the chain rules depends on the shape of the segmented objects, i.g. liver shapes. It maps the boundary information as the number of their

vertex which is in touch with the bounding contour of the pixels (Salem et al., 2005). The CC based systems hold a great potential for compressing binary medical data.

In this dissertation, a combined pipeline of run-length and chain code is designed for bi-level medical images, see in Figure 5.15.

Having transformed every slice of the $I(x,y,z)$ volumetric image to chain symbols using $F8$ rule, the run-length approach is employed to reveal redundancy of chain symbols. The Huffman coding is applied to (r_c, v_c) pairs as symbol-to-data operations. Eventually, the raw three-dimensional is compressed as $C(k), k \in \mathbb{N}$ code stream. The chain block has been experienced utilizing various chain rules such as $F8$ and $F4$ see in Figure 5.14. The proposed systems designed as given in Figure 5.15 has been applied to CT data set and achieved satisfactory compression ratio. Aforementioned chain rules aim to reduce entropy by reordering contour pixel.

5.3 Transform based Compression System

The transformation is a common method employed by state-of-the-art standards. Transform based systems aim to convey the raw image to a domain where the redundancy becomes more discernible. The Fourier, discrete cosine, and wavelet transforms are frequency domains transformations. The predictive mapping is a spatial transformation that reshapes the raw image in a low-entropy. And thus, they extend the boundary of lossless compression. The predictive coding is used by prominent standards such as PNG, JPEG.

5.3.1 Predictive Mapping and RLE based Hybrid Compression

A modified lossless compression scheme has been proposed for binary biomedical data. The image is exposed to one-to-one reversible transform, i.e., predictive coding.

Predictive mapping is operated as the lossless transformation to decrease the entropy of the $I \in \mathbb{R}^3$ volumetric image. After the first step, \hat{I} image is transformed

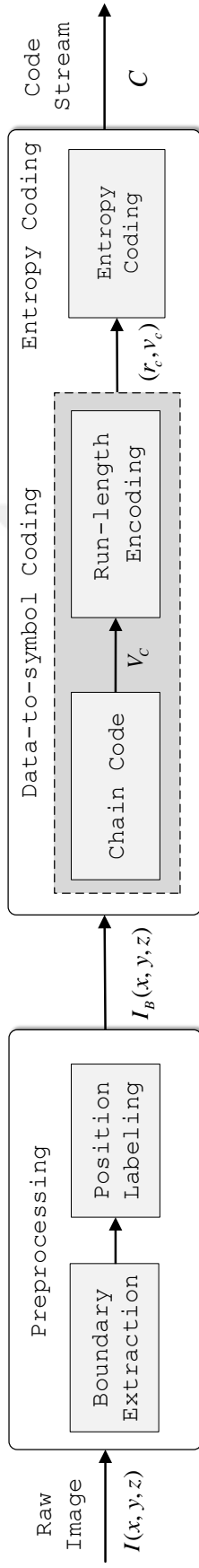


Figure 5.15 Main block diagram for chain code based compression

into symbols by the predictive model. Then the RLE data-to-symbol encoding is exploited. As the last step of the coding phase, the symbols are converted into the coded bit stream by the entropy coders. Huffman coding method is used as entropy coding by the system. $I(x,y,z)$ is an 3D image data where x , y , are spatial and z is temporal coordinates, respectively. Suggested predictors models for 3D image data are given below ;

1. $\hat{I}(x,y,z) = \alpha I(x-1,y,z)$
2. $\hat{I}(x,y,z) = \alpha I(x,y-1,z)$
3. $\hat{I}(x,y,z) = \alpha I(x-,y-1,z-1)$
4. $\hat{I}(x,y,z) = \alpha I(x,y-1,z-1) + \beta I(x-1,y,z-1) - \theta I(r-1,c-1,s-1)$
5. $\hat{I}(x,y,z) = \alpha I(x-1,y-1,s) + \beta(I(x,y+1,z) - \theta I(x,y,z+1))/3$
6. $\hat{I}(x,y,z) = \alpha I(x-1,y,z) + \beta(I(x,y-1,z) + \theta I(x-1,y-1,z-1))/2$
7. $\hat{I}(x,y,z) = \alpha(I(x,y-1,z-1) + \beta I(x-1,y,z-1)) + \theta I(x-1,y-1,z-1)/3$

where α and β parameters are arbitrary selected scalar. Since there is no universal parameters which is optimal for all images, these parameters are determined according to the image characteristics. The 3D predictors are applied to medical data set and the results show that the predictor contribute the performance of gray-scale compression algorithms (Aldemir et al., 2018b).

5.3.2 *Embedded Zerotree Wavelet Image Coding*

In this chapter, proposed algorithm, Embedded zerotree wavelet (EZW) coefficients coding has been introduced in details and have been applied to natural and medical data. The EZW is a well defined and numerically easy to apply transform based compression algorithm. The technique is proposed by Shapiro (Shapiro, 1993) for 2D images. It is initially applied on 2D natural data and furthermore, is improved for one-dimensional natural and medical data (Dehkordi et al., 2011; Tohumoglu & Sezgin, 2007; Brechet et al., 2007; Cho et al., 2004). Through last decades, EZW has been developed in various modified approaches and becomes the fundamental concept of the modern compression algorithm such as JPEG2000, JPEG-LS. There are still ongoing study on the EZW for multi-dimensional data (Cheng & Dill, 2014;

Pearlman et al., 2002).

The EZW compression method consists of three processes in encoder: **wavelet transformation** for obtaining decomposition coefficients. In wavelet transformation block, the coefficients are truncated related to their algorithm of significance and coded based an algorithm defined in Figure 5.20. The second process is to apply **scalar quantizer** to the obtained wavelet coefficients. The last step is to perform entropy encoding which is specifically **adaptive arithmetic encoder** in EZW.

Due to that embedded zerotree coding is analogous to the precision of a binary finite-precision representation of real numbers, an encoded bit stream can be terminated at any point for desired compression/distortion rate, by using an embedded algorithm. At the same time, the code can reproduce the same image using the remaining code from the halted encoded bit stream (Shapiro, 1993). In the following subsections, the wavelet transform and the EZW algorithm have introduced briefly.

5.3.3 Wavelet Transform

Wavelet transform provides multi-resolution analysis which is an effective tool for compression. The property allows developing practical and simple algorithms commonly used to compress the data in medical applications. Wavelet based algorithms such as EZW, Set Partitioning In Hierarchical Trees (SPIHT) algorithm etc. lead high compression rate thus high dimensional data can be compressed efficiently (Cho et al., 2004). Having defined the wavelet transform for 1D data, it can be adapted to the function of 2D matrix by applying the same process to rows and columns analogously. Wavelet transform for 1D discrete signal $f(n)$ with M length is expressed as follows,

$$W_{\phi}(j_0, k) = \frac{1}{\sqrt{M}} \sum_n f(n) \phi_{j_0, k}(n), \quad j \leq j_0 \quad (5.2)$$

$$W_\psi(j, k) = \frac{1}{\sqrt{M}} \sum_{j=j_0}^{\infty} f(n) \psi_{j,k}(n), \quad j \leq j_0 \quad (5.3)$$

where $\phi_{j_0,k}(n)$ and $\psi_{j,k}(n)$ are basis function that defines in range of $[0, M - 1]$. The signal $f(n)$ can be reconstructed by operating inverse wavelet transform as described,

$$f(n) = \frac{1}{M} \sum_k W_\phi(j_0, k) \phi_{j_0,k}(n) + \sum_{j=j_0}^{\infty} W_\psi(j, k) \psi_{j,k}(n) \quad (5.4)$$

where $W_\phi(j_0, k)$ states for the low frequency component (approximation coefficients) and $W_\psi(j, k)$ states for high frequency components (detail coefficients). $f(n)$ is reconstructed by approximation and detail coefficients. Two-level decomposition in rows of 2D signal is given in Figure 5.16. For the column decomposition same process is repeated.

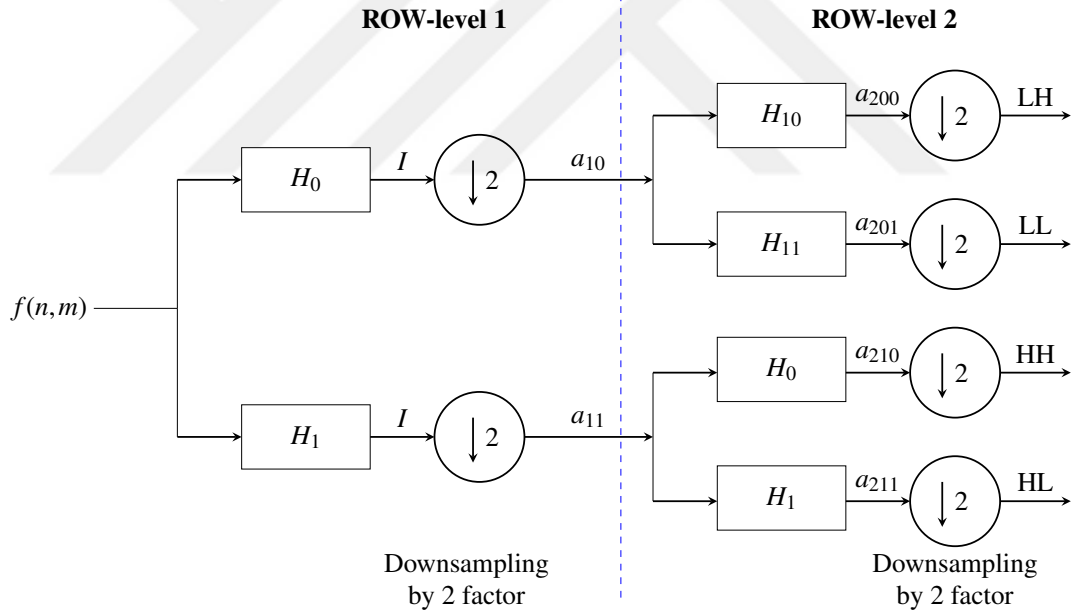
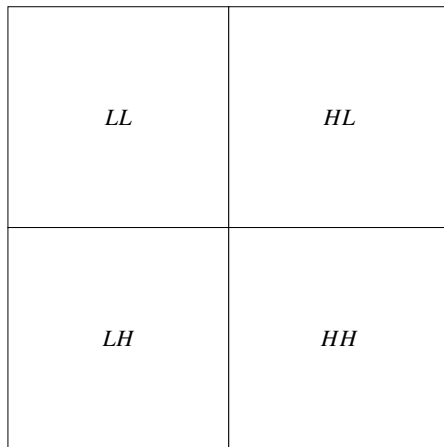
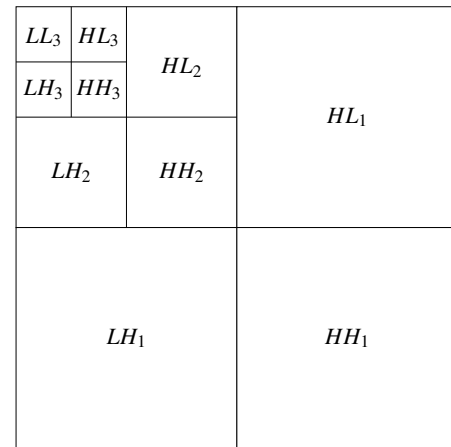


Figure 5.16 Two level wavelet decomposition for 2D data

where $f(n, m)$ is 2D image data, H_0 and H_1 are low and high pass filters respectively. Wavelet coefficients a_{klm} , $k, l, m \in \mathbb{Z}$ and k indicate the level of the wavelet scale, indexes l and m show the detail and approximation coefficients. Multiple levels can be made by repeating the low-pass H_0 and high-pass H_1 filtering simultaneously. The sub-band labeling scheme is shown in Figure 5.17.



(a) Subband labeling for 1 level



(b) Subband labeling for 2 level

Figure 5.17 Subband scheme for 1 and 2 level, 2D wavelet transform

While, the Fourier transform maps the discrete signal $f(n)$ into a one-dimensional sequence of the number called harmonics, the wavelet transform maps 1D data into the two-dimensional arrays, called detail and approximation coefficients. The wavelet has an importance that is pertinent to the localization of components. Therefore, the wavelet is significantly important for tool transient signals, considering on 2D data features: high-frequency component and unpredictable structure of the medical/natural images. The property that is so useful for the compression is to provide the resolution scalable.

Various users in the medical data network have desired to achieve compressed data in a range of resolutions. For providing this demand, the EZW uses resolution scalable property of wavelet. Additionally, unlike the compression methods, quality scalable properties of wavelet based algorithms provides to get compressed data with various Signal Noise to Ratio (SNR) in proportion to numbers of scales. This makes medical data networks more flexible and practical in the aspect of bandwidth usage.

This section has aimed to explicate the concept of the wavelet transform that has been pertinent to EZW algorithm in general. More information can be found in (Sydney et al., 1998; Usevitch, 2001; Shapiro, 1993). Application of the separable wavelet decomposition on natural and medical data have been shown in Figure 5.18 and 5.19. The application of wavelet decomposition has been employed using

separable wavelet filter on 2D coronal view MRI slices. Discrete wavelet transform

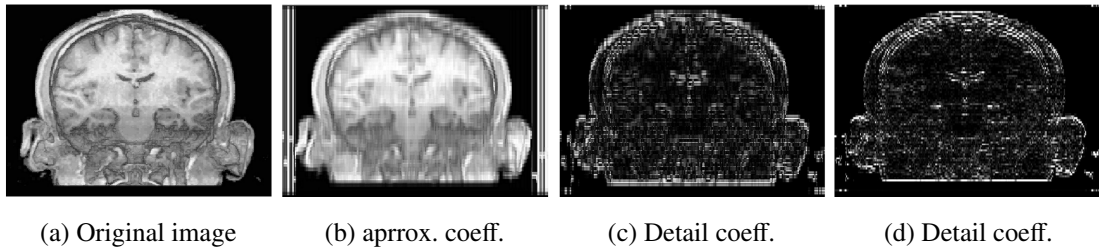


Figure 5.18 Decomposition of 2D medical data (Sudheimer et al., 2019)

has been applied on natural image in two-scale as detail and approximation coefficients and the results are shown in Figure 5.19.

5.3.4 *Embedded Zerotree Wavelet Algorithm*

EZW coding is a simple algorithm that is compatible with numerical applications. Due to that EZW is based on transform based algorithm and using the wavelet in transformation block, it directly affects the performance of both the quantization and the entropy coding. Another remarkable property of the EZW is that bits in code stream is generating according to their *importance* whose algorithm is given Figure 5.20 below whose output is converted the code.

The properties of the EZW algorithm are described below:

- Embedded coding that enables to truncate code stream according to *importance*,
- Transform based compression that provides better entropy and quantization performance,
- Providing well-established subband analysis and compact multi-resolution expression of the data by using wavelet transform,
- Outstanding performance on numerical realisation
- Easily applicable and has computational simplicity

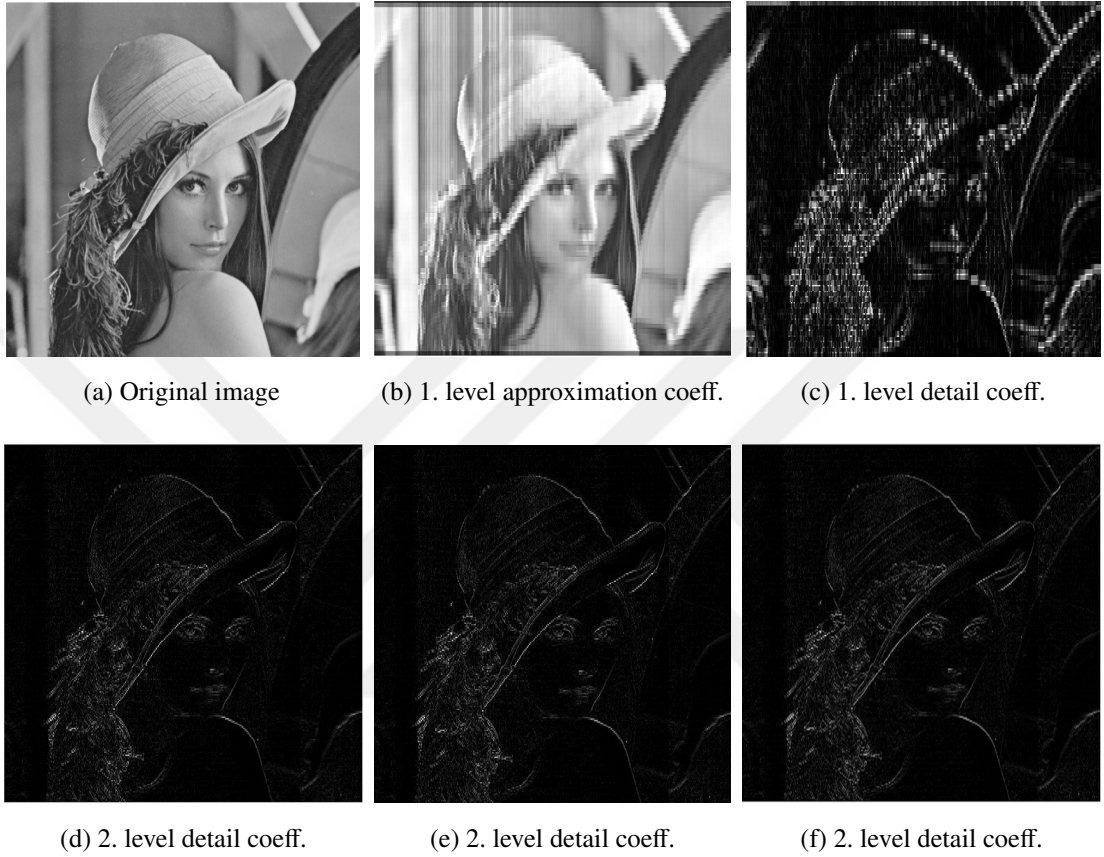


Figure 5.19 Decomposition of 2D natural data (Sudheimer et al., 2019)

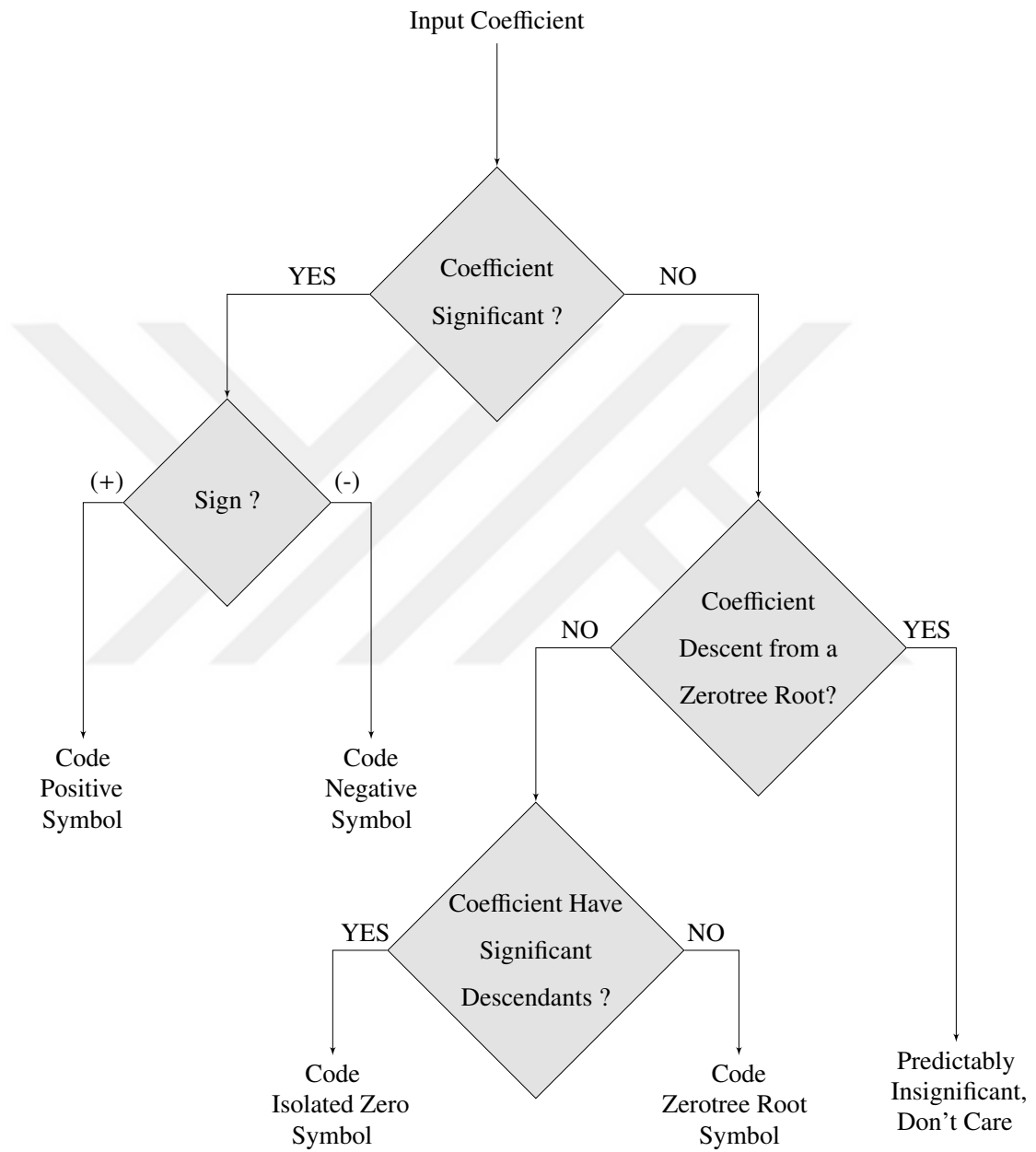
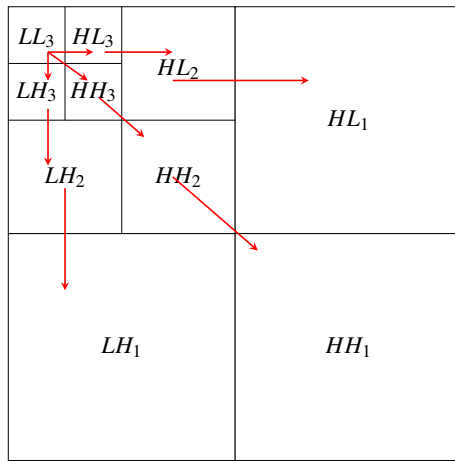
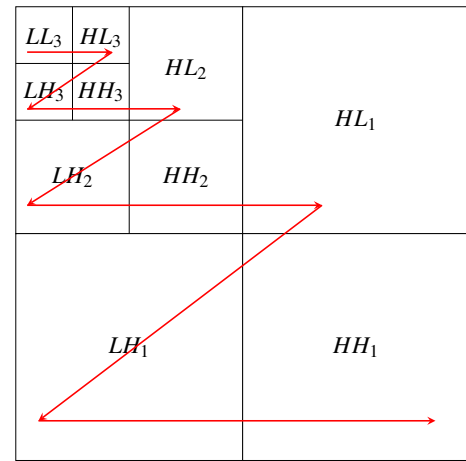


Figure 5.20 Significance map for EZW encoding



(a) Parent child dependency of subbands



(b) Scanning order of the subband for significance map

Figure 5.21 Scanning order of the subband for encoding a significance map (a) The sub-band of the parents to the sub-band of the children is indicated by the arrows. The sub-band of the lowest frequency is located at the top of the left and the maximum one is located at the lowest part of the right (b) Parent should be scanned before the children

- Adaptive multilevel entropy coding with no need to training or pre- stored tables or codebooks and prior information

A discrete wavelet transform which provides a compact multi-resolution representation of the image. Then the coefficients are scanned as a prioritization protocol whereby the ordering of importance is obtained that. The ordering of importance for the coefficient and scanning of direction are shown in 5.21a and 5.21b, respectively.

Application of the EZW algorithm is explained in detail by (Shapiro, 1993). EZW algorithm has applied the discrete wavelet transform to obtain a multiresolution representation of the image. Zerotree coding has created a significance map which indicates the position of the significant coefficients in binary. Successive approximation block has provided embedded coding and multiprecision representation of significant coefficients. Then ordering of the importance has been obtained by a prioritization protocol in terms of precision, magnitude, scale, and spatial localization shown in 5.21a. In importance criteria, larger coefficients have

been considered as more important than smaller ones, independent from the scales that scanned (Shapiro, 1993). Unlike the transitional method, EZW has used adaptive multilevel arithmetic coding in the entropy block. An adaptive coding does not need training or code tables.

Additionally, adaptive codes have been faster than classical methods. Finally, iterative of the algorithm could be terminated at any level of application which provides a wide range of scale for distortion of the metric from losses to lossy compression. The EZW is applied on human brain MRI, the 3D slice of sagittal view with different bases.

5.3.5 Sparse Representation Approach

Wavelet sparse decomposition approach which is used to reconstruct the original image by linearly combining a concise subset of the bases can be used for data compression. Images are represented in separable bases into wavelet space as shown in Figure 5.19. Assume that an $I \in \mathbb{C}^N$ image data with $N \times M$ dimension is given, then define an orthogonal basis as $\{\psi_m\}_m$ where $\psi \in L^2([0, 1]^3)$ and $m \in \mathbb{N}$. Then decomposition of the I image is given as,

$$I = \sum_m \langle I, \psi_m \rangle \psi_m \quad (5.5)$$

m can be restricted as

$$K_M = \{m \in \mathbb{N} : |\langle I, \psi_m \rangle| > T_M\} \quad (5.6)$$

Then the representation of I with the new set of K_M becomes

$$\hat{I} = \sum_{m \in K_M} \langle I, \psi_m \rangle \psi_m \quad (5.7)$$

in the representation of equation (5.7), K_M states for a set of the m that largest inner product whose amplitude above T_M threshold value (Stéphane, 2009). As a result equation (5.7) indicates that an image data I can be represented in a sparse way as \hat{I} . Motivated by this fact, \hat{I} can be regarded as a representation of I signal with the

removal of the redundancy of the original signal. The level of the redundant data can be determined by an appropriate threshold value applied on the wavelet coefficients. In this thesis, hard and soft thresholds have been applied to the images for compression. Eliminating wavelet coefficients have been regarded as redundant. Obviously seen that the coefficients below the threshold have led to the loss of information.

Considering a large class of signals, the number of wavelet coefficients is diminishing rapidly. This property is called unconditional basis that makes wavelets so effective in data denoising and removal of the redundancy for compression (Sydney et al., 1998). Additionally, it has been shown that the wavelets in fields of denoising, data compression, and detection have been nearly optimal for a broad class of signals (Donoho, 1993). Motivated by the theory of sparsity, coefficients in K_M set have been related to redundancy. Conversely, the coefficients which have been in the set $m \in K_M$ belonged to approximated data considering significant coefficient. Therefore, the performance of compression has been directly affected by an efficient threshold estimator. Hard and soft threshold has been used and the results have been assessed according to Mean Square Error(MSE) and Peak Signal to Noise Ratio (PSNR) distortion metrics.

CHAPTER SIX

SIMULATIONS AND RESULTS

In this thesis, a wide range of medical data set is compressed by proposed algorithms and up-to-date standards. For bi-level images, the run-length encoding (2D-RLE and 3D-RLE) and chain rule based (CrS) compression schemes have been developed. For gray level images, the EZW algorithm utilizing different wavelets experienced on the gray-level images data set, and sparse representation approach is suggested to compress medical images.

In this chapter, in turn, the experimental data sets have been demystified, proposed bi-level techniques and their results are presented together with the state-of-the-art standards, and finally, the simulation results of the EZW and sparsity-based methods are presented.

6.1 Medical Image Data Sets

The data sets for testing proposed compression schemes are chosen from several modalities and anatomical objects with diverse spatial structures so that the performance of the compression techniques can be evaluated for a wide range of applications. The abdominal region and vasculature are categories of the performed data set. Expert physicians manually segmented each of the organs of interest to create the bi-level data set. Abdominal CT data sets were acquired after the contrast agent injection at the portal phase with the spiral scanning option. This allows acquisitions in a spiral path as the patient goes through the gantry and offers several advantages for 3D visualization, such as reducing misregistration between slices. This is especially important for compression if the algorithm uses 3D scanning forms. The CT series of 20 data sets are collected from the PACS of Dokuz Eylül University Radiology Department randomly, and the liver is manually segmented for each image individually. All of the image series has 3–3.2 mm inter-slice distance (ISD), and this corresponds to a slice number around 90 (minimum 77, maximum 105 slices).

Sample images for MR-T1 sequence and abdominal aortic aneurysms aortic tree (CT-Angiography) are presented in Figure. 6.1. Four abdominal organs are extracted, including liver, right/left kidneys, and spleen (Figure 2.a). For T2-SPIR, ISD value changes between 7.7 mm and 9 mm and has an average value equal to 8.6 mm. Moreover, the x-y spacing in this sequence varies between 1.63 mm and 1.89 mm, with an average of 1.53 mm. The number of slices for T2-SPIR sequence is 26 as a minimum, 36 as maximum and 30 as average. On the other hand, T1-DUAL sequences include two different series mentioned above. Each series has the same x-y spacing, ISD, and number of slices. For T1-DUAL sequences, ISD has a value between 5.5 mm and 9 mm with an average of 7.84 mm. The x-y spacing value in this sequence is between 1.44 mm and 1.89 mm, and the average value is 1.61 mm. While the average number of slices is 32.8, the minimum number is 26, and the maximum number is 50.

The third data set, see in Figure 6.1g, consists of segmented objects in the second category: vascular trees, see in Figure 6.1h to Figure 6.1l. The proposed compression methods are tested in 19 CT angio data sets from 19 different patients having Abdominal Aortic Aneurysms (AAA) using four different modalities (Figure 2.b) (10). The first data set is acquired by a 16-row detector CT scanner with 3.2 mm ISD from PACS located at our institution. The remaining data sets were selected among acquisitions, which reflect the challenges of daily clinical practice Six data sets (i.e., data sets from 2 to 7) were acquired with a 320-row detector CT scanner with 3.0 mm ISD, six data sets (i.e., data sets from 8 to 13) were acquired with a 64-row detector CT scanner with 5.0 mm ST obtained. The performance of the proposed compression methods for 3.0 and 5.0 mm ISD values are chosen to represent the efficiency of the compression methods as these values are the most frequent ISD values used in clinical routine. Six data sets (i.e., data sets from 14 to 19) were acquired using the 320-row detector CT scanner with 0.8 mm ISD. In total, 3649 DICOM images, which have 512×512 pixel resolution, are segmented manually to extract aorta and the main vessels departing from it.

The figure shows rendered abdominal images Figure 6.2a, segmented in Figure

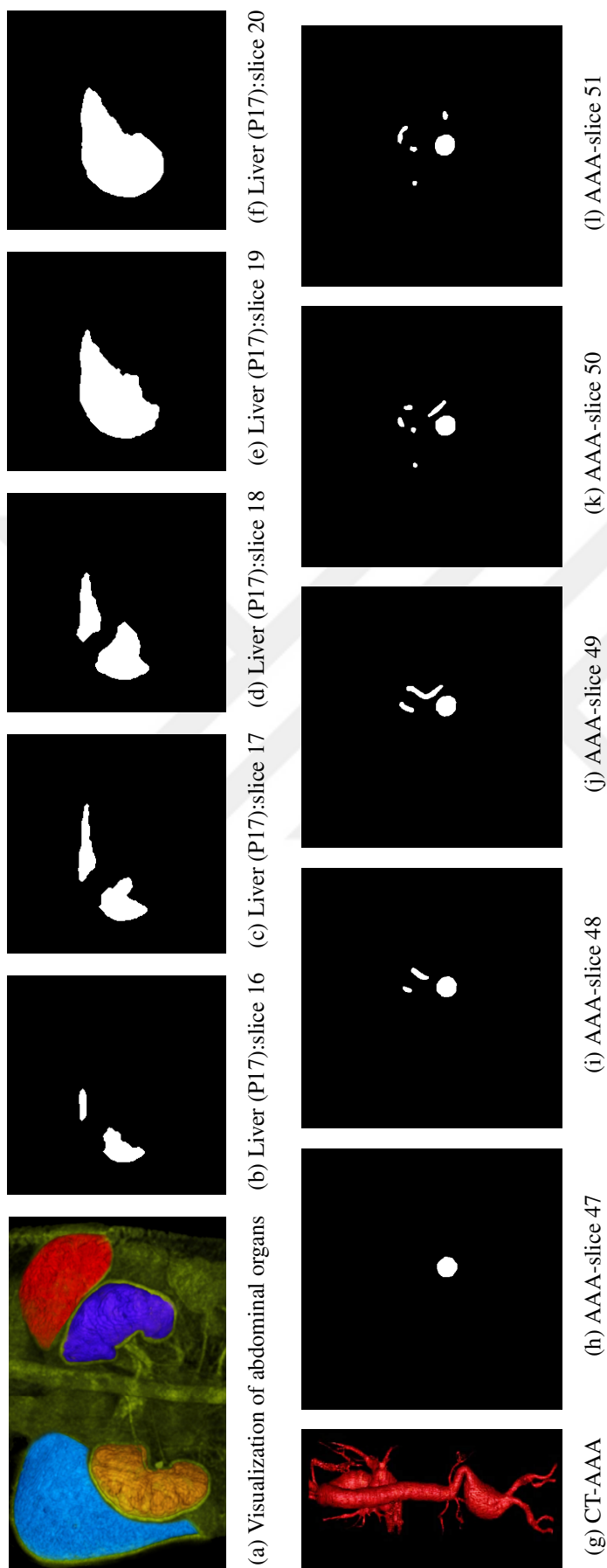


Figure 6.1 Images data set: (b)-(f) T1 weighted segmented bi-level MR sequence (h)-(l) abdominal aortic aneurysms aortic (AAA) tree (CT-Angiography)

6.2b and uniformly distributed data in Figure 6.2c example of volumetric images. It is obvious that the characteristics of the images, such as correlation between inter-slice and intra-slice, compactness, are completely different from each other.

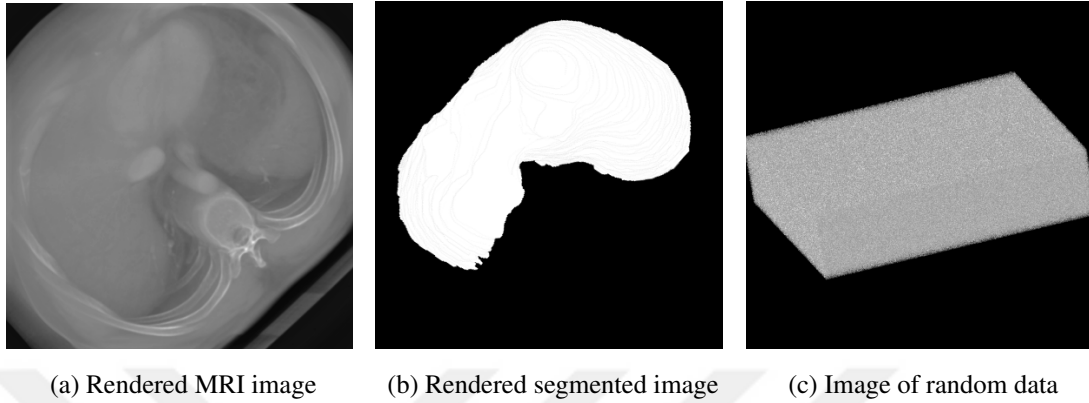


Figure 6.2 Test data: (a) Rendered MRI image (b) rendered segmented binary image and (c) uniformly distributed random data

The gray level medical images are obtained from public brain atlas data set of Michigan State University, Brain biodiversity Bank (Sudheimer et al., 2019). The image are acquired from MRI sagittal section with resolution of 658×500 . Since the scope of the thesis broadly covers lossless compression of medical data, the application of the lossy methods remains in a limited range. The MSE and PSNR are the assessment metrics for lossy techniques.

The data sets of abdominal MR and CT are controlled and approved by the Dokuz Eylül University Medical School Hospital Ethics Committee under grant number 2445-GOA. These data set are outcome of the projects supported by The Scientific and Technological Research Council of Turkey (TÜBİTAK) -Scientific and Technological Research Projects Funding Program- under grant number 116E133.

6.2 State-of-The-Art Binary Image Compression Standards

The proposed methods 3D-RLE and the CrS are compared to up-to-date lossless bi-level compression techniques listed in Table 6.1 for comprehensive verification.

These standards, except the PNG, are only the container of the image data. The PNG has a special register to keep the embedded metadata, which is text information. The metadata may consist of patient knowledge, such as name, gender, demographic statistics, etc. Thus it is a significant instrument for medical images. It is a network-friendly, patent-free architecture that is truly cross-platform and has the features that are useful for teleradiology. Among these features are housing the data (e.g. annotations, patient data, image contributor information) in the alphanumeric string and allowing private information to be access by particular applications. Furthermore, the addition of new meta-information to an image file, combining deflate with pixel prediction, and wide-range control of transparency are some main advantages of the format (Graham et al., 2005). The JBIG and JBIG2 are two most

Table 6.1 Categories of the compression strategy according to lossy and lossless approaches

Method	Approaches		Images	
	Lossless	Lossy	Bi-level	Gray-level
JBIG	✓		✓	✓
JBIG2	✓	✓	✓	
CCITT-G4	✓		✓	
JPEG-XR	✓	✓	✓	✓
JPEG-2000	✓	✓	✓	✓
JPEG-LS	✓	✓		✓
LZW	✓		✓	✓
PNG	✓		✓	✓
ZIP	✓		✓	✓
ABIC	✓		✓	

succeeding bi-level techniques. However, they do not support metadata transmission and does not designed in praöteric form. The ABIC standards is designed by IBM group and achieves considerable compression performance. However, it does not employed by a common application, that may be the result of the patent restrictions.

The compression results of listed methods have been assessed by quantitative lossless compression metrics compression ratio (CR) and bit per pixel (bpp).

6.3 Run-Length Encoding based Compression Scheme

The Run-length encoding is easy-to-implement and well-defined lossless compression algorithm. It is designed in two-dimensional and volumetric approaches (Xu et al., 2004; Rajan & Fred, 2019). Modern compression standards utilize it as data-to-symbol coding as an auxiliary module (Qin et al., 2018; Anantha Babu et al., 2016). Despite these advantages of the algorithm, the compression pipelines harness only standard scanning procedures which restrict the performance of the method. In this dissertation, the RLE is improved from two aspects: firstly, the scanning procedure is widened to capable of new scanning rules and orders. These modifications give rise to morphological coherence between the physical mold of the binary object (i.e., segmented organ) and the procedure of scanning. And Thus, the redundant data could reveal more effectively. The simulation results given in Figure 6.3 shows compression performance for standard zigzag and perimeter scanning rules. The 3D-image (CT segmented liver image of patient number 1) set has 97 slices resolutions of 512×512 . Size of the raw and compressed images are given in Table

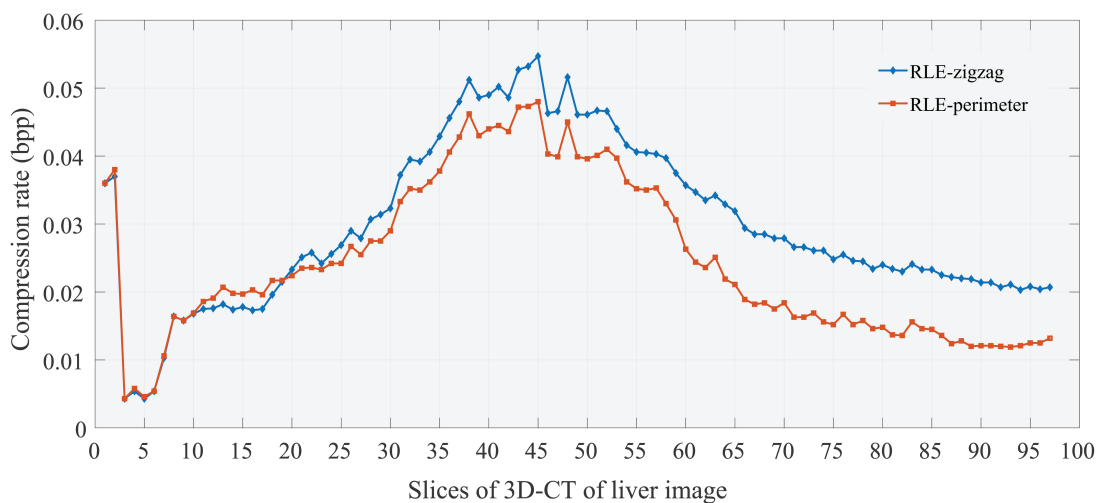


Figure 6.3 Compression performance of the RLE for zigzag and perimeter scanning

6.2. Since the energy of the first images (1 to 10 slices) are remains low level, it is

Table 6.2 RLE techniques applied using standard zigzag and perimeter scanning rule

Method	Image Sets					
	12 th sl.	24 th sl.	36 th sl.	64 th sl.	80 th sl.	total(3D)
Raw data	256	256	256	256	256	24832
RLE-zigzag	4.51	6.55	11.67	8.42	6.14	740
RLE-perimeter	4.89	6.20	10.39	5.61	3.79	609

shown that the scanning rules cannot appreciably affect the compression efficiency. However, the effects of the scanning rules are noticeable in the remaining slices (slice 10 to 97). Consequently, the results show that appropriate scanning rules can significantly contribute the performance of the RLE even if without entropy coder that reform the symbols using variable length coding.

The RLE based proposed method is experienced in two-dimensional mode, namely 2D-RLE. The algorithm has been extended by boustrophedonic, spiral (perimeter), quadrant scanning (Morton), Pi (Hilbert), and chevron besides to generally employed by the systems, see the scanning form in Figure 6.4. It shown that the perimeter,

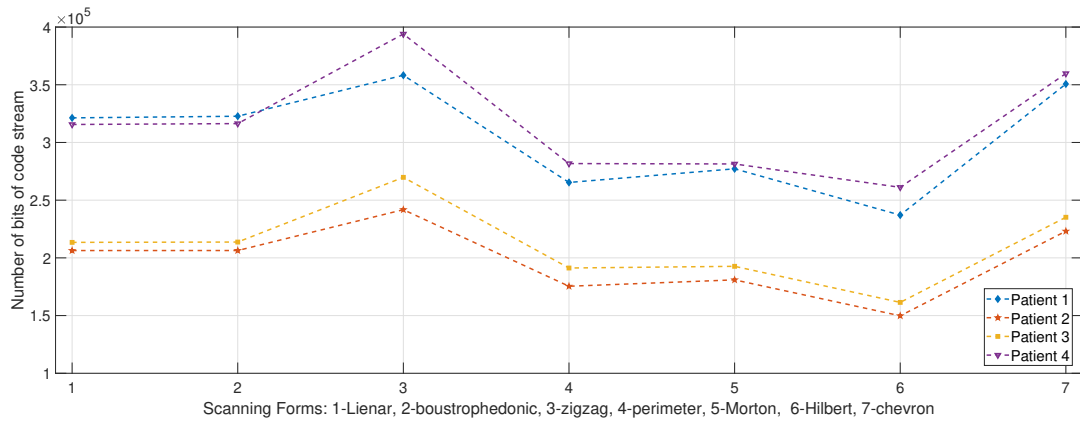


Figure 6.4 Compression performance for the RLE system using different scanning forms

Morton, and Hilbert are three forms that achieve minimum number of bit, which imply the best compression efficiency (Aldemir et al., 2018a).

6.3.1 Volumetric RLE based Compression Algorithm: 3D-RLE

The RLE algorithm is developed for 3D-volumetric images, called 3D-RLE. The technique utilizes the scanning pattern, which are expressed by scanning rules and orders parameters, considering the correlation between the pixels of binary images. When the general forms of segmented binary images have been taking into account, the scanning procedure provides a flexible solution to remap the image matrix in low-entropy sequence. The 3D-RLE is applied on volumetric medical images to unveil the maximum amount of redundancy.

The method was first tested on two-dimensional slices of 3D MRI data and yielded more successful results than the method operated classical scan form. In other words, the algorithm is employed in case of $\mathcal{D} = 1$. Then, the methods is experienced geared various slice-depth and scanning procedure parameters. The Figure 6.5 shows CT data set performance 2D-RLE ($\mathcal{D} = 1$) and the 3D-RLE (optimal \mathcal{D}_o slice depth which is determined as 4) methods compared to existing bi-level compression standards.

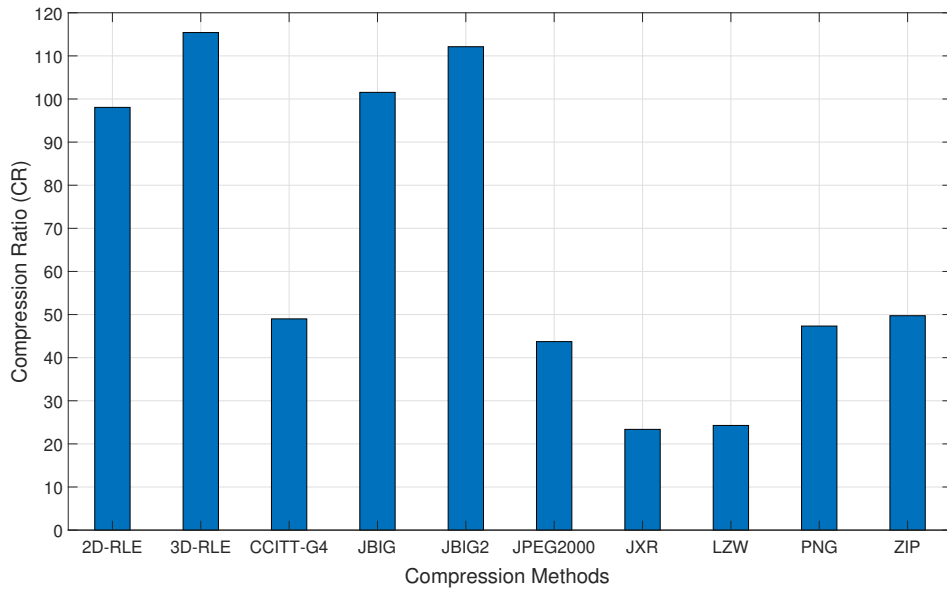


Figure 6.5 The compression efficiencies of proposed and state-of-the-art techniques for the CT images set (the average for all patients)

The Figure 6.6 shows the compression achievement for MR-liver data set (average of MR-T1 and MR-T2 weighted imaging sections) of the 2D-RLE (the slice-depth is

set to $\mathcal{D} = 1$) and the 3D-RLE (the slice depth is determined as optimal \mathcal{D}_o) methods compared to existing bi-level compression standards.

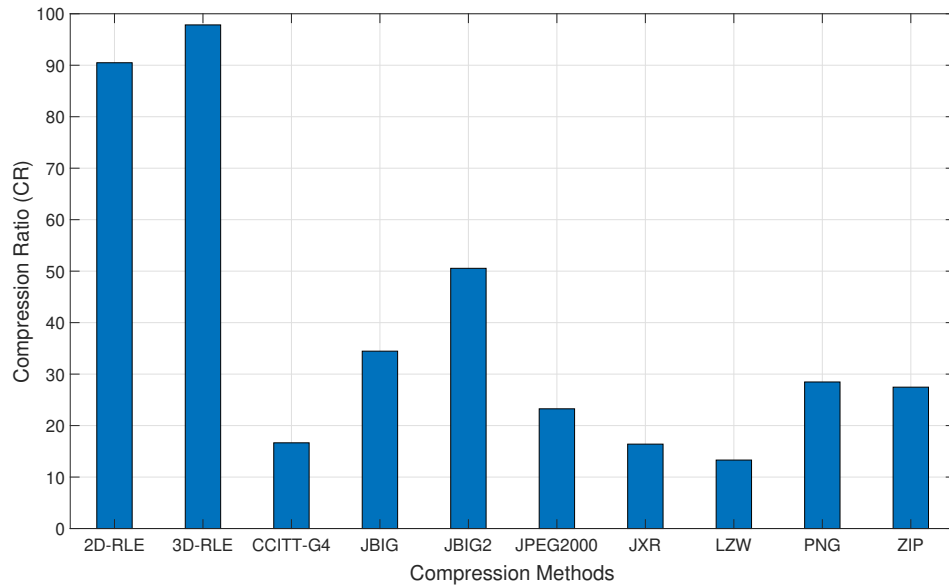
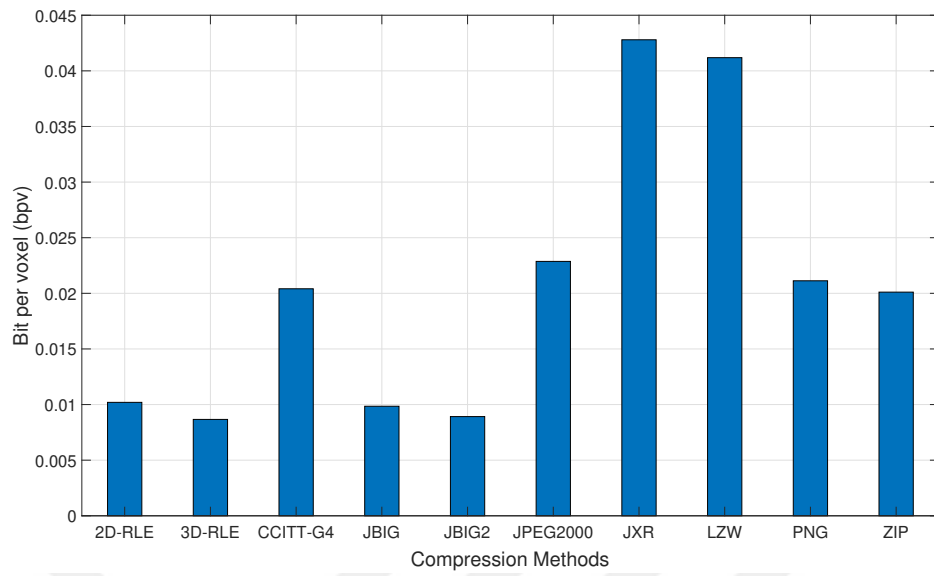


Figure 6.6 The compression efficiencies of proposed and state-of-the-art techniques for the MR images set (the average for all patients)

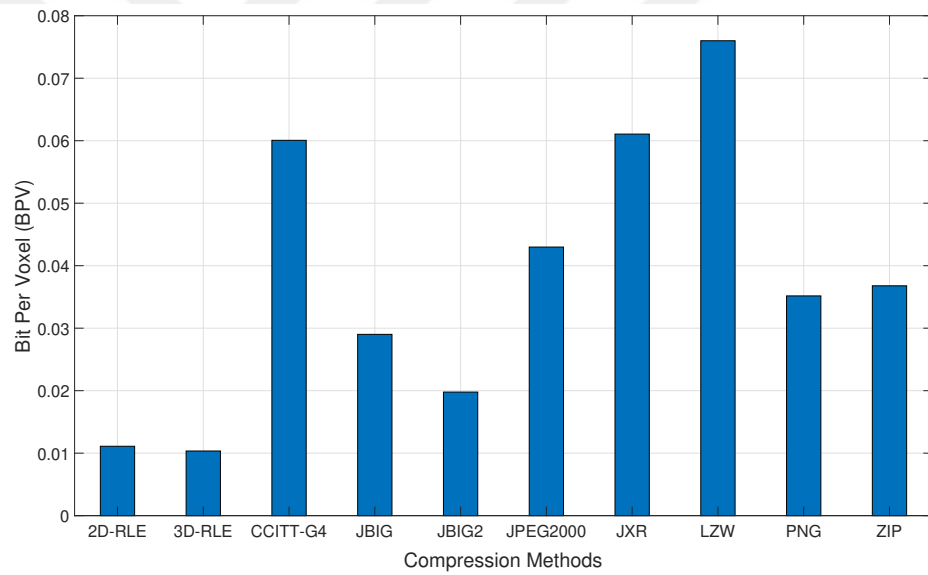
The bit per voxel (bpv) metrics for CT and MR data sets are presented in Figure 6.7a and Figure 6.7b, respectively. One pixel of the raw images could be presented by under 0.01 pixels using the proposed methods. This achievement can unburden the bandwidth capacity of the telemedicine networks.

The optimal slice depth of MR data set is determined as 2 – 3 which indicate less inter-slice relationship compared to the optimal depth of CT images which have slice depth 4. This difference stems from the image acquisition mechanism and is a significant parameter that affects the compression performance. The scanning form are Hilbert, perimeter, in general, for both Figure 6.5 and 6.6.

In point of view of the-state-of-the-art techniques, the performance of the methods remain under the 3D-RLE techniques because of that the algorithm is specifically designed to reveal the redundancy of medical images. The foremost consideration of the 2D-RLE and 3D-RLE methods is to utilize coding redundancy by providing morphological coherence between the shape of the segmented objects and scanning



(a) The performance of the scanning froms for CT data set

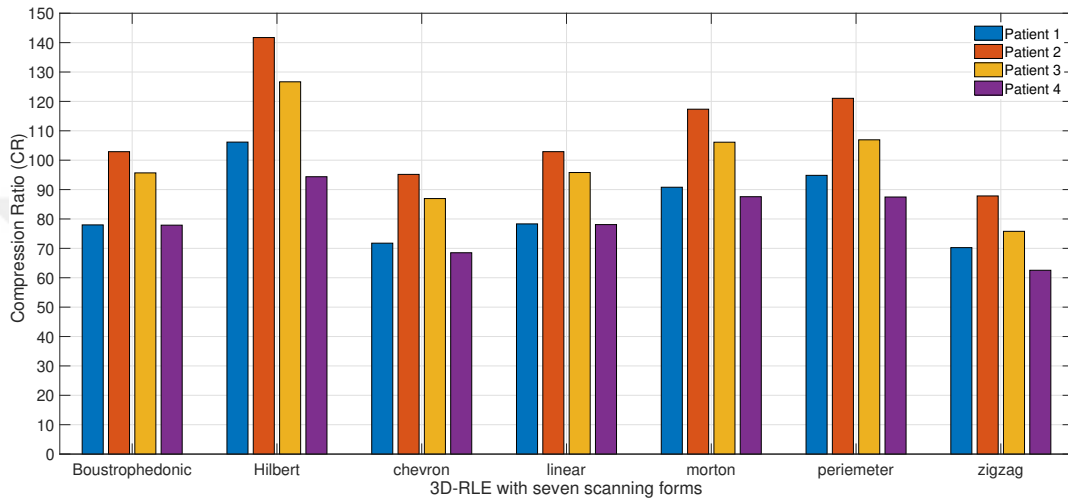


(b) The performance of the scanning froms for MR data set

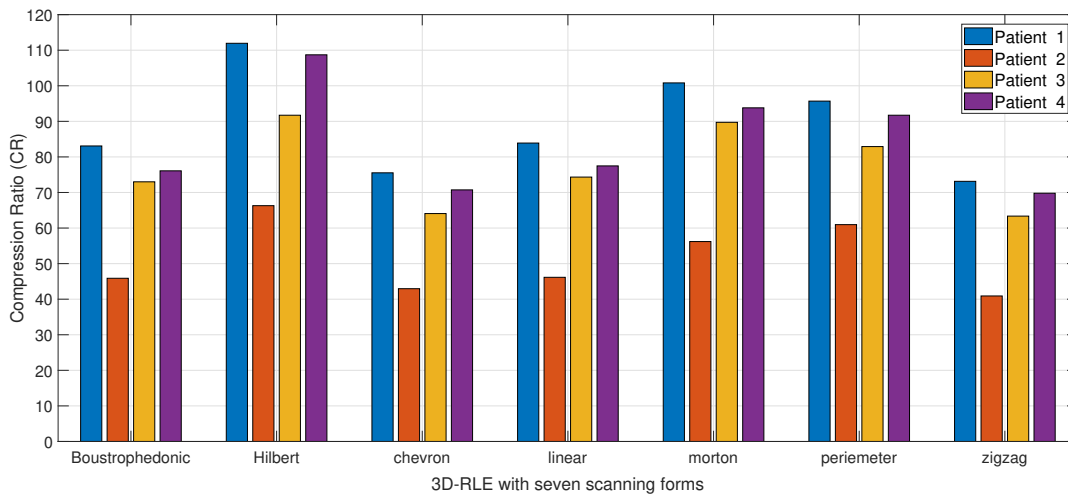
Figure 6.7 The bit per voxel metric for (a) CT and (b) MR data set

procedure. As a result of this motivation, a flexible scanning procedure catch this coherence and resulting in the best compression ratio compared the given group state-of-the-art methods.

The extended scanning form have important impact on the accomplishment of the RLE-based method. The Figure 6.8a and Figure 6.8b present the compression ratios for CT and MR data set, respectively. The Hilbert, which is fractal scanning rule,



(a) The performance of the scanning froms for CT data set



(b) The performance of the scanning froms for MR data set

Figure 6.8 The performance of the scanning froms for (a) CT and (b) MR data set

perimeter and Morton are three most successful scanning form of the proposed 3D-RLE method. An important observation is that the level of CR of MR data set fluctuate in a broad range, which may be regarded as disadvantes of the methods. The

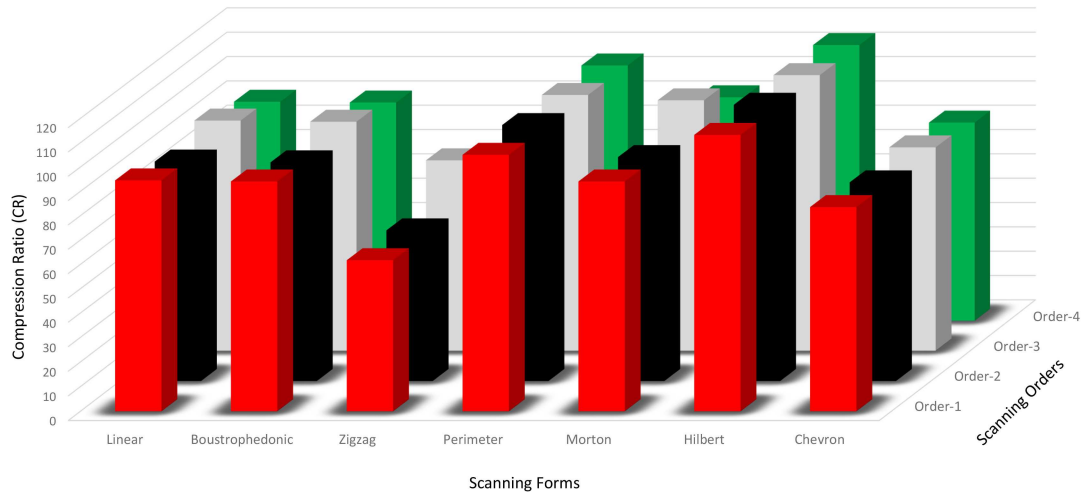
reason of this instabilities arise from the level of non-stationarity. In other words, the non-stationarity of CT is higher than of MR data set. This lead the performance undulate of the method.

A notable observation for the Figure 6.5 and Figure 6.6 is that the overall compression performances on CT data set of RLE based system are greater than the performance for MR data sets. This main reason behind this result is that the ISD of CT-liver volumetric images is fewer than of MR volumetric images. Note that, the higher the ISD, the lower the inter-slice coding redundancy. Considering the other characteristics of medical images, the energy of the CT images is higher of the MR images. This indicates an obvious difference in the amount of information being coded.

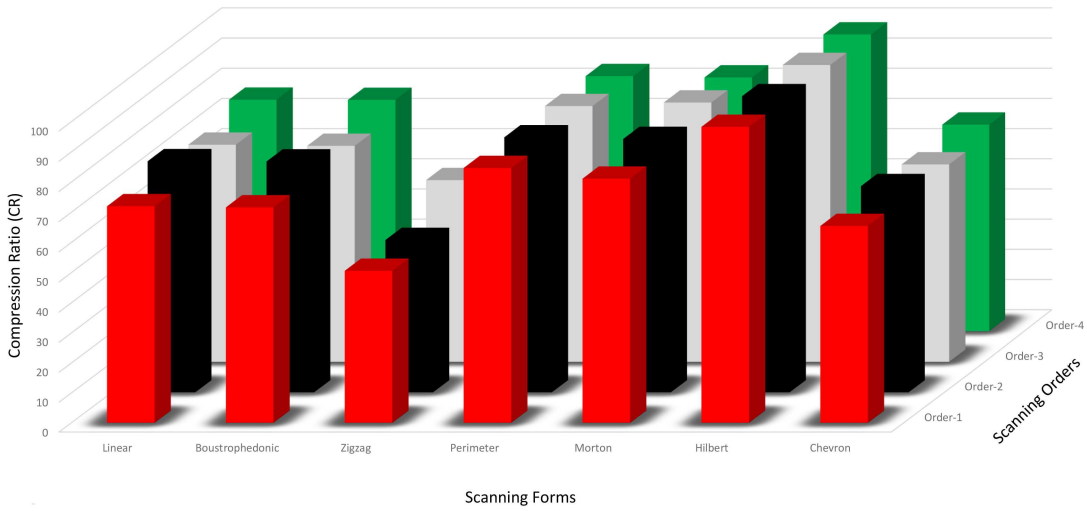
The order is the parameter that indicate the starting and end position of the scanning procedure. This parameter has also impact on the overall performance of the compressed scheme. The effects of the 4 orders for 7 different scanning forms is presented in Figure 6.9a and Figure 6.9b for CT and MRI data sets, respectively. The determination optimal order parameter of the methods is significant in the sense of revealing more redundant data. In this context, order 3 provides the best compression ratio for CT data set, in general. For MRI data set, the optimal order is determined as number 3. Considering CT data set, The performance of the method has the least dependency on the order parameter in the case of Hilbert, perimeter, and chevron. On the contrary, zigzag, boustrophedonic, and linear are the orders that make fluctuation on the performance of the methods in case of utilizing different orders. The same analysis is valid for MR data set - which is expected.

In the case of a data set consists of non-symmetrical objects, one can conclude that the performance of the method is more dependent on order parameters. It is suggested that the compression parameters, including order, should be determined by taking into account the image characteristics to obtain optimal compression rates.

The 3D-RLE also employs inter-slice correlation beside the intra-slice correlation. The slice depth parameter indicates how many slices are figured out to unearth the



(a) Compression efficiency for 3D-RLE employing 7 scanning forms, 4 orders and $\mathcal{D} = 4$ for CT data set



(b) Compression efficiency for 3D-RLE employing 7 scanning forms, 4 orders and $\mathcal{D} = 4$ for MR data set

Figure 6.9 Test data: computed tomography slice and uniformly distributed random data

correlations. For CT and MR image data sets, change of the CR according to the slice number \mathcal{D} is presented in Figure 6.10. It shows that while increasing the slice number, the compression ratio increase until the bound in which the slices are not correlated, or does not have enough correlation. Once this the number of the frame depth is exceeded the optimal case, the volumetric approach losses its ability of the redundancy revealing. In MR imaging, the ISD values of slices are lower than those of CT images. Thus, the

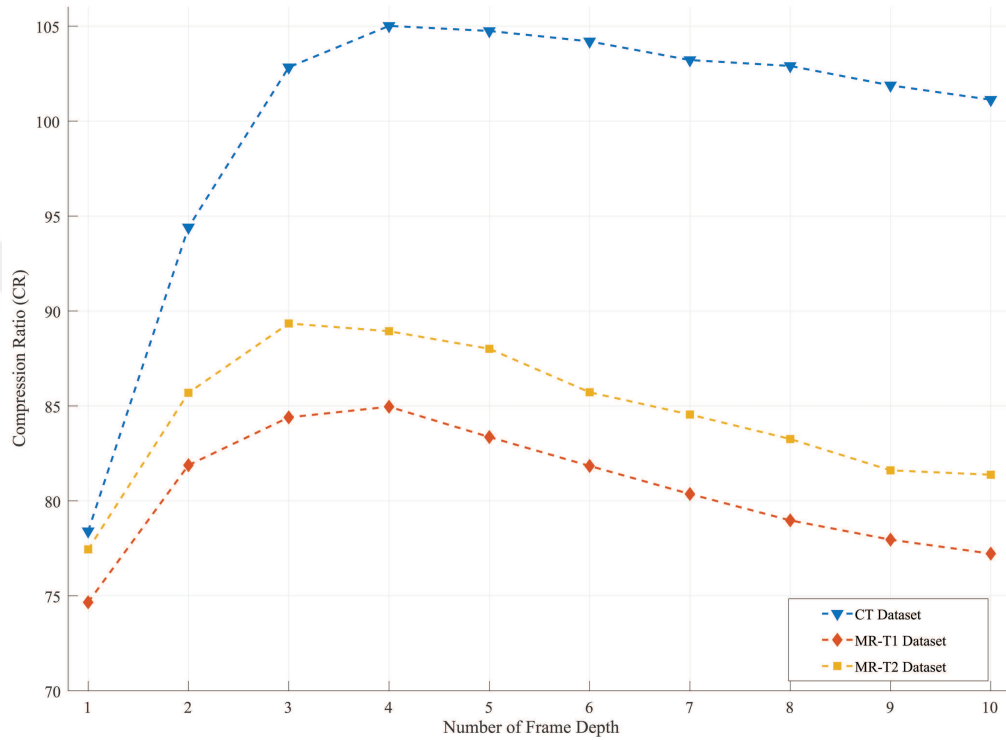


Figure 6.10 Optimality of slice depth

number of correlated slices must be fewer for MR images. This fact can be observed from the Figure 6.10 in which the optimal slice depth of MR (2-3) is less than those of CT images (4-5). Non-stationarity is another fact that contributed to this result. Let's make it clear, the non-stationarity is a measure of common data between consecutive slices.

The simulation has been extended by embodying ABIC and JPEG-LS standards for a more comprehensive assessment. Furthermore, abdominal aortic aneurysms (AAA) data set have a different level of compactness, energy, and non-stationarity properties from the abdominal CT and MR data sets. More importantly, the entropy level of the AAA is completely varies from the liver or kidney images. The results are presented in

Table 6.3 in terms of CR. The metrics indicates that adaptive (ABIC) and context-based (proposed RLE methods) are two the best techniques that achieve more than 100 CR values.

To reflect the achieved CR percentages according to a reference, a second metric called Relative CR_r , which defined in Chapter 2 is calculated by taking the JPEG 2000 format the reference. The results are given Table 6.4. The RLE based systems are designed as context based approaches by considering morphological shape of the organs to determine optimal parameters. The relative compression performance of context-based and adaptive techniques reach over 95%, in general, for all image data sets. The PNG, which can store metadata for telemedicine networks, remains between 70% and 80% ratios for all data set. Besides the considerable performance of ABIC, the method is not designed in parametric form, which makes it not appropriate for e-health networks. A noticeable observation is that the standard deviation of the context-based methods remains in a limited range. This is can be interpreted that the method could provide an appropriate scanning procedure for all objects having different morphological and other characteristics.

Figure 6.11a and Figure 6.11b collectively illustrate the CR for all abdominal organs when MR modality is utilized via T1-DUAL and T2-SPIR pulse sequences, respectively. It is observed from the results that the 3D-RLE ($CR_r = 94.98\%$, $CR = 171 \pm 88$) and the ABIC ($CR_r = 95.49\%$, $CR = 188 \pm 94$) significantly outperform the well-known techniques such as PNG ($CR_r = 77.18\%$, $CR = 36 \pm 13$), JPEG-LS ($RCR = 83.84\%$, $CR = 52 \pm 26$), *JPEG – XR* ($CR_r = 61.99\%$, $CR = 22 \pm 7$), CCIT-G4 ($CR_r = 88.23\%$, $CR = 72 \pm 31$), LZW ($CR_r = 53.19\%$, $CR = 18 \pm 8$), JBIG2 ($CR_r = 87.16\%$, $CR = 68 \pm 33$), and ZIP ($CR_r = 81.4\%$, $CR = 45 \pm 19$). For MR data sets of kidneys, the performance of the context-based and adaptive methods achieve more compression ratio compared to data set of liver and spleen. Besides achieving the best results by far, the performances of 3D-RLE and ABIC vary considerably for different organs due to their data-driven approach. Their average CR performances are found as 105.1 (3D-RLE) and 139.63 (ABIC) for liver, 118 (3D-RLE) and 146.15 (ABIC) for spleen, and 191.15 (3D-RLE) and 184.8 (ABIC) for kidneys showing

Table 6.3 Compression ratios for all data sets

Method	Liver		Spleen		Right Kidney		Right Kidney		CT	
	MR-T1	MR-T2	MR-T1	MR-T2	MR-T1	MR-T2	MR-T1	MR-T2	Liver	AAA
RLE	91.7	91.5	91.6	87.7	183.0	168.8	179.7	169.3	98.1	260.3
3D-RLE	101.1	98.9	118.6	117.4	199.2	181.4	203.9	180.1	115.4	393.3
PNG	23.4	23.1	31.1	30.5	37.4	36.4	36.8	35.5	36.0	70.3
JPEG-LS	28.7	29.6	40.4	40.4	54.7	53.1	53.8	51.4	49.6	212.3
JPEG-XR	16.9	18.0	17.8	17.6	21.2	20.6	21.4	20.4	22.6	40.7
CCITT-G4	48.9	47.6	58.6	58.1	64.4	63.8	64.8	63.6	98.7	151.8
LZW	12.5	12.5	14.0	14.0	15.2	15.2	21.4	15.0	24.2	38.3
JBIG2	49.2	51.7	51.6	51.2	56.2	55.6	56.2	55.1	107.6	148.5
ZIP	26.5	26.7	35.4	34.7	46.7	44.9	45.5	44.9	48.1	94.8
ABIC	104.4	100.3	148.2	144.1	188.3	181.9	189.3	179.7	214.2	432.8

Table 6.4 Relative compression ratios for all data sets (reference is jpeg2000 which is common standard employed by telemedicine networks)

	Liver		Spleen		Right Kidney		Right Kidney		CT	
	MR-T1	MR-T2	MR-T1	MR-T2	MR-T1	MR-T2	MR-T1	MR-T2	Liver	AAA
RLE	95.4	95.6	92.6	92.3	94.9	94.9	94.8	94.7	92.7	92.1
3D-RLE	95.8	96.0	94.3	94.2	95.3	95.2	95.4	95.0	93.8	94.8
PNG	81.9	82.7	78.1	77.9	75.1	76.2	74.6	74.5	80.0	70.8
JPEG-LS	85.2	86.5	83.2	83.3	83.0	83.7	82.6	82.4	85.5	83.1
JPEG-XR	74.9	77.9	61.8	61.6	56.1	58.0	56.2	55.7	68.1	49.6
CCITT-G4	91.3	91.6	88.4	88.4	85.6	86.4	85.6	85.8	92.7	86.5
LZW	66.1	68.1	51.4	51.8	38.8	42.9	56.2	40.0	70.2	46.4
JBIG2	91.4	92.3	86.8	86.8	83.4	84.4	83.4	83.6	93.3	86.2
ZIP	84.0	85.3	80.8	80.5	80.1	80.7	79.5	79.9	85.0	78.4
ABIC	95.9	96.0	95.4	95.3	95.1	95.2	95.1	95.0	96.6	95.3

increased CR directly proportional to the compactness of the organ ($P < 0.05$). However, the algorithms, which have limited performance, show very similar compression ratios independent of structural characteristics.

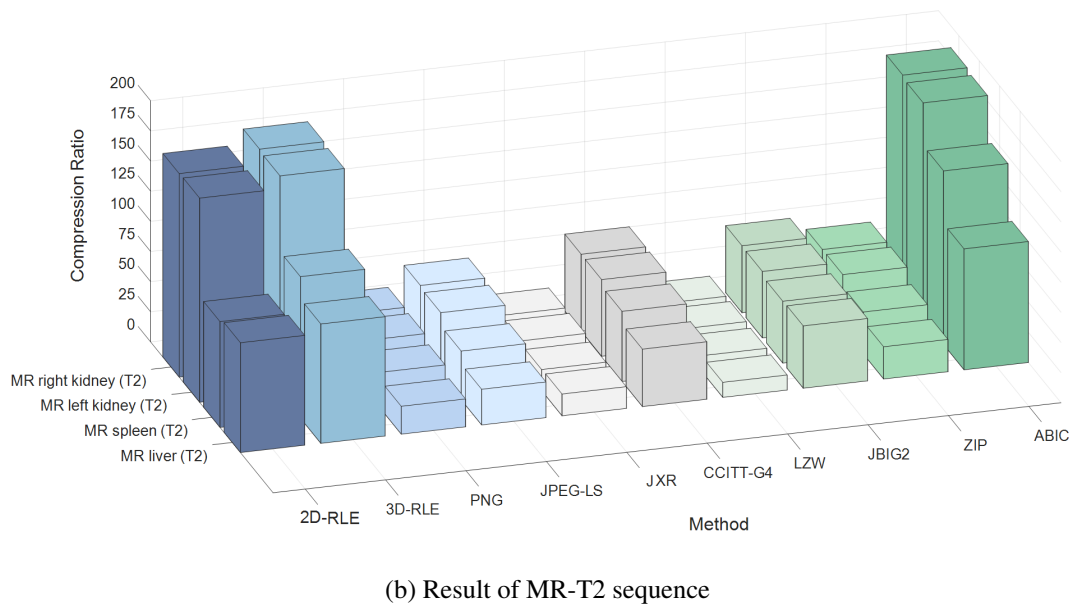
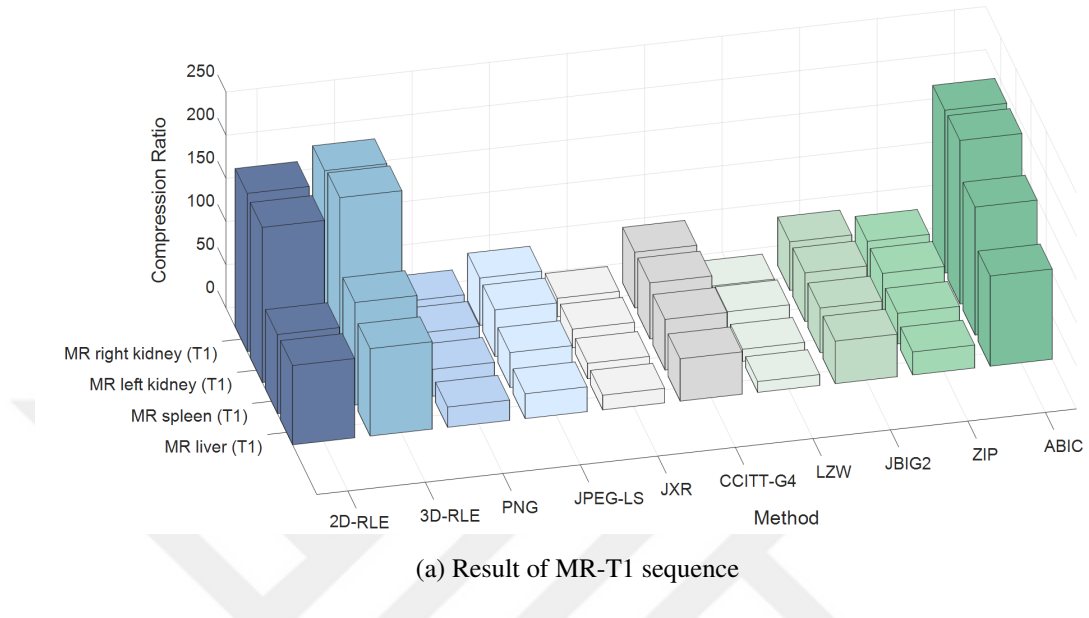


Figure 6.11 Compression ratio for segmented binary abdominal organs acquired by (a) MR-T1 and (b) MR-T2 sequences

In general, the method achieves the highest CR for the kidneys and the lowest CR for the liver. Considering 3D-RLE, this result can be attributed to the sensitivity of the method to spatial coherence, which changes due to compactness, entropy, and

structural morphology of the organs to be compressed. Since the 3D-RLE algorithm releases the inter-slice redundancy, the lower the ISD of the data set, the higher the compression performance. The results attest to the hypothesis as CR of CT images is higher than the MR data sets. The independent sample test is performed and the $P < 0.01$ for all data sets.

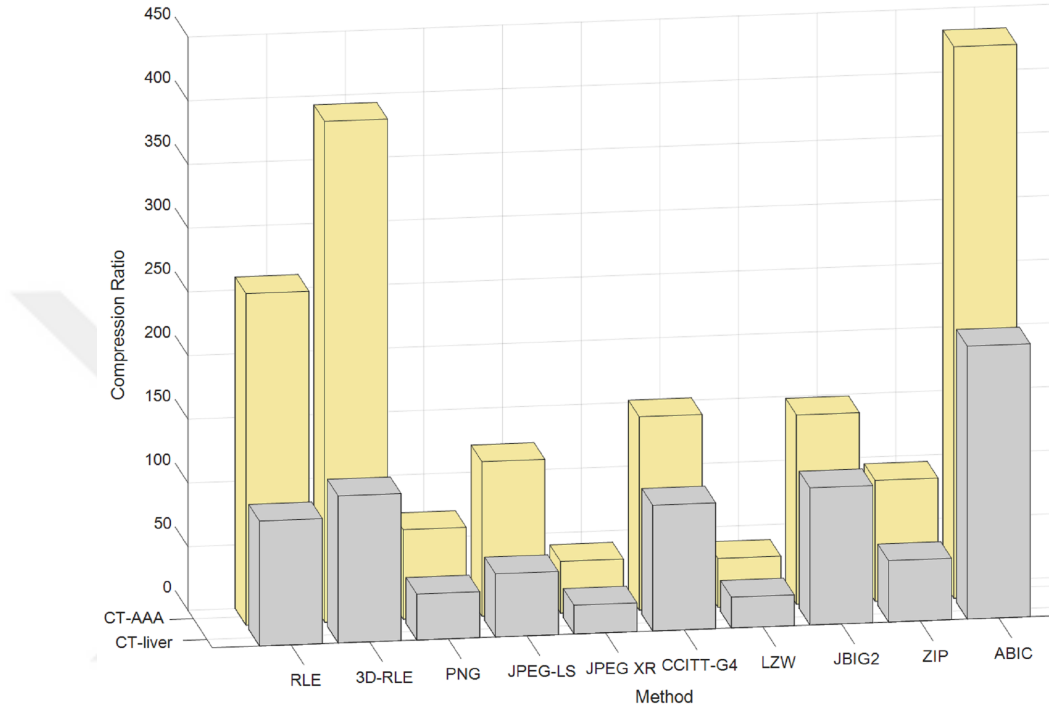


Figure 6.12 Compression Ratios for segmented organs acquired by CT (CT-AAA and CT-liver)

Considering all CT result in Figure 6.3, the 3D-RLE and ABIC (214 ± 21) outperform all other methods by providing significant compression efficiency. Although 3D-RLE also has high CR (115 ± 8), it is less than half of ABIC and very close to JBIG2 performance (108 ± 7). On the other hand, when MR is considered, 3D-RLE and ABIC performances are almost equal to each other and they are both significantly better than the rest of the algorithms. This can be supported by the fact that the redundancy of the high-dimensional (more spatial detail) data can be released more efficiently by the adaptive and context-based algorithms employed by the ABIC and 3D-RLE, respectively. A noticeable observation is that the standard deviation of the context-based methods remains in a limited range. This can be interpreted that the method could provide an appropriate scanning procedure for all objects having different morphological and other characteristics.

Consequently, experimental results have shown that a specially established compression algorithm can outperform general-purpose compression standards. This achievement is accomplished by providing a flexible scanning procedure for RLE algorithm. This approach is reconsidered by suggested a novel volumetric algorithm (3D-RLE) to unveil the inter-slice redundancy existing in the medical images. Furthermore, the proposed methods have been designed in parametric to be able to be integrable into telemedicine networks. Hereby, the 3D-RLE method achieved an approximate 5% and 25% higher CR than the best state-of-the-art method for CT and MRI data set, respectively.

The simulation results have shown that the scan forms and orders have primarily affected compression performance of the methods. Therefore, determining appropriate scan form and order for medical data taking into account the physical mold of the segmented organs is the crucial point for accomplish higher compression ratios. The results have been compared to up-to-date standardization of compression such as JPEG family, PNG, BMP, TIFF, GIF.

The 2D-RLE and 3D-RLE lossless compression strategies have been simulated on CT, MR-T1, MR-T2 and CT-Angiography data sets. Firstly, 20 patients three-dimensional images have been compressed slice by slice via 2D-RLE algorithm.

Boustrophedonic, spiral, quadrant, Pi, linear, chevron, and zig-zag scan forms have been used during the numerical simulations. Hilbert, which is a fractal scanning form, has been determined as optimal scan form because that has been provided the most successful compression ratio in general.

The CT data set is compressed by proposed pipelines and state-of-the-art techniques. The results are presented in terms of CR that is shown in Figure 6.12. The results confirm that the proposed RLE based system is able to reveal a considerable redundancy regardless of that it utilizes 2D or 3D approaches.

The MR data sets are compressed by proposed pipelines and state-of-the-art techniques. The results, the average value of the T1-weighted and T2-weighted

imaging sequences, are given in terms of CR, in Figure 6.11.

The methods achieve higher compression ratio for CT data set, compare to the compression efficiency for CT and MR data set. The causation behind this result is that the intra- and inter-slice correlation in CT data set is higher than the those of the magnetic imaging data set. Since the 3D-RLE algorithm releases the inter-slice redundancy, the lower the ISD of the data set, the higher the CR. The results confirm the hypothesis as CR of CT is higher than the MR data sets.

The run length coding based two lossless compression methods namely 3D-RLE has been proposed for binary biomedical data. Both algorithms have been extended scan forms besides to commonly used zig-zag and linear scan forms. The simulation results have shown that the scan forms and orders have primarily affected compression performance of the methods. Therefore, determining appropriate scan form and order for medical data taking into account the physical mold of the organs is the vital point for unearth high level of redundancy.

The proposed 3D-RLE method is designed to be lossless, since any information loss may cause a diagnostic error. All blocks of the pipeline are also lossless processes as explained in the following: the first block is the volumetric matrix scanning that scans the image in a volumetric manner and codes voxels having the same intensity level as identical. Otherwise, a header h_i is used as the escape character for non-identical voxels through the depth D to satisfy the Uniquely Decipherable (UD) requirement, where i subscript denotes the index for voxel position. The details of mathematical expression for the header is given in the revised manuscript (see the pseudo code of the proposed algorithm in Table 5.3 and Table 5.4). The second block is Run that creates the vector of symbols corresponding to the sequence constructed in the previous step. These symbols are the number of re-occurrence together with the intensity of the voxels. This process also satisfies UD. In the last step, entropy-Huffman coding is performed as a variable length coding to create compressed data, i.e. bitstream.

Compressed images can be perfectly reconstructed by the 3D-RLE decoder which performs the identical inverse operations of the encoder. As the 3D-RLE and the

state-of-the-art methods are lossless, CR and bpv are used as the figures of merits instead of the lossy compression metrics: the SNR and the NMSE. All compressed images are tested during the reconstruction process of the decoder. The compressed data are also controlled by radiology specialists of the Dokuz Eylül University Radiology department since the method is going to be integrated into a DICOM 3D-presentation state object. Consequently, the decoded images are tested by the quantitative assessment metrics to avoid any loss of information.

6.4 The Chain Rule based Compression System

By the proposed Crs system, the chain code is employed as data-to-symbol coding and run-length encoding is employed to reveal the redundancy of the chain code symbols. The run-length symbols are finally transformed to codestream by Huffman entropy coding block. The segmentation algorithm in study of (Selver et al., 2008) is performed to obtain segmented bi-level liver images. The data sets are compressed by the CrS system of which the pipeline was illustrated in Chapter 5.2.

Since the CrS is designed in two-dimensional approach, every slice of volumetric images is compressed slice-by-slice. The method extracts the boundary of the segmented liver and executes the chain rule for obtaining symbols. In the case of the liver having 2 or more independent pixels areas, which are the most common case, a sample for liver as shown in Figure 6.13, regions in the image are separated by labeling algorithm and then the chain is exploited. These independent regions of the symbols are codified using a *header* for being able to decipher the volume in decoder block.

The simulation results of the RLE-based and the chain system are compared to PNG for 5 patients in Figure 6.14a in terms of the number of bits of compressed data. The accomplishment for remaining patients are presented in Figure 6.14b. From the figure it is apparent that the CrS can uncover the redundancy part more than of the RLE based and PNG systems, as it is expected.

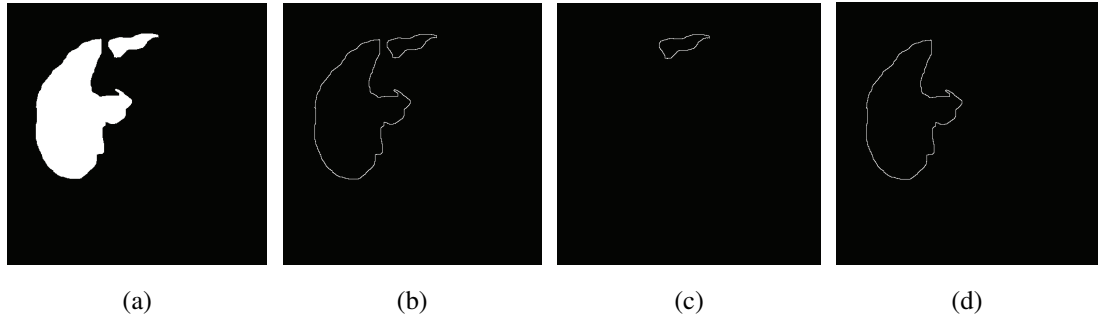
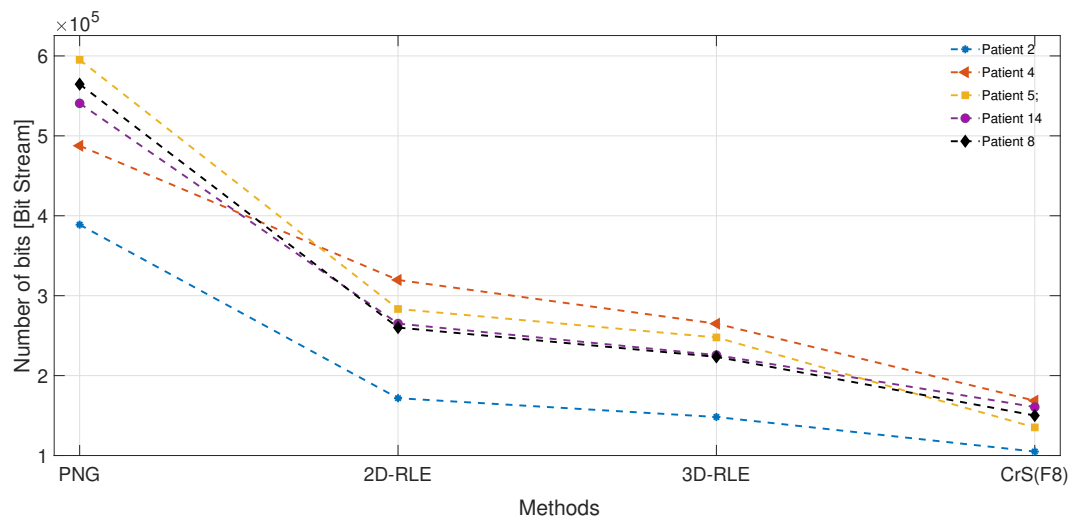


Figure 6.13 Segmentation boundary extraction of the independent regions of the livers (a) Segmented liver slice (b) Boundary extracted form of the segmented liver slice (c) The first part of separated slice (d) The second part of separated slice

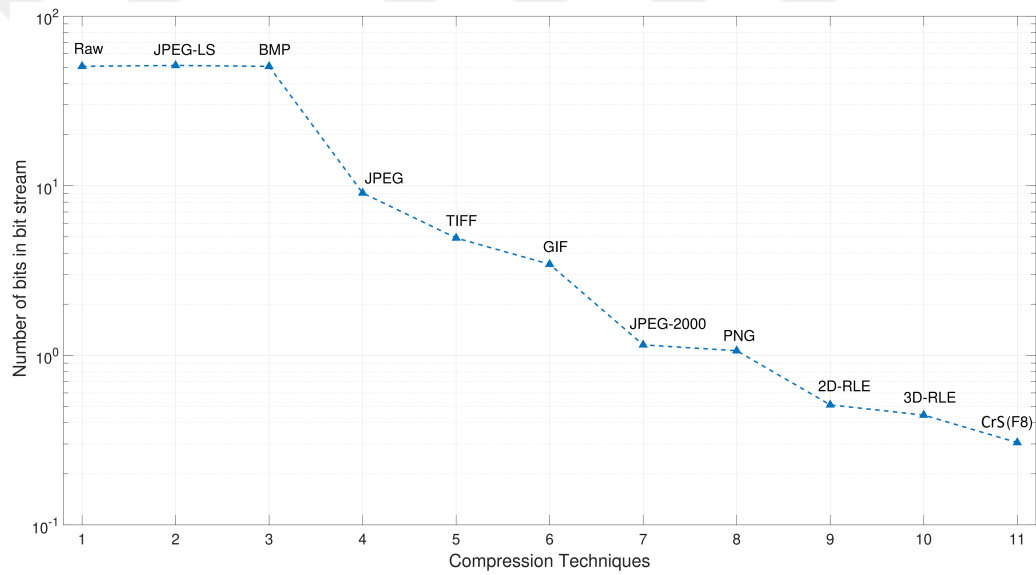
The simulations (average) results of the proposed methods and the state-of-the-art standards for all patients have been reported in Table 6.6a (MR-T1), Table 6.6b (MR-T2), and Table 6.6 (CT) in terms of number of bits. The results are presented as the number of bits because of that the CrS system achieves almost 10000:1 compression ratios, which is hard to illustrate together with the state-of-the-art whose performance remains under the 500:1 ratios. The data sets consist of various organs such as kidney, liver, spleen, and aortic aneurysm.

The performance of some state-of-the-art and proposed CrS technique are shown in Figure 6.15a and Figure 6.15b for CT-AAA and CT-liver data sets, respectively. The chain code based system outperforms the RLE based systems and the other state-of-the-art techniques in the sense of quantitative assessment metrics. It employed by the F8, F4, 3OT, NAD, and MNAD chain rule, which has plenty of movement capabilities, for data-to-symbol coding. The system can be extended with extra chain rules such as vertex and in volumetric approach. The MNAD rules employed idle symbols such as {30,31,32} to reduce the entropy of the resulting chain code symbol sequences.

The chain code based system (the CrS) has been applied to M-T1 and MR-T2 weighted image data sets: left and right kidney, spleen and vessel images. The performance of the chain code based system for various chain rule is presented in Table 6.6a for MR-T1 weighted, Table 6.6b for MR-T2 weighted and Table 6.6 for



(a) Compression performance of the proposed method and modern standards(for typical 5 patients)



(b) Average (20 patients) compression performance of the method and modern standards

Figure 6.14 Compression performance of the CrS system employed *F8* compared to other standards

Table 6.5 Efficiency of compression for the CrS compression systems on MR data sets

Dataset	Chain Rule									
	F4	F4-RLE	F8	F8-RLE	3OT	3OT-RLE	NAD	NAD-RLE	MNAD	MNAD-RLE
Liver	13272	15910	13608	11019	9559	10278	10209	7689	7614	10222
left kidney	2847	3344	3012	20616	2082	2395	1599	2039	1611	2085
right kidney	2726	3188	2918	2004	1988	1934	1509	1972	1523	2007
spleen	4732	5858	4771	3733	3388	3576	2689	3571	2684	3591

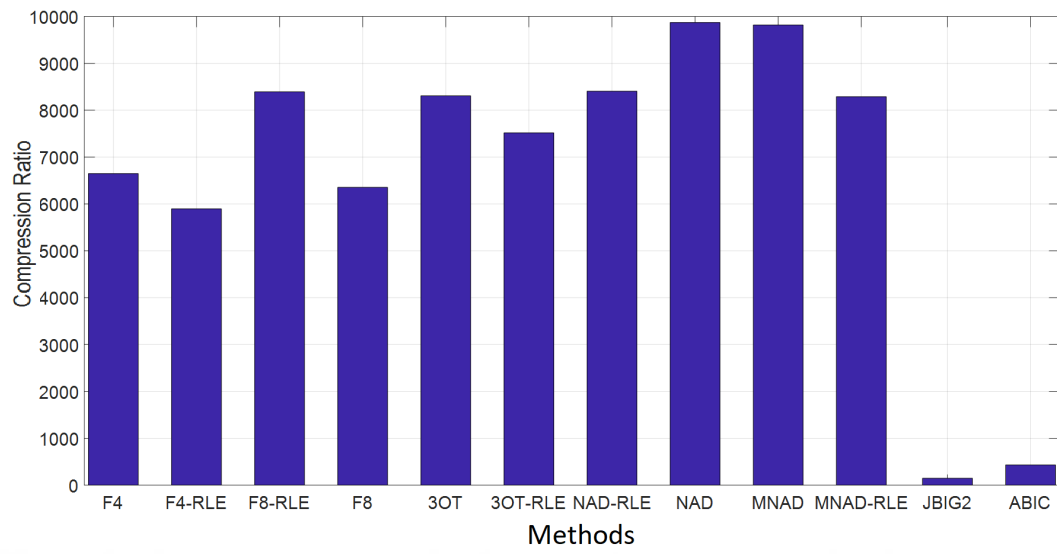
(a) MR-T1 Weighted

Dataset	Chain Rule									
	F4	F4-RLE	F8	F8-RLE	3OT	3OT-RLE	NAD	NAD-RLE	MNAD	MNAD-RLE
Liver	10361	12392	10772	8799	7473	8069	6051	7986	5970	7958
Left kidney	2853	3341	3031	2065	2068	1982	1569	2004	1566	2040
Right kidney	2758	3202	2949	2046	2011	1973	1526	1970	1530	2003
Spleen	4862	5935	4926	3672	3493	3576	2716	3525	2702	3565

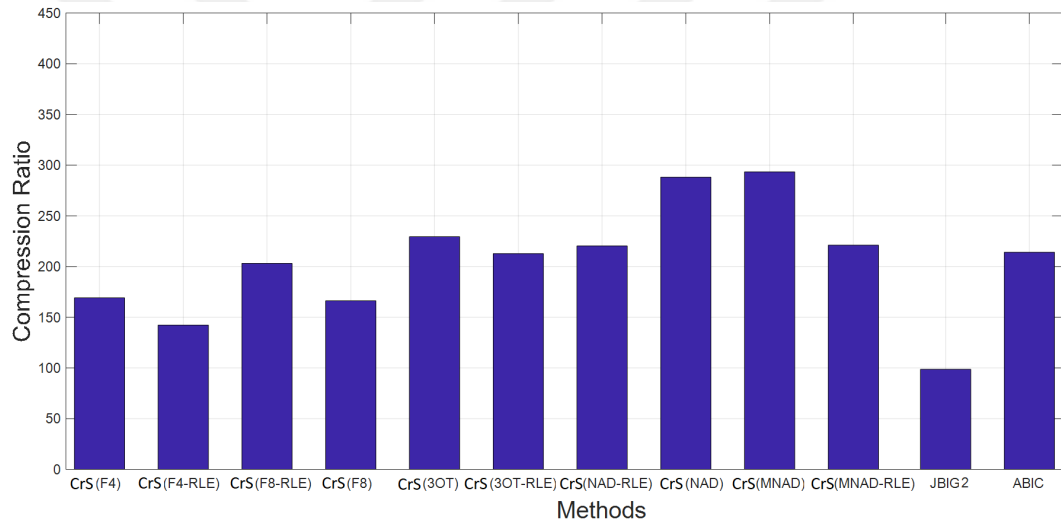
(b) MR-T2 Weighted

Table 6.6 Efficiency of compression for the CrS compression systems on CT data sets

Dataset	Chain Rule									
	F4	F4-RLE	F8	F8-RLE	3OT	3OT-RLE	NAD	NAD-RLE	MNAD	MNAD-RLE
Vessel	4852	5366	5034	4026	4059	4387	3552	4026	3566	4067
Liver	148955	177044	151511	124013	109794	118418	87417	114323	85860	113961



(a) CT-AAA image data set



(b) CT-liver image data set

Figure 6.15 Compression performance of CrS system compared to other standards

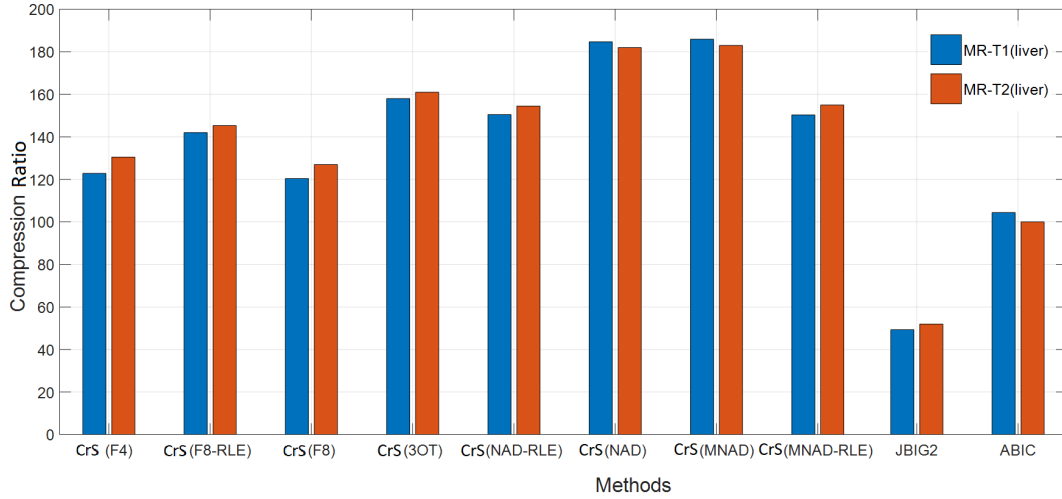


Figure 6.16 Compression ratios for MR-T1 and MR-T2 using the CrS

CT image data sets. The results show that since chain code compress the images using only the boundary and location information of the segmented objects, it outperforms the state-of-the-art compression standards. The performance of the system depends on the chain rule. The entropy of the resulting chain symbol sequence decreases significantly in the case of optimal selection of the chain rules. The CrS has some disadvantages in sense of the high-entropy existing. Since the algorithm extract the boundary and store location pixel of every object, codestream for high-entropy image increase and compression efficiency decreases. On the other hand, the chain code based system generally achieve more than 1000:1 compression ratios which are considerably higher than the ratio of the up-to-date compression standards such as JBIG family.

6.5 The EZW Compression

Since the termination of the wavelet coefficients was performed corresponding to importance map, the image artefacts generally seen in DCT based techniques such as JPEG, did not occurred in EZW.

6.6 Sparse Representation based Compression

The simulations have been done on medical images for haar and curvelet bases shown in Figure 6.17 with hard and soft threshold. The results of haar bases have been shown in Figure 6.19 and Figure 6.19, and the soft threshold results have been shown in Figure 6.20 and 6.21. Curvelet results for hard and soft threshold has been shown in Figure 6.22 and 6.23, respectively.

The threshold level has a significant impact on the compression performance. As the threshold level increases, the compression performance significantly improves considering both groups of data and all bases. On the other hand, the processing time for encoding and decoding increases proportional to the decrease of the threshold level. Therefore, in the fields that the loss of information is not so crucial, lower threshold level can be preferred. On the other hand, in the cases in which the image quality is indispensable, the level of threshold can be determined as low as possible. As a result, the threshold level and processing time are two trade-offs of the compression.

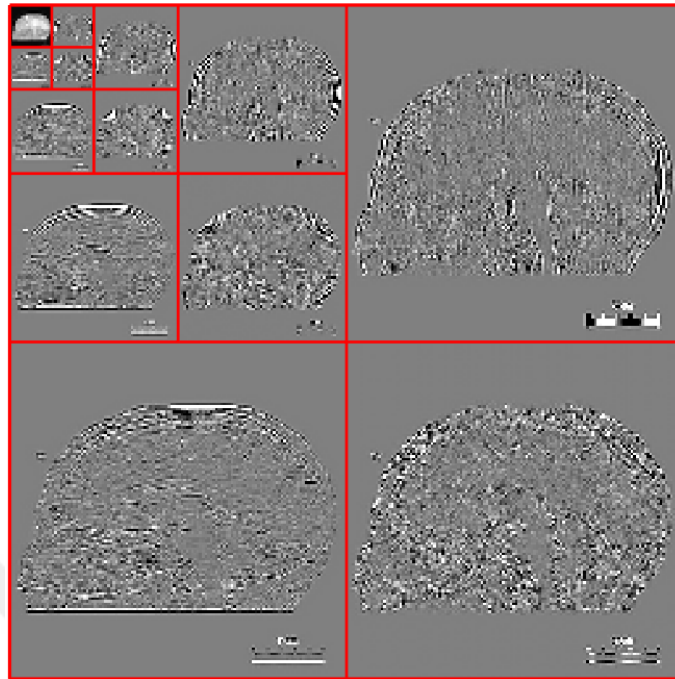
Result of sparse approach in compression using hard threshold (haar basis) are presented in Figure 6.19 and Figure 6.18.

Result of sparse approach in compression using soft threshold (haar basis): Result of sparse approach in compression using soft threshold (haar basis):

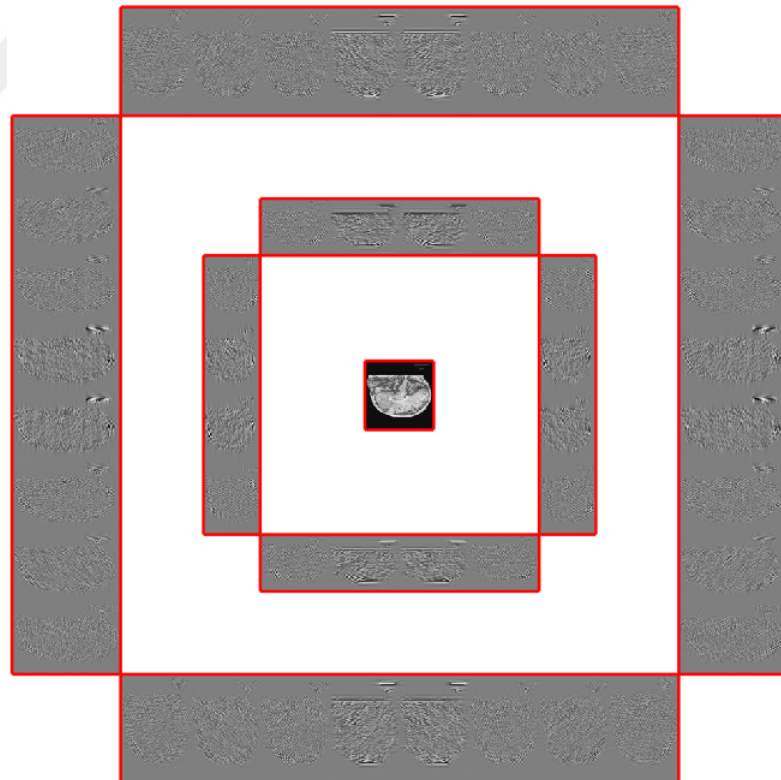
Table 6.7 PSNR metrics assessment (medical image)

	Threshold Value									
	4.5		1.5		0.15		0.075		0.015	
Bases	hard	soft	hard	soft	hard	soft	hard	soft	hard	soft
Haar	65	66	68	67	77	74	82	77	97	88
Curvelet	57	56	71	63	76	74	79	76	90	83

Consequently, the sparsity-based lossy compression scheme has been applied to the 16 bit gray level DICOM images. Since there exists a high level of correlation between



(a) 4 level haar decomposition



(b) 4 level curvelet decomposition

Figure 6.17 Haar and curvelet decomposition for sparse approach (Sudheimer et al., 2019)

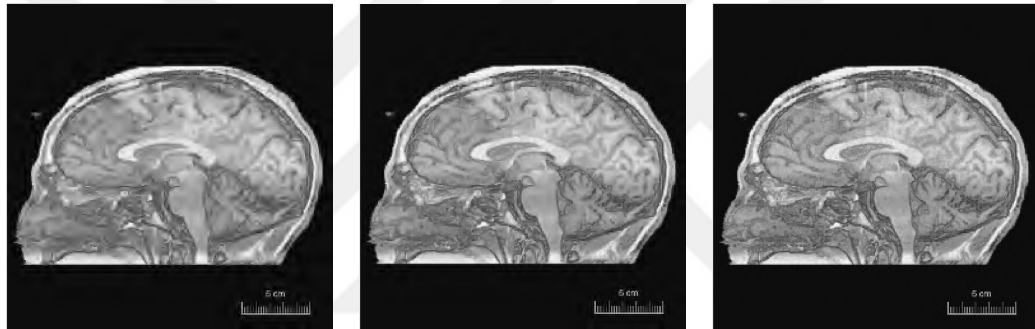


(a) Human MRI sagittal view

(b) Hard threshold=4.5

(c) Hard threshold=1.5

Figure 6.18 Sparse approach in compression using haar basis with hard threshold (Sudheimer et al., 2019)



(a) Hard threshold value=0.15

(b) Hard threshold value=0.075

(c) Hard threshold value=0.015

Figure 6.19 Sparse approach in compression using haar basis with hard threshold (Sudheimer et al., 2019)

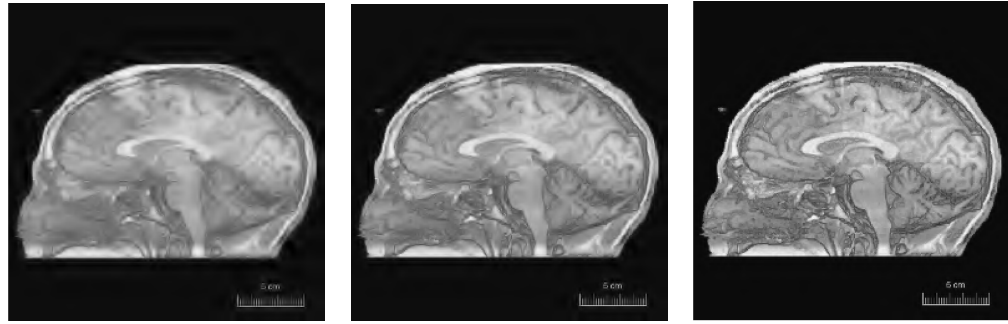


(a) Human MRI sagittal view

(b) Soft threshold value=4.5

(c) Soft threshold value=1.5

Figure 6.20 Sparse approach in compression using haar basis with soft threshold (Sudheimer et al., 2019)



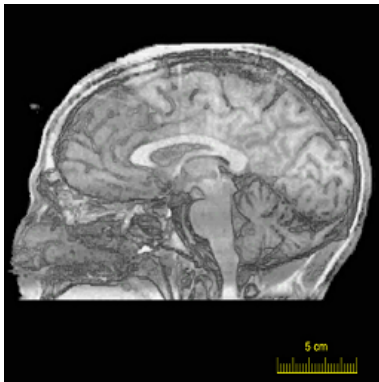
(a) Soft threshold value=0.15 (b) Soft threshold value=0.075 (c) Soft threshold value=0.015

Figure 6.21 Sparse approach in compression using haar basis with soft threshold (Sudheimer et al., 2019)

Table 6.8 PSNR metrics assessment (natural image)

	Threshold Value									
	4.5		1.5		0.15		0.075		0.015	
Bases	hard	soft	hard	soft	hard	soft	hard	soft	hard	soft
Haar	64	66	68	67	77	74	82	77	93	87
Curvelet	55	54	69	61	77	74	80	77	87	83

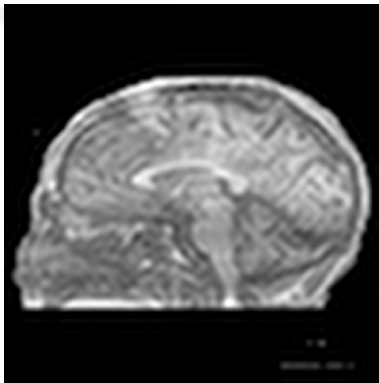
Result of sparse approach in compression using hard threshold (Curvelet basis):



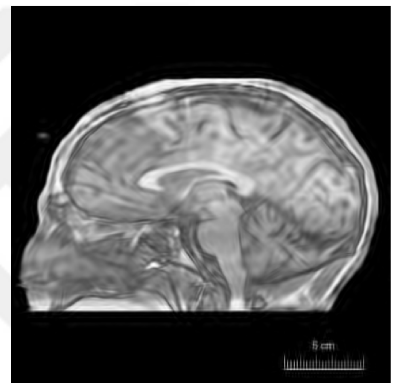
(a) Human MRI sagittal view



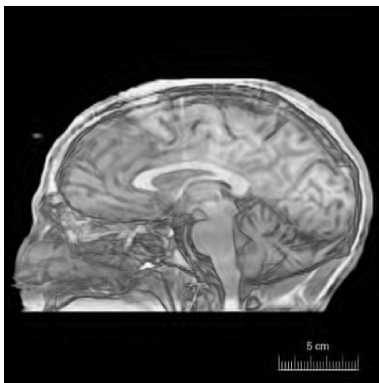
(b) Hard threshold value=4.5



(c) Hard threshold value=1.5



(d) Hard threshold value=0.15



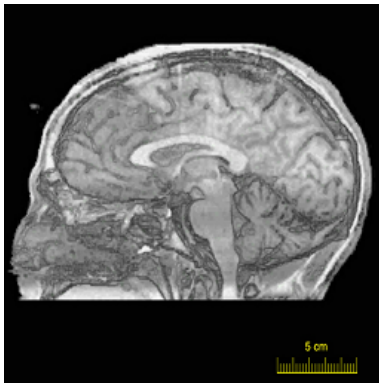
(e) Hard threshold value=0.075



(f) Hard threshold value=0.015

Figure 6.22 Sparse approach in compression using curvelet basis with hard threshold (Sudheimer et al., 2019)

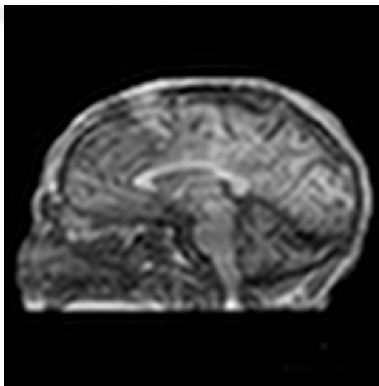
Result of sparse approach in compression using soft threshold (Curvelet basis):



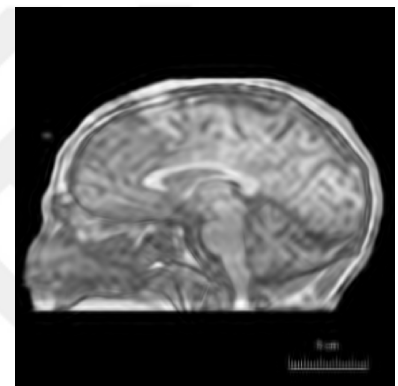
(a) Human MRI sagittal view



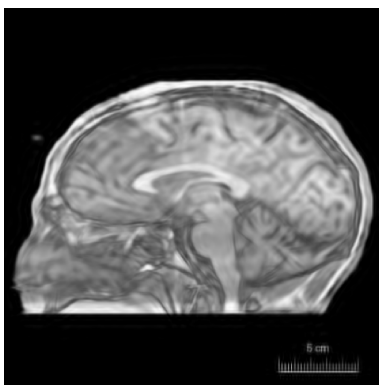
(b) Hard threshold value=4.5



(c) Hard threshold value=1.5



(d) Hard threshold value=0.15



(e) Hard threshold value=0.075



(f) Hard threshold value=0.015

Figure 6.23 Sparse approach in compression using curvelet basis with soft threshold (Sudheimer et al., 2019)

the consecutive pixels, this strategy achieves considerable compression performance. However, the loss of information may be crucial for medical images.

6.7 The Implementation Challenges

Besides the compression performance, the implementation is an important consideration for compression systems. The issues of implementation are taken up for proposed systems 3D-RLE and the CrS.

6.7.1 The 3D-RLE

Performance is a major parameter for the efficiency of the whole telemedicine system. In recent years, there are various implementation patents based on the RLE approaches due to the fact that run-length is a simple and easy-to-implement algorithm (Watanabe et al., 2019; Chen & Chang, 2019). The algorithm extends the 2D-RLE approach to the volumetric scanning using a simple algorithm that can be implemented on the telemedicine platforms. The 3D-RLE method is developed in MATLAB 2017b environment and have been implemented on the JAVA platform for the efficient telemedicine networks and DICOM presentation states. The optimal slice depth and other parameters should be considered for satisfactory compression performance.

6.7.2 The Chain Rule-based Compression System

The chain rule-based systems (the CrS) achieves the best compression performance which may exceed over 1000:1 ratio. This level of achievement is the tremendous performance that general-purposed lossless bi-level methods cannot obtain. However, there exist some issues must be considered before implementation of the chain-code based systems. The principle of systems is to codify the only boundary of a bi-level object instead of cipher all the pixel of the matrix. While the methods dramatically

decrease the number of bits required for the reconstruction process, it also needs extra complicated processes for compression and decompression, as follows. Recall that all independent region in the bi-level image must be segmented, boundary extracted and position labeled. These operations are time-consuming.

In this dissertation, the chain-code symbols are created in both JAVA and MATLAB 2017b development environments. Considering medical data, the system extracts the boundary of the organs and codify the boundary in acceptable computational complexity and execution time for off-line applications. Moreover, the systems can be experienced through the on-line e-health networks for a comprehensive evaluation. The image characteristics such as compactness and entropy can give information about the burden of processes. Consequently, the images should be analyzed whether the process raises difficulties for telemedicine implementations.

CHAPTER SEVEN

CONCLUSIONS AND FUTURE WORKS

Removing the geographical restriction for medical data circulation and spreading the medical services to the vast majority of the population by establishing a distributed collaborative platforms of medical data is becoming a significant requirement is associated with considerable improvement of communication technologies. In recent years, effective and lossless compression of images provides an efficient communication facility by the decreasing total amount of stored data, transmission time, bandwidth and cost rate that is the essential requirement for e-health networks standards such as DICOM and PACS. Accordingly, it is essential to compress and transmit medical data in telemedicine systems, which involve interactive transmission within and between health-care facilities using public and special networks.

Image compression systems are designed to meet specific requirements, such as to reduce the number of bits to store the image or to achieve required bit rate. They must satisfy the quantitative/qualitative distortion metrics and computation complexity affordable for the applications during the reconstruction process. In other words, image compression systems seek out for reducing the number of bits involved in reproducing of raw data that is used in a specially designed for medical data processing or health archiving systems. The success of image compression algorithms depends on their capabilities of revealing redundancy existing in the image data. Over the last decade, the still images have become diversified, e.g., natural, scientific, and medical images. However, the majority of the common compression standards are designed for natural images and multimedia records. Consequently, the performance of the general-purposed compression standards remains in a limited range for medical images. In this thesis, new compression strategies are suggested to uncover the redundancy of the medical images. To overcome the limitation of the current techniques, the characteristics of the medical data have been taken into account during the process of the compression by the proposed techniques.

In this dissertation, it has been shown that the characteristics of the medical images considerably differ from their of the natural ones in the sense of the entropy, compactness, energy, and non-stationarity. Considering the characteristic of medical images contributes to the redundancy removing capabilities of the methods. Thus, they could uncover a considerable amount of redundancy that can not be detected by the current standards. The three-dimensional run-length encoding, the 3D-RLE, (context-oriented), the chain code based, embedded zerotree wavelet and sparsity based systems are the techniques that are designed in characteristic-considering strategy.

The 3D-RLE and the CrS methods are the lossless methods for bi-level medical images that can faithfully reconstruct the images. The proposed methods which are volumetric run-length encoding (3D-RLE) and contour based systems (CrS) are lossless and bi-level compression techniques. The 3D-RLE has been utilized the inter-slice and the intra-slice correlation between the image elements. The method has suggested a new volumetric scanning algorithm that sweeps the voxels along a path coherent with the shape of the organs. The CrS has compressed the binary image by codifying only the boundary pixel of the organs. Thus, it reaches the remarkable compression achievement that exceeds tenfold more than those of the conventional compression standards such as JBIG and CCITT.

The sparsity and the EZW approaches are designed in a lossy mode for gray-scale medical images. These techniques utilizing different wavelets such as curvelet and wavelets with soft and hard thresholding are applied to the medical data sets.

The proposed methods have been simulated on different data sets such as abdominal bi-level (segmented) images and gray-scale brain image sets. The simulation results show that the proposed methods outperform the state-of-the-art compression standards in terms of the common lossless compression evaluation metrics. The context-oriented based strategy, namely the 3D-RLE, can reveal the redundancy of the medical data up to 200:1 ratio. And the CrS system exceeds the ratio of 1000:1 for the medical segmented image, on average. These achievements

show that context-oriented and contour based systems obtain notable results for medical images compared to the state-of-the-art bi-level compression standards.

7.1 Future Works

Compression performance for the run-length encoding primarily depends on the scanning procedures. Fractal space-filling curves, e.g. Hilbert and spiral, are the most successful forms. Thus, extended fractal forms such as Sierpiński curve, Peano curve, Koch snowflake, Dragon curve, H-tree curve will be designed as the RLE scanning procedures. Partitioning the image matrix while applying the RLE and Burrow-Wheeler transform will be employed to unearth the redundant data in the 3D-RLE symbols.

REFERENCES

- Ageenko, E., & Fränti, P. (2000). Lossless compression of large binary images in digital spatial libraries. *Computers and Graphics (Pergamon)*, 24(1), 91–98.
- Aguilar, W., & Bribiesca, E. (2015). Symmetry detection in 3D chain coded discrete curves and trees. *Pattern Recognition*, 48(4), 1416–1435.
- Aja-Fernandez, S., Estepar, R. S. J., Alberola-Lopez, C., & Westin, C.-F. (2006). Image quality assessment based on local variance. In *2006 International Conference of the IEEE Engineering in Medicine and Biology Society*, 4815–4818, IEEE.
- Aldemir, E., & Tohumoglu, G. (2016). Denoising of 3d medical imaging using sparse decomposition. *2016 International Conference on Image Processing, Wavelet and Applications (IWW2016)*, 1(1).
- Aldemir, E., Tohumoglu, G., & Alper, S. M. (2018a). Lossless compression of segmented 3d binary data for efficient telemedicine applications. In *Radiological Society of North America 2018 Scientific Assembly and Annual Meeting*, 1–1, Chicago IL.
- Aldemir, E., Tohumoglu, G., Dicle, O., & Selver, M. A. (2018b). Improvement of entropy coding performance for medical images using 3d predictors. In *Signal Processing and Communications Applications Conference (SIU)*, 1–4, IEEE.
- Aldemir, E., Tohumoglu, G., & Selver, M. A. (2019). Binary medical image compression using the volumetric run-length approach. *The Imaging Science Journal*, 67(3), 123–135.
- Anantha Babu, S., Eswaran, P., & Senthil Kumar, C. (2016). Lossless compression algorithm using improved RLC for grayscale image. *Arabian Journal for Science and Engineering*, 41(8), 3061–3070.
- Ansari, R., Guillemot, C., & Memon, N. (2009). Chapter 17 - jpeg and jpeg2000. In Bovik, A. (Ed.), *The Essential Guide to Image Processing*, 421 – 461, Boston: Academic Press.

- Anusuya, V., Raghavan, V. S., & Kavitha, G. (2014a). Lossless compression on mri images using swt. *Journal of Digital Imaging*, 27(5), 594–600.
- Anusuya, V., Raghavan, V. S., & Kavitha, G. (2014b). Lossless Compression on MRI Images using SWT. *Journal of Digital Imaging*, 27(5), 594–600.
- Associated, C., & Adverse, W. (2015). (12) United States Patent (10) Patent No : (45) Date of Patent :. 2(12).
- Babu, D. V., & Alamelu, N. (2009). Wavelet based medical image compression using roi ew. *International Journal of Recent Trends in Engineering*, 1(3), 97.
- Bailey, D. G. (2010). Chain coding streamed images through crack run-length encoding. *International Conference Image and Vision Computing New Zealand*.
- Bairagi, V. K. (2017). *Big data analytics in telemedicine: a role of medical image compression*, 123–160. Cham: Springer International Publishing.
- Bankman, I. (2008). *Handbook of medical image processing and analysis*. Burlington MA: Elsevier.
- Bassbouss, L., Pham, S., & Steglich, S. (2018). Streaming and playback of 16k 360 degree videos on the web. In *2018 IEEE Middle East and North Africa Communications Conference (MENACOMM)*, 1–5, IEEE.
- Bradley, S. (1969). Optimizing a scheme for run length encoding. *Proceedings of the IEEE*, 57(1), 108–109.
- Brahimi, T., Boubchir, L., Fournier, R., & Nait-Ali, A. (2017a). An improved multimodal signal-image compression scheme with application to natural images and biomedical data. *Multimedia Tools and Applications*, 76(15), 16783–16805.
- Brahimi, T., Laouir, F., Boubchir, L., & Ali-Chérif, A. (2017b). An improved wavelet-based image coder for embedded greyscale and colour image compression. *AEU - International Journal of Electronics and Communications*, 73, 183–192.

- Brechet, L., Lucas, M.-F., Doncarli, C., & Farina, D. (2007). Compression of biomedical signals with mother wavelet optimization and best-basis wavelet packet selection. *IEEE Transactions on Biomedical Engineering*, 54(12), 2186–2192.
- Bribiesca, E. (1997). Measuring 2-d shape compactness using the contact perimeter. *Computers & Mathematics with Applications*, 33(11), 1–9.
- Bribiesca, E. (1999). A new chain code. *Pattern Recognition*, 32(2), 235–251.
- Bribiesca, E. (2008). An easy measure of compactness for 2D and 3D shapes. *Pattern Recognition*, 41(2), 543–554.
- Bribiesca, E. (2016). A contour-oriented approach to shape analysis via the slope chain code. *International Journal of Contemporary Mathematical Sciences*, 11(2), 65–84.
- Bribiesca, E., & Bribiesca-Contreras, G. (2014). 2D tree object representation via the slope chain code. *Pattern Recognition*, 47(10), 3242–3253.
- Bruylants, T., Munteanu, A., & Schelkens, P. (2015). Wavelet based volumetric medical image compression. *Signal Processing: Image communication*, 31, 112–133.
- Candès, E. J., & Wakin, M. B. (2008). An introduction to compressive sampling. *IEEE Signal Processing Magazine*, 25(2), 21–30.
- Chang, C.-L., Zhu, X., Ramanathan, P., & Girod, B. (2006). Light field compression using disparity-compensated lifting and shape adaptation. *IEEE Transactions on Image Processing*, 15(4), 793–806.
- Chen, K., & Chang, C.-C. (2019). High-capacity reversible data hiding in encrypted images based on extended run-length coding and block-based msb plane rearrangement. *Journal of Visual Communication and Image Representation*, 58, 334–344.
- Chen, T., Zhang, M., Wu, J., Yuen, C., & Tong, Y. (2016). Image encryption and compression based on kronecker compressed sensing and elementary cellular automata scrambling. *Optics & Laser Technology*, 84, 118–133.

- Chen, Y.-W., & Lee, S. (1991). The C-chain code-a new method for coding 3D curves. *Conference Record of the Twenty-Fifth Asilomar Conference on Signals, Systems & Computers, 1*, 1–5.
- Cheng, K.-J., & Dill, J. C. (2014). An improved ezw hyperspectral image compression. *Journal of Computer and Communications, 2*(02), 31.
- Cho, S., Kim, D., & Pearlman, W. A. (2004). Lossless compression of volumetric medical images with improved three-dimensional spiht algorithm. *Journal of Digital Imaging, 17*(1), 57–63.
- Choplin, R. H., Boehme 2nd, J., & Maynard, C. (1992). Picture archiving and communication systems: an overview. *Radiographics, 12*(1), 127–129.
- Cover, T. M., & Thomas, J. A. (2005). *Elements of information theory*. Hoboken, New Jersey: Wiley Interscience.
- Creusere, C. D. (1997). A new method of robust image compression based on the embedded zerotree wavelet algorithm. *IEEE Transactions on Image Processing, 6*(10), 1436–1442.
- Dehkordi, V. R., Daou, H., & Labeau, F. (2011). A channel differential ezw coding scheme for eeg data compression. *IEEE Transactions on Information Technology in Biomedicine, 15*(6), 831–838.
- Donoho, D. L. (1993). Unconditional bases are optimal bases for data compression and for statistical estimation. *Applied and Computational Harmonic Analysis, 1*(1), 100–115.
- Fang, L., Li, S., Kang, X., Izatt, J. A., & Farsiu, S. (2015). 3-d adaptive sparsity based image compression with applications to optical coherence tomography. *IEEE Transactions on Medical Imaging, 34*(6), 1306–1320.
- Foundation, N. S. (2019). *Akiyo video frames*. Retrived April 25, 2019, from <http://trace.eas.asu.edu/yuv>.

- Fowler, B., Arps, R., Gamal, a. E., & Yang, D. (1995). Quadtree based JBIG compression. *Proceedings DCC '95 Data Compression Conference*.
- Freeman, H. (1961). On the encoding of arbitrary geometric configurations. *IRE Transactions on Electronic Computers*, 10(2), 260–268.
- Freeman, H. (1974). Computer processing of line-drawing images. *Computing Surveys*, 6(1), 58–97.
- Gantz, J., & Reinsel, D. (2012). The digital universe in 2020: Big data, bigger digital shadows, and biggest growth in the far east. *IDC iView: IDC Analyze the Future*, 2007(2012), 1–16.
- Gonzalez, R., & Woods, R. (2008). *Digital image processing*. New Jersey, USA: Prentice Hall.
- Goyal, V. K. (2001). Theoretical foundations of transform coding. *IEEE Signal Processing Magazine*, 18(5), 9–21.
- Graham, R. N., Perriss, R., & Scarsbrook, A. F. (2005). Dicom demystified: a review of digital file formats and their use in radiological practice. *Clinical Radiology*, 60(11), 1133–1140.
- Graps, A. (1995). An introduction to wavelets. *IEEE Computational Science and Engineering*, 2(2), 50–61.
- Guo, Y., Lu, C., Allebach, J. P., & Bouman, C. A. (2017). Model-based iterative restoration for binary document image compression with dictionary learning. *arXiv preprint arXiv:1704.07019*.
- Hampel, H., Arps, R. B., Chamzas, C., Dellert, D., Duttweiler, D. L., Endoh, T., et al. (1992). Technical features of the jbig standard for progressive bi-level image compression. *Signal Processing: Image Communication*, 4(2), 103–111.
- Hara, Y., & Kawano, T. (2015). Run-length encoding graphic rules applied to dna-coded images and animation editable by polymerase chain reactions. *Journal of Advanced Computational Intelligence*, 19(1).

- Hoffman, M. W. (2003). Lossless Bilevel Image Compression. In Sayood, K. (Ed.), *Lossless Compression Handbook*, chap. 17 327–349, California: Academic Press.
- Howard, P. G., Kossentini, F., Martins, B., Forchhammer, S., & Rucklidge, W. J. (1998). The emerging jbig2 standard. *IEEE Transactions on Circuits and Systems for Video Technology*, 8(7), 838–848.
- Hsu, W.-Y. (2015). Segmentation-based compression: new frontiers of telemedicine in telecommunication. *Telematics and Informatics*, 32(3), 475–485.
- Huerta-Hernández, C. E., & Sánchez-Cruz, H. (2014). Chain code histograms for rotation invariance. *Proceedings - 2014 International Conference on Computational Science and Computational Intelligence, CSCI 2014*, 1, 190–193.
- Kadhim, A. K., Merchany, A. B. S., & Babakir, A. (2019). An improved image compression technique using ezw and sphit algorithms. *Ibn AL-Haitham Journal For Pure and Applied Science*, 32(2), 145–155.
- Karadimitriou, K., & Tyler, J. M. (1997). Min-max compression methods for medical image databases. *ACM SIGMOD Record*, 26(1), 47–52.
- Karam, L. J. (2009). Chapter 16 - lossless image compression. In Bovik, A. (Ed.), *The Essential Guide to Image Processing*, 385 – 419, Boston: Academic Press.
- Karimi, N., Samavi, S., Soroushmehr, S., Shirani, S., & Najarian, K. (2016). Toward practical guideline for design of image compression algorithms for biomedical applications. *Expert Systems with Applications*, 56, 360–367.
- Khan, A., Khan, A., Khan, M., & Uzair, M. (2017). Lossless image compression: application of bi-level burrows wheeler compression algorithm (bbwca) to 2-d data. *Multimedia Tools and Applications*, 76(10), 12391–12416.
- Kim, S.-C., & Kim, E.-S. (2009). Fast computation of hologram patterns of a 3D object using run-length encoding and novel look-up table methods. *Applied Optics*, 48(6), 1030.

- Lee, H., Desbrun, M., & Schröder, P. (2003). Progressive encoding of complex isosurfaces. *ACM Transactions on Graphics*, 22(3), 471–476.
- Liaghati, A. L., & Pan, W. D. (2016). Evaluation of the biased run-length coding method on binary images generated by a modified ising model. In *SoutheastCon, 2016*, 1–8, Norfolk VA: IEEE.
- Lih-Jen Kau (2003). Lossless image coding using adaptive predictor with automatic context modeling. In *10th IEEE International Conference on Electronics, Circuits and Systems, ICECS*, 116–119, Sharjah: IEEE.
- Liu, F., Hernandez-Cabronero, M., Sanchez, V., Marcellin, M. W., & Bilgin, A. (2017). The current role of image compression standards in medical imaging. *Information*, 8(4), 131.
- Liu, X., Wu, X., Zhou, J., & Zhao, D. (2015). Data-driven sparsity-based restoration of jpeg-compressed images in dual transform-pixel domain. In *Proceedings of the IEEE Conference on Computer Vision and Pattern Recognition*, 5171–5178, Boston, MA.
- Liu, Y. K., Malik, B., Wang, P. J., & Podgorelec, D. (2012). Directional difference chain codes with quasi-lossless compression and run-length encoding. *Signal Processing: Image Communication*, 27(9), 973–984.
- Liu, Y. K., Wei, W., Jie Wang, P., & Žalik, B. (2007). Compressed vertex chain codes. *Pattern Recognition*, 40(11), 2908–2913.
- Liu, Y. K., & Žalik, B. (2005). An efficient chain code with Huffman coding. *Pattern Recognition*, 38(4), 553–557.
- Lu, Y., & Tan, C. L. (2003). Document retrieval from compressed images. *Pattern Recognition*, 36(4), 987–996.
- Maglogiannis, I., Doukas, C., Kormentzas, G., & Pliakas, T. (2009). Wavelet-based compression with roi coding support for mobile access to dicom images over

- heterogeneous radio networks. *IEEE Transactions on Information Technology in Biomedicine*, 13(4), 458–466.
- Maniccam, S., & Bourbakis, N. G. (2001). Lossless image compression and encryption using scan. *Pattern Recognition*, 34(6), 1229–1245.
- Marks, K. M. (1998). A jbig-abic compression engine for digital document processing. *IBM Journal of Research and Development*, 42(6), 753–758.
- Martínez, L. A., Bribiesca, E., & Guzmán, A. (2016). Chain coding representation of voxel-based objects with enclosing, edging and intersecting trees. *Pattern Analysis and Applications*, 1–20.
- Memon, N. D., & Sayood, K. (1995). Lossless image compression a comparative study. In *Proceedings of Still-Image Compression*, 8–21, Vancouver, BC.
- Miano, J. (1999). *Compressed image file formats: Jpeg, png, gif, xbm, bmp*. Reading, Massachusetts: ACM Press.
- Miaou, S. G., Ke, F. S., & Chen, S. C. (2009). A lossless compression method for medical image sequences using jpeg-ls and interframe coding. *IEEE Transactions on Information Technology in Biomedicine*, 13(5), 818–821.
- Method, system, and program for decoding compressed data at multiple points* (2004). US Patent 6,690,832.
- Moursi, S. G., & El-Sakka, M. R. (2007). Improving calic compression performance on binary images. Poznań: Citeseer.
- Munkres, J. (2014). *Topology*. Essex: Pearson Education.
- NEMA (2017). *DICOM Strategic document*. Retrived September 2, 2018, from <http://dicom.nema.org/dicom/geninfo/Strategy.pdf>.
- Olshannikova, E., Ometov, A., Koucheryavy, Y., & Olsson, T. (2015). Visualizing big data with augmented and virtual reality: challenges and research agenda. *Journal of Big Data*, 2(1), 22.

- Ono, F., Rucklidge, W., Arps, R., & Constantinescu, C. (2000). Jbig2-the ultimate bi-level image coding standard. *I*, 140–143.
- Pearlman, W. A., Kim, B.-J., & Xiong, Z. (2002). *Embedded video subband coding with 3D SPIHT*. New York: Springer.
- Peter D. Johnson, G. A. H. D. H., Jr. (2003). *Introduction to information theory and data compression*. Florida: Chapman and Hall/CRC.
- Petitcolas, F. A. P. (2018). *The boat image*. Retrived September 2, 2018, from <https://homepages.cae.wisc.edu/ece533/images>.
- Prabhu, K. M. M., Sridhar, K., Mischi, M., & Bharath, H. N. (2013). 3-d warped discrete cosine transform for mri image compression. *Biomedical Signal Processing and Control*, 8(1), 50–58.
- Pu, I. M. (2005). *Fundamental data compression*. Oxford: Butterworth-Heinemann.
- Qin, Y., Wang, Z., Wang, H., & Gong, Q. (2018). Binary image encryption in a joint transform correlator scheme by aid of run-length encoding and qr code. *Optics & Laser Technology*, 103, 93–98.
- Rajan, P. V. S., & Fred, A. L. (2019). An efficient compound image compression using optimal discrete wavelet transform and run length encoding techniques. *Journal of Intelligent Systems*, 28(1), 87–101.
- Ramabadran, T. V., & Chen, K. (1992). The use of contextual information in the reversible compression of medical images. *IEEE Transactions on Medical Imaging*, 11(2), 185–195.
- Ramakrishnan, B., & Sriraam, N. (2006). Internet transmission of dicom images with effective low bandwidth utilization. *Digital Signal Processing*, 16(6), 825–831.
- Rani, S. S., Rao, G. S., & Rao, B. P. (2018). Ezw, spiht and wdr methods for ct scan and x-ray images compression applications. In *International Conference on ISMAC in Computational Vision and Bio-Engineering*, 1517–1525, Switzerland: Springer.

- Rao, K., & Yip, P. (1990). *Discrete Cosine Transform: Algorithms, Advantages, Applications*. San Diego, CA, USA: Academic Press Professional, Inc.
- Regentova, E. E., Latifi, S., Chen, D., Taghva, K., & Yao, D. (2005). Document analysis by processing jbig-encoded images. *International Journal of Document Analysis and Recognition (IJDAR)*, 7(4), 260–272.
- Rissanen, J., & Langdon, G. G. (1979). Arithmetic coding. *IBM Journal of Research and Development*, 23(2), 149–162.
- Rodríguez-Dagnino, R. M. (2005). Compressing bilevel images by means of a three-bit chain code. *Optical Engineering*, 44(9), 097004.
- Salem, A.-b. M., Sewisy, A. A., & Elyan, U. A. (2005). A vertex chain code approach for image recognition boundary extraction. *Image (Rochester, N.Y.)*, 5(March), 1–8.
- Salomon, D. (2008). *A concise introduction to data compression*. London: Springer.
- Salomon, D., & Motta, G. (2010). *Handbook of data compression*. London: Springer.
- Sánchez-Cruz, H., Bribiesca, E., & Rodríguez-Dagnino, R. M. (2007). Efficiency of chain codes to represent binary objects. *Pattern Recognition*, 40(6), 1660–1674.
- Sánchez-Cruz, H., & Rodríguez-Díaz, M. A. (2009). Coding long contour shapes of binary objects. In *Lecture Notes in Computer Science (including subseries Lecture Notes in Artificial Intelligence and Lecture Notes in Bioinformatics)*, 15–52, LNCS.
- Sayood, K. (2003). *Lossless compression handbook*. San Diego: Academic Press.
- Sayood, K. (2017). *Introduction to data compression*. Waltham MA: Morgan Kaufmann.
- Schelkens, P., Munteanu, A., Barbarien, J., Galca, M., Giro-Nieto, X., & Cornelis, J. (2003). Wavelet coding of volumetric medical datasets. *IEEE Transactions on Medical Imaging*, 22(3), 441–458.

- Schiopu, I., & Tabus, I. (2013). Lossless contour compression using chain-code representations and context tree coding. In *Workshop on Information Theoretic Methods in Science and Engineering (WITMSE)*, 6–13, Tokyo.
- Scholl, I., Aach, T., Deserno, T. M., & Kuhlen, T. (2011). Challenges of medical image processing. *Computer Science - Research and Development*, 26(1), 5–13.
- Seeram, E. (2015). *Computed tomography: physical principles, clinical applications, and quality control*. Amsterdam: Elsevier Health Sciences.
- Selver, M. A., Kocaoğlu, A., Demir, G. K., Doğan, H., Dicle, O., & Güzeliş, C. (2008). Patient oriented and robust automatic liver segmentation for pre-evaluation of liver transplantation. *Computers in Biology and Medicine*, 38(7), 765–784.
- Shapiro, J. M. (1993). Embedded image-coding using zerotrees of wavelet coefficients. *IEEE Transactions on Signal Processing*, 41(12), 3445–3462.
- Shen, L., & Rangayyan, R. M. (1997). A segmentation-based lossless image coding method for high-resolution medical image compression. *IEEE Transactions on Medical Imaging*, 16(3), 301–7.
- Shusterman, E., & Feder, M. (1994). Image compression via improved quadtree decomposition algorithms. *IEEE Transactions on Image Processing*, 3(2), 207–215.
- Skodras, A., Christopoulos, C., & Ebrahimi, T. (2001). The jpeg 2000 still image compression standard. *IEEE Signal Processing Magazine*, 18(5), 36–58.
- Soille, P. (2013). *Morphological image analysis: principles and applications*. Berlin Heidelberg: Springer Science & Business Media.
- Stéphane, M. (2009). Chapter 1 - sparse representations. In Stéphane, M. (Ed.), *A Wavelet Tour of Signal Processing*, 1 – 31, Boston: Academic Press.
- Strasser, B., Botea, A., & Harabor, D. (2015). Compressing optimal paths with run length encoding. *Journal of Artificial Intelligence Research*, 54, 593–629.

- Sudheimer, K. D., Winn, B. M., Garrett M. Kerndt, Shoaps, J. M., Davis, K. K., J., A., Jr., F., & Johnson, J. I. (2019). *The Human Brain Atlas*. Retrived April 25, 2019, from [https://msu.edu/ brains/brains/human/index.html](https://msu.edu/brains/brains/human/index.html).
- Suresh, K. (2015). Lossless compression using adaptive integer wavelet for medical images. *ISRN Biomedical Engineering*, 2(2), 167–170.
- Sydney, B. C., Remesg, A., & Haito, G. (1998). *Introduction to wavelets and wavelet transform*. New Jersey: Prentice-Hall International, Inc.
- Taquet, J., & Labit, C. (2012). Hierarchical oriented predictions for resolution scalable lossless and near-lossless compression of ct and mri biomedical images. *IEEE Transactions on Image Processing*, 21(5), 2641–2652.
- Toennies, K. D. (2017). *Guide to medical image analysis*. London: Springer.
- Tohumoglu, G., & Sezgin, K. E. (2007). Ecg signal compression by multi-iteration ezw coding for different wavelets and thresholds. *Computers in Biology and Medicine*, 37(2), 173–182.
- Tu, C., & Tran, T. D. (2002). Context-based entropy coding of block transform coefficients for image compression. *IEEE Transactions on Image Processing*, 11(11), 1271–1283.
- Usevitch, B. E. (2001). A tutorial on modern lossy wavelet image compression: foundations of jpeg 2000. *IEEE Signal Processing Magazine*, 18(5), 22–35.
- Venugopal, D., Mohan, S., & Raja, S. (2016). An efficient block based lossless compression of medical images. *Optik-International Journal for Light and Electron Optics*, 127(2), 754–758.
- Verdoja, F., & Grangetto, M. (2017). Efficient representation of segmentation contours using chain codes. In *2017 IEEE International Conference on Acoustics, Speech and Signal Processing (ICASSP)*, 1462–1466, New Orlenias: IEEE.
- Wallace, G. K. (1992). The jpeg still picture compression standard. *IEEE Transactions on Consumer Electronics*, 38(1), xviii–xxxiv.

- Watanabe, K., Nakashima, Y., Inenaga, S., Bannai, H., & Takeda, M. (2019). Shortest unique palindromic substring queries on run-length encoded strings. *arXiv preprint arXiv:1903.06290*.
- Wu, X., & Memon, N. (1996). Calic-a context based adaptive lossless image codec. 4, *IEEE International Conference on Acoustics, Speech and Sig. Proc.*, 1890–1893, GA.
- Xiong, Z., Wu, X., Cheng, S., & Hua, J. (2003). Lossy-to-lossless compression of medical volumetric data using three-dimensional integer wavelet transforms. *IEEE Transactions on Medical Imaging*, 22(3), 459–470.
- Xu, D.-H., Kurani, A. S., Furst, J. D., & Raicu, D. S. (2004). Run-length encoding for volumetric texture. In *International Conference on Visualization, Imaging and Image Processing (VIIP)*, 452–458, Marbella: IASTED.
- Xu, Z., Bartrina-Rapesta, J., Blanes, I., Sanchez, V., Serra-Sagristà, J., García-Bach, M., & Francisco Muñoz, J. (2016). Diagnostically lossless coding of X-ray angiography images based on background suppression. *Computers & Electrical Engineering*, 53, 319–332.
- Yang, E. H., & Wang, L. (2009). Joint optimization of run-length coding, Huffman coding, and quantization table with complete baseline JPEG decoder compatibility. *IEEE Transactions on Image Processing*, 18(1), 63–74.
- Zahir, S., Dhou, K., & George, B. P. (2007). A new chain coding based method for binary image compression and reconstruction. *PCS, Lisbon, Portugal*, 1321–1324.
- Žalik, B., & Lukač, N. (2014). Chain code lossless compression using move-to-front transform and adaptive run-length encoding. *Signal Processing: Image Communication*, 29(1), 96–106.
- Žalik, B., Mongus, D., Liu, Y. K., & Lukač, N. (2016). Unsigned Manhattan chain code. *Journal of Visual Communication and Image Representation*, 38, 186–194.
- Žalik, B., Mongus, D., & Lukač, N. (2015). A universal chain code compression method. *Journal of Visual Communication and Image Representation*, 29, 8–15.

Zhou, N., Pan, S., Cheng, S., & Zhou, Z. (2016). Image compression–encryption scheme based on hyper-chaotic system and 2d compressive sensing. *Optics & Laser Technology*, 82, 121–133.

Ziv, J., & Lempel, A. (1977). A universal algorithm for sequential data compression. *IEEE Transactions on Information Theory*, 23(3), 337–343.

Ziv, J., & Lempel, A. (1978). Compression of individual sequences via variable-rate coding. *IEEE Transactions on Information Theory*, 24(5), 530–536.

